N° d'ordre : 40623

THÈSE

PRÉSENTÉE A

L'UNIVERSITE LILLE I

ÉCOLE DOCTORALE SCIENCES POUR L'INGÉNIEUR UNIVERSITÉ LILLE NORD-DE-FRANCE

Jan, ZELENY

POUR OBTENIR LE GRADE DE

DOCTEUR

SPÉCIALITÉ : Micro et Nano-technologies, Acoustique et Télécommunications

COMPENSATION NUMERIQUE DES NON-LINEARITES DES AMPLIFICATEURS DE PUISSANCE AVEC IDENTIFICATION AU NIVEAU RECEPTEUR

Architecture and Algorithms for Estimation and Compensation of Power Amplifiers Nonlinearities in Wireless Transceivers

Thèse soutenue le 4 octobre 2011

Jury :

M. GAQUIERE Christophe	Professeur IEMN Lille	Président
M. GHAZEL Adel	Professeur Sup'Com Tunis	Rapporteur
M. KERHERVE Eric	Professeur Laboratoire IMS Bordeaux	Rapporteur
M. DEHOS Cedric	Ingénieur CEA Grenoble	Encadrant
M. KAISER Andreas	Directeur de recherche CNRS IEMN Lille	Directeur
M. MARTINEAU Baudouin	Docteur STMicroelectronics Crolles	Membre

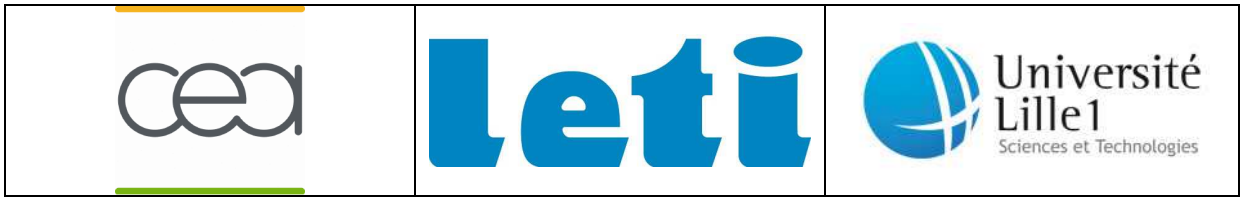

Université Lille 1Sciences et Technologies
CEA/LETI/DACLE/LAIR

A mon grand père

A ma famille

A la mémoire de Patrick

et à ceux qui me sont chers.

Abstract

Architecture and Algorithms for Estimation and Compensation of Power Amplifiers Nonlinearities in Wireless Transceivers

Keywords—Power Amplifier, Consumption Reduction, Predistortion, Software feedback, Look Up Table, Algorithm Complexity, LTE, LTE advanced, WiMAX, Rapp model, Base station, Mobile Station, Relay Station, Transmitter architecture, Receiver Aided.

Abstract— In this work a novel scheme of predistortion of power amplifier nonlinearities is developed and demonstrated. The originality of the proposed system architecture is that the estimation of nonlinearities is carried out at the receiver thanks to a training sequence, and sent back to the transmitter for predistortion. The proposed architecture achieves efficient compensation of power amplifier nonlinearities on WiMAX and LTE standards without extra hardware. An evaluation of consumption savings is carried out, considering digital consumption of the estimation algorithm at the receiver and predistortion Look Up Table refreshment at the transmitter. The results show that the suggested architecture can be applied for high data rate systems at base stations, relay stations and mobile stations as well.

Résumé

Compensation numérique des non-linéarités en amplificateurs de puissance.

Les mots clés — Amplificateurs de puissance, Économie d'énergie, Pré-Distorsion, Boucle d'asservissement logicielle, Radio Émetteurs avec l'aide de récepteur en Systèmes de communications sans fil, Look Up tableau, Complexité des algorithmes, LTE, LTE advanced, WiMAX, Model de Rapp, Station de base, Station mobile, Station Relay.

Résumé — Dans ce travail, un nouveau schéma de prédistorsion de non-linéarités amplificateur de puissance est développé et démontré. L'originalité de l'architecture du système proposé est que l'estimation des non-linéarités est réalisé grâce au récepteur à une séquence de formation, et renvoyé à l'émetteur pour la prédistorsion. L'architecture proposée réalise indemnisation efficace des non-linéarités amplificateur de puissance sur les normes WiMAX et LTE, sans matériel supplémentaire. Une évaluation des économies de consommation est effectuée, compte tenu de la consommation numérique de l'algorithme d'estimation au niveau du récepteur et de prédistorsion Look Up Table de rafraîchissement à l'émetteur. Les résultats montrent que l'architecture proposée peut être appliquée pour les systèmes de données à haut taux de stations de base, les stations relais et également aux stations mobiles.

Acknowledgments

I would like to thank in the memory of Dr. Patrick Wurm of being my advisor for the first part of the work. I would like to tell my sincere thanks to Mr. Cedric Dehos, who has taken over after the demise of Patrick, for motivation, guidance and expertise and encouragement especially in difficult moments of this thesis. I also would like to show my gratitude to Mr. Patrick Rosson for his time and precious help with measurements, Mr. Lionel Rudant and Mr. Maxime Robin for the help with test bed in anechoic chamber and Mr. Jerome Prouvée for his help with power amplifiers. I am very grateful to my thesis supervisor Prof. Andreas Kaiser from IEMN Lille, for his valuable academic advices and supervision.

I also thank to the jury members: Prof. Adel Ghazel and Prof. Eric Kerhervé, for accepting to participate to the Jury as reporters, Prof. Christophe Gaquiere and Mr. Baudouin Martineau for accepting to participate the Jury as members.

I would like to thank Mr. Pierre Vincent, head of LAIR laboratory in CEA-LETI and Mr. Jean-Réné Lequepeys, head of DACLE department, for accepting me for this PhD thesis and for giving me motivation and encouragement in difficult parts of the thesis. I am very grateful for the entire laboratory LAIR for help to make the work possible. I would like also to thank the entire DACLE department especially Miss Armelle De Kerleau for her sympathy and for telling me about the Grenoble Kayak Club and Dr. Marc Belleville for his useful scientific advises.

Contents

List of Figures

List of Tables

Chapter 1 : Introduction

1-1 Introduction

Worldwide energy consumption increases dramatically every year. As 78% of worldwide energy comes from fossil fuels, this energy produces green house effect CO_2 gas. If today only 0.2% of global CO_2 emissions come from mobile radio networks [1], the demand of transferred data in all countries is expected to skyrocket in the next years to 3 to 5%, which will increase very significantly its contribution to CO_2 emissions. In the meantime energy cost should rise. Figure 1 sketch highlights the balance between revenue from telecommunication industries and traffic growth. During the "voice era", revenues and costs were directly linked with the amount of users speaking. Now the quantity of data exchanged increases rapidly without correlated money feedback, but expensive energy consumption. In order to maintain the operator margins, the energy per bit needs to be reduced within the cellular network.

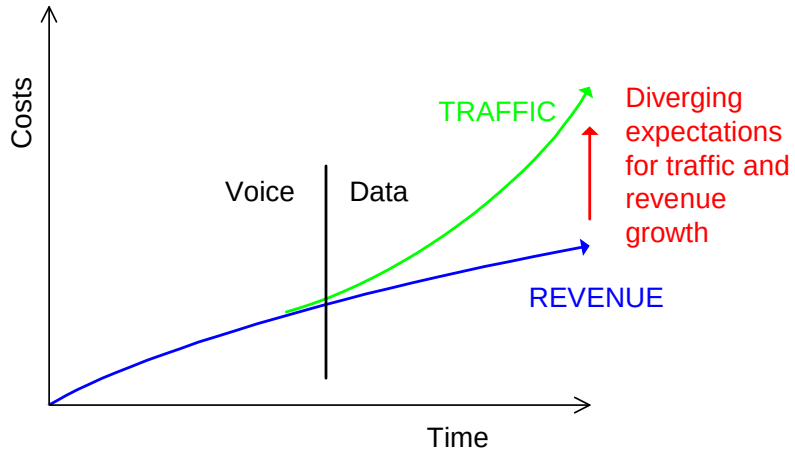

Figure 1 - Traffic/Revenue [7]

1-1.1 Cellular network operator energy consumption

As an example, for an UK cellular network operator consuming 40MW of total power [6], the power consumption budget is detailed in Figure 2.

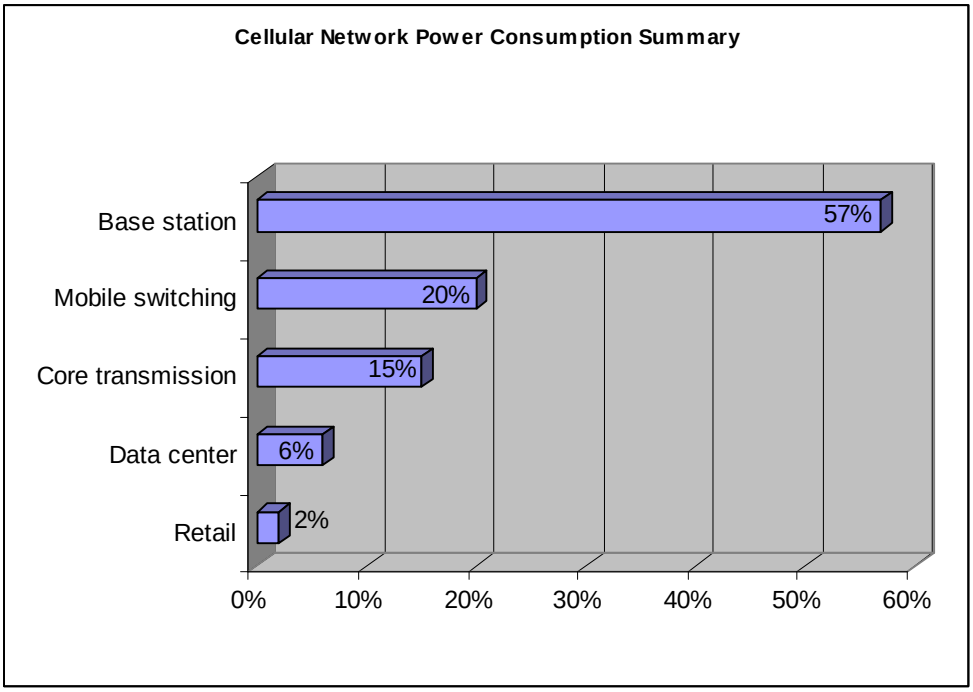

Figure 2 – Cellular Network Operator Power Summary [6]

The most power-hungry part is base station since 57% (22.8MW) of power consumption is consumed there. Indeed a conventional CDMA S3/3/3 base station consumes 2,2kW [2].

To tackle the cellular network consumption issue, [3] lists clues for power consumption and CO_2 emission reduction:

- ***Use renewable energy sources***
- ***Minimize number of BTS sites***
- ***Minimize BTS energy consumption***

Use of renewable energy sources becomes interesting in appropriated areas especially those without infrastructure. Nowadays in rural areas the BTS are more often powered by two diesel generators [4]. These generators produce a large quantity of CO_2 and they are harmful for environment. An important problem also is vandalism and fuel thefts. Hence renewable energy infrastructures, especially solar panels and wind micro power stations are win-win solutions.

The second possibility is to minimize the number of BTS sites. For this purpose article [3] suggests to extend cell coverage, to use lower frequency bands, to develop 6-sector sites and to use smart antennas.

The third possibility is at last to minimize the intrinsic BTS energy consumption by:

- ***Improving energy efficiency***
- ***Use system level features***
- ***Optimize BTS site solutions***

The energy efficiency can mainly be improved at the power amplifier. By using more efficient power amplifiers less supply power is dissipated. Power amplifier efficiency could also be enhanced by using well known linearization techniques such as polar loops, feedback techniques, or predistortion.

The second mean of improvement is related to the remote control of the BTS, in order to optimize the trade-off between BTS performances and consumption. For instance during low traffic period, part of the BTS can be shut down by the network manager, saving huge part of the power consumption.

The last mean of improvement is to take advantage of the site where BTS is installed for reducing the use of cooling fans. For example, by putting special weather proof on the components in outdoor sites, the BTS shelter can be removed. Then heat transfer from components is facilitated and power hungry cooling fans are no longer needed.

1-1.2 Challenge

Figure 3 shows the typical distribution of BTS power consumption [6]. From the pie chart there are four major sources of power consumption having shares larger than 10%:

- ***Power amplifier*** ***22%***
- ***Transmitter Idling*** ***19%***
- ***Power Supply*** ***16%***
- ***Cooling fans*** ***13%***

All these consumption sources are related together by temperature. For a power efficient PA, less power is dissipated in heat, and less cooling is needed. Also less time the transmitter is on, less power is dissipated in power amplifier and less power is consumed by cooling fans. A solution in [4] for optimizing the cooling is to put equipment outside of the shelter, which reduces power consumption by 30-40%. Another solution for optimizing Transmitter Idling is developed in [5]. By switching off radio resources when they are not needed, in low traffic periods, up to 25% of the energy consumption can be saved. A PA digital predistortion based solution with intelligent carrier control [2] reduces power consumption for CDMA S3/3/3 BTS up to 61%, compared to a conventional BTS. Then the diesel generators could be replaced by a combination of solar panels, wind power stations and batteries as power supply. When applying all these mitigation methods together we could save up to 68% of energy for a WCDMA BTS, according to [3].

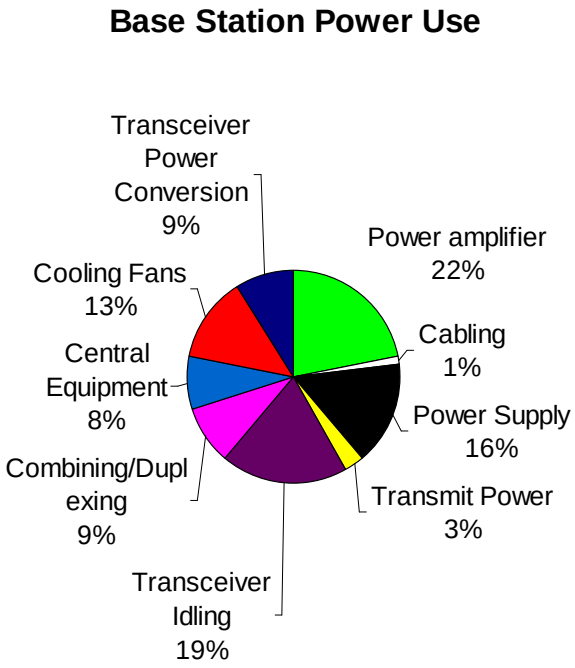

Figure 3 – Base station power use [6]&[8].

The challenge is then to keep the energy consumption of base station as low as possible, in the context of ever growing data traffic in new telecommunication networks. In the following, the work is focused on the power amplifier, where the consumption gain could be maximal.

1-1.3 Summary

The thesis work embraces the concept of Green Radio whose goal is to optimize mobile operator networks in energy consumption and CO_2 emission reduction. Eco-friendly, low consumption and energy independent BTS are being developed. This requires that the most power-hungry part of BTS, i.e. the power amplifier, improves its efficiency while limiting heat dissipation and power-hungry cooling.

1-2 Power Amplifier Characteristics

The power amplifier is the key component of radio architecture. As a most consuming part of base station the power amplifier governs other power hungry systems such as cooling fans. The overall design of transmitters needs to be optimized with respect to the power amplifier used and standard for which the transmitter is intended for.

1-2.1 PA function

At the Digital to Analog (DAC) converter output, the signal is often weak and needs strongly to be amplified before being emitted. For instance the standard [9] specifies an emitted power of 43dBm at base station and 23dBm at mobile station for WiMAX and 46dBm at base station and 24dBm at mobile station for LTE. Hence, after up conversion, the signal passes through a power

amplifier to be amplified up to the needed power level. Unfortunately the PA is not an ideal component. It adds imperfections, such as noise and nonlinearity that designers have to cope with. To be able to compare the various PAs, their different parameters and figures of merit are defined below.

1-2.2 Figures of merit

In this paragraph the power amplifier parameters and figures of merit are described. Each figure of merit qualifies some power amplifier property, which is directly included in standard specification or related to signal-defined figure of merit which is included in standard specification. The principal power features are gain, bandwidth, efficiency, linearity, noise figure and dynamic range.

1-2.2.1 Gain

The gain is obviously given by the ratio of input and output power, Eq. 1. Typically the gain is quantified in dB.

$$G = 10 \cdot \log\left(\frac{P_{OUT}}{P_{IN}}\right)[dB] \qquad \text{Eq. 1}$$

For an ideal power amplifier, the gain would be constant until its point of saturation, where the signal is clipped and the gain decreases as a linear function with increasing input power until the breakdown power is reached. In a real power amplifier, the output power is a nonlinear function of input power; hence the gain is also a nonlinear function of input power.
The gain is also closely related to power consumption. If the amplification requires a perfect linear signal, more power is needed for the same gain, in order to shift the nonlinear region higher in the P_{OUT}/P_{IN} characteristic.

1-2.2.2 Bandwidth

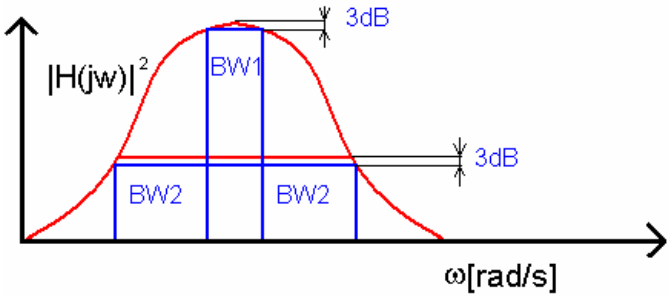

Figure 4 – An Amplifier Transfer Function

The bandwidth is defined as the part of the transfer function where the actual squared absolute value of transfer function is -3dB from maximal gain. On Figure 4 we can see how we can increase bandwidth using negative feedback. Negative feedback makes the gain constant on a wider interval, but the gain is not as large as maximal gain without feedback.

1-2.2.3 Efficiency

Efficiency measures how much power is used for amplifying the signal and how much power is dissipated. Efficiency is strongly related to the power amplifier classes which are given by the conduction angle.

The simplest definition of efficiency is the drain efficiency of Eq. 2, where P_{OUT} is the output power and P_{DC} is the supply power.

$$\eta = \left(\frac{P_{OUT}}{P_{DC}} \right) \qquad \text{Eq. 2}$$

Power Added Efficiency (PAE) is defined by Eq. 3, where P_{OUT} is output power P_{IN} is input power and P_{DC} is supply power.

$$PAE = \left(\frac{P_{OUT} - P_{IN}}{P_{DC}} \right) \qquad \text{Eq. 3}$$

PAE is always lower than drain efficiency. For high gain PAs, the PAE becomes closer to drain efficiency. Improving PA efficiency and PAE is the key issue for lower consumption of transmitters.

1-2.2.4 Linearity

Linearity is a key parameter of the power amplifiers. The need of signal linearity affects the power efficiency, which increases power consumption. The trade-off between linearity requirements and power consumption is defined by the power back off from the 1dB gain compression point as defined in the figure below. This trade-off is widely analyzed in [10].

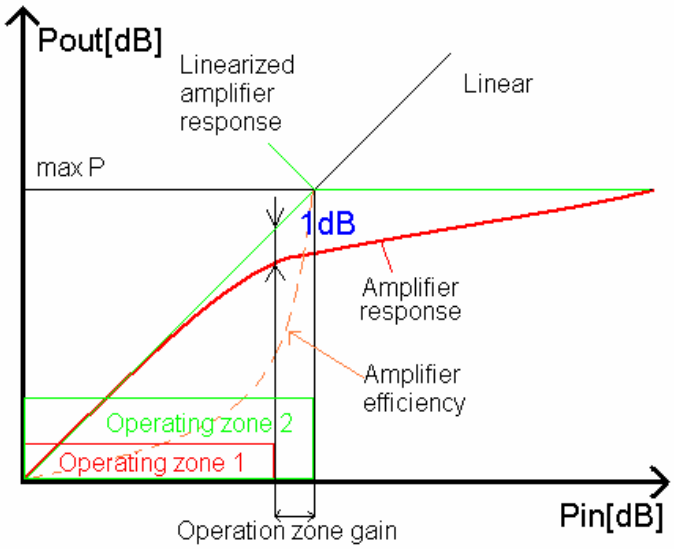

Figure 5 –Nonlinear power amplifier AM/AM conversion

The linearization techniques aim at changing the amplifier power response from the nonlinear red curve to the linear green curve up to the saturation point.

1-2.2.5 Noise figure

The noise figure measures the degradation of the signal to noise ratio (SNR) by the device, Eq. 4, at standard noise temperature T_0=290K.

$$F = \left(\frac{SNR_{IN}}{SNR_{OUT}} \right) \quad \text{Eq. 4}$$

In radio architecture, which is composed from cascaded blocks the final noise figure is given by Friis formula, Eq. 5, where F are device noise factors and G are device power gains.

$$F = F_1 + \frac{F_2 - 1}{G_1} + \frac{F_3 - 1}{G_1 G_2} + \ldots + \frac{F_n - 1}{G_1 G_2 \ldots G_{n-1}} \quad \text{Eq. 5}$$

Attenuators or devices with no gain a have noise factor equal to their attenuation.

1-2.2.6 Output dynamic range

The dynamic range is defined as the difference between the smallest and the greatest output level. On Figure 6 the dynamics ranges for nonlinear amplifier response (zone 1) and linearized amplifier response (zone 2) are roughly illustrated. Dynamic range is related to the Peak to Average Power Ratio of the input signal. For nonlinear power amplifiers, power has to be reduced (back off from P1dB) for the PA to operate within its linear zone. Ideally linearized PAs can operate up to the saturation point.

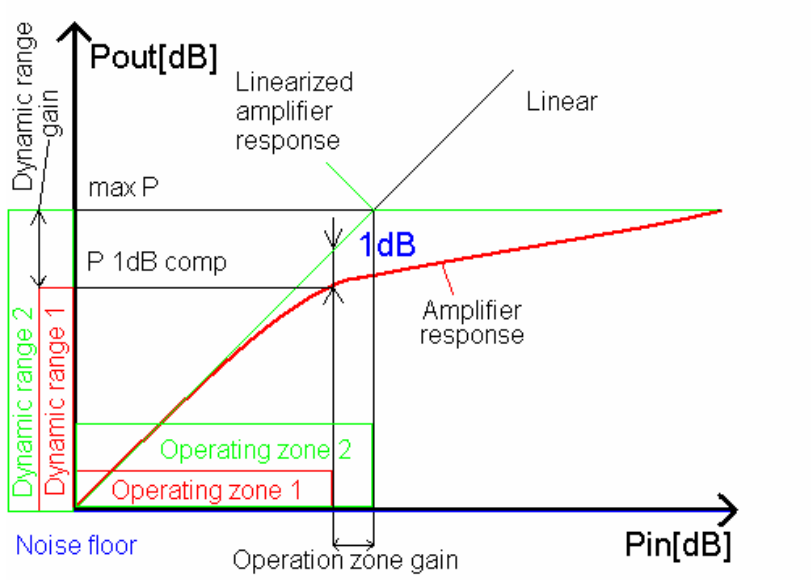

Figure 6 –Dynamic range

1-2.3 Summary on power amplifiers

The challenge of power amplifiers is to optimize linearity and efficiency together, more precisely increasing PA's efficiency while keeping the PA's linearity. Clever compromises need to be made to optimize the transmitter architecture to dedicated use cases.

1-3 High PAPR signals for high data rate applications

In this paragraph the signal properties of the considered standards are described. Modulated signals for high data rate applications are mostly OFDM-based waveforms, which suffer from high peak-to-average-ratio (PAPR). This high PAPR puts emphasis on PA's linearity. Indeed PA nonlinearities change signal properties such as its statistical distribution, variance and mean power, because of clipping and distortion caused by the nonlinear power amplifier. In the first part of this section the considered high data rate signals are presented. Then signal figures of merit defined by standard's specifications are explained. Finally the interactions with nonlinear devices are described.

1-3.1 High data rate application

OFDM-based waveforms are widely used in WLAN high data rate systems. Indeed multicarrier modulation is relevant for mitigating the effect of multi-path indoor environment. Each subcarrier is modulated by quadrature amplitude modulation (QAM), whose constellation can have many points. For instance in the following developments, we consider modulations up to 64QAM. Then the signal power is given as a sum of modulated carrier signals. At some instants the signals are all summed in phase, and peaks appear with amplitude far higher than the average amplitude. For a large number of subcarriers (up to 2048 subcarriers for WiMAX) Peak to Average Power Ratio (PAPR) is then very high. To guarantee their integrity, high PAPR signals demand large dynamic range in RF components like power amplifiers and digital to analogue converters.

PAPR is defined by Eq. 6 as an instantaneous maximal power divided by the mean power in a considered time window.

$$PAPR = \left(\frac{P_{PEAK}}{P_{AVERAGE}} \right) = \frac{\max\left(\left| s(t)^2 \right| \right)}{E\left(\left| s(t)^2 \right| \right)} \qquad \text{Eq. 6}$$

Mean value is defined as a first statistical moment by Eq. 7 a) where $f_X(u)$ is probability density function. Eq. 7 b) defines mean value for periodic signals. For non periodic signals (such as OFDM), the PAPR is dependent on the time window where it is measured. For OFDM signals PAPR can be measured on a symbol or on a frame. Usually PAPR refers in the OFDM case to the average of the measured PAPR on an OFDM symbol.

$$\text{a) } E(x) = \int_{-\infty}^{+\infty} u \cdot f_X(u) du \qquad \text{b) } E(x) = \frac{1}{T} \int_{0}^{T} u \cdot f_X(u) du \qquad \text{Eq. 7}$$

If the power amplifier has a nonlinear amplitude response, it is necessary to apply a power back-off to high PAPR signal, by reducing the power at the PA input. The peaks of signal having large PAPR stay undistorted. Figure 7 shows the decrease of efficiency of the PA due to power

back-off. The blue curve is the efficiency of a class A PA, magenta curve is the efficiency of a class B PA and class AB PAs are between these two, depending on the conduction angle. For instance in a worst case, a signal having a large PAPR has to pass through a class A PA not being clipped or distorted, the input back off to be applied can be as much as 15dB. In that case of no-clipping, the PA efficiency falls to 1.6%. Then for a WiMAX mobile station with an output power of 23dBm, we would need 41dBm (12W) of supply power and for WiMAX base station with an output power of 43dBm, we would need 61dBm (1200W) of supply power.

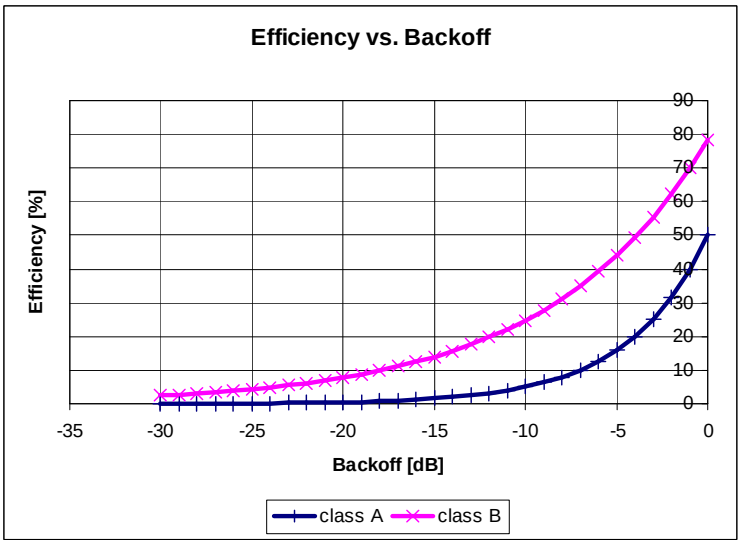

Figure 7 –Efficiency vs. Backoff

In more realistic conditions, low distortion is tolerated at the PA output, function of the Error Vector Magnitude (EVM) required by the standard. For example in a transmitter architecture, where the input signal PAPR equals 15dB, the output signal is distorted and clipped by a class A power amplifier, up to an EVM of 5%. The power amplifier is then driven with Input Back Off (IBO) of 5.85dB, corresponding to 13% efficiency. Then for the same WiMAX mobile station with 23dBm of output power we need 31.86dBm (1,5W) and for the same WiMAX base station with output power 43dBm, we would need 51.86 dBm (153W). The power amplifier's consumption is significantly reduced.

1-3.2 Signal properties

In this paragraph the signal properties and figures of merit are defined. The figures of merit stand for comparing the signal quality at the emitter output compared to the quality required by the standards.

1-3.2.1 EVM

Error vector magnitude is shown in Figure 8 as the error vector in the complex plane between the reference and the measured signal.

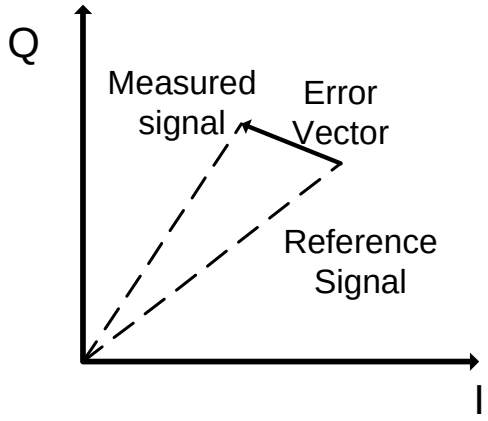

Figure 8 –Error vector [11]

Eq. 8 defines EVM as the square root of the ratio between the error power and the reference power.

$$EVM = \sqrt{\frac{P_{ERROR}}{P_{REFERENCR}}} = \sqrt{\frac{1}{N_f}\sum_{i=1}^{N_f}\frac{\sum_{j=1}^{Lp}\sum_{k\in S}\left(\left(I(i,j,k)-I_0(i,j,k)\right)^2+\left(Q(i,j,k)-Q_0(i,j,k)\right)^2\right.}{\sum_{j=1}^{Lp}\sum_{k\in S}\left(I_0(i,j,k)^2+Q_0(i,j,k)^2\right)}} \quad \text{Eq. 8}$$

Where the definition of the symbols is taken from standard norm [9]

- L_p is the length of the time packet
- N_f is the number of frames for the measurement
- $(I_0(i,j,k),Q_0(i,j,k))$ is the ideal symbol point in the i-th frame, j-th OFDMA symbol of the frame and k-th subcarrier of the OFDMA symbol in the complex plane.
- $(I(i,j,k),Q(i,j,k))$ is the measured symbol point in the i-th frame, j-th OFDMA symbol of the frame and k-th subcarrier of the OFDMA symbol in the complex plane.
- S is the group of modulated data subcarriers, where the measurement is performed

Allowed EVM values for IEEE 802.16e standard are given by Table 1 with regard to the used subcarrier modulation and data coding.

Burst type	**Relative constellation error [dB]**	**EVM [%]**
QPSK-/2	-15	17.78
QPSK-3/4	-18	12.6
16-QAM-1/2	-20.5	9.44
16-QAM-3/4	-24	6.3
64-QAM-1/2	-26	5
64-QAM-2/3	-28	4
64-QAM-3/4	-30	3.16

Table 1 - Allowed relative constellation error versus data rate for IEEE 802.16e standard

For high PAPR signal, PA characteristics needs to be more linear. As a result power Input Back-Off (IBO) needs to be increased to keep the signal EVM below the standard requirements of Table 1.

IBO is defined in Eq. 9, where P_{SIGNAL} is the signal RMS power and the 1dB compression point (P_{1dB}) is the power for which the gain of PA becomes stressed by nonlinearity by 1dB.

$$IBO = \frac{P_{SIGNAL}}{P_{1dB}} \qquad \text{Eq. 9}$$

1-3.2.2 Output mean power

Base Stations, Relay Stations and Mobile Stations are limited in LTE and WiMax standards with maximal output mean power (Table 2). The relay station which is localized outdoor uses BS PA while RS which is localized indoor uses MS PA.

	WiMAX		LTE	
Terminal	BS	MS	BS	MS
PA output power [dBm]	43	23	46	24

Table 2 - PA output power for LTE&WiMAX

1-3.2.3 Spectral Mask

Transmission of information shall be done without interfering users in adjacent or alternate frequency band. However the output of a nonlinear device signal suffers from spectral regrowth. The spectral regrowth interferes with other devices communicating in adjacent channels. To avoid the interference between communicating devices a spectral mask was introduced in standards. It quantifies the maximal allowed spectral regrowth. Spectral mask for 20MHz and 10MHz channel bandwidth is drawn on Figure 9 with values marked in Table 1. The x-axis is an offset frequency from frequency of the carrier. The y-axis is a maximal allowed spectrum regrowth related to carrier power.

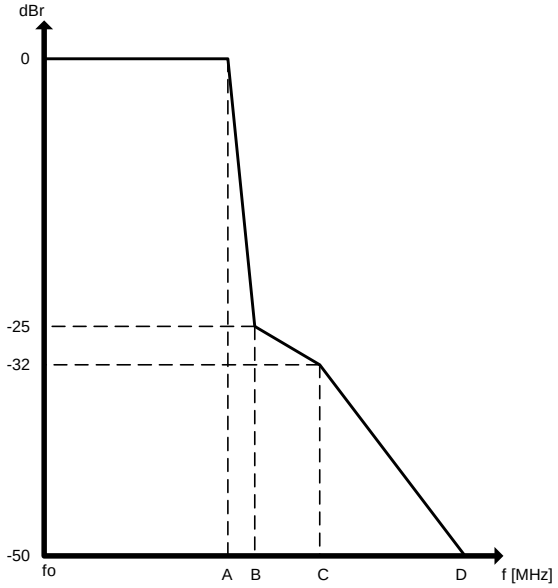

Figure 9 –WiMAX spectral mask [11]

Channel Bandwidth [MHz]	A	B	C	D
20	9.5	10.9	19.5	29.5
10	4.75	5.45	9.75	14.75

1-3.3 Nonlinear power amplifier and signal distortion

When the modulated signal passes through a nonlinear power amplifier it becomes distorted. From Gaussian distribution, the amplitude distribution changes, with a limitation of the highest amplitude. Distortion in [12] is defined as an undesirable signal change. The input signal is defined in Eq. 10

$$x(t) = A \cdot e^{j(2\cdot\pi\cdot f\cdot t+\varphi)} \qquad \text{Eq. 10}$$

Where A is signal amplitude f is signal frequency φ is signal phase. When the signal passes through a nonlinear device such as power amplifier it becomes distorted.

$$y(t) = G(x(t)) = G_1\left(|x(t)|^2\right)A \cdot e^{j\left(2\cdot\pi\cdot f\cdot t+\varphi+G_2\left(|x(t)|^2\right)\right)} \qquad \text{Eq. 11}$$

G is a function of memory or memory-less power amplifier characteristic. It is decomposed into two parts depending on the input power. The first part G_1 is gain as a function of the input power and the second part G_2 is a phase addiction dependent of the input power.

In the case of a linear power amplifiers the G_1 function is constant for input power from zero to the saturation power. For real amplifiers G_1 is a nonlinear monotonous function towards the saturation point. The amplitude distortion is usually given for a device by its AM/AM conversion shown on Figure 6 (the red curve). For modulated signals, AM/AM distortion causes spectral regrowth, i.e. signal spectrum overlaps onto adjacent channels. The nonlinearities generate n^{th} order spectral regrowth as depicted on Figure 10 with carrier offset frequency on x-axis and power spectral density on y-axis. Wireless standards require that that regrowth does not exceed their spectral mask (Figure 9).

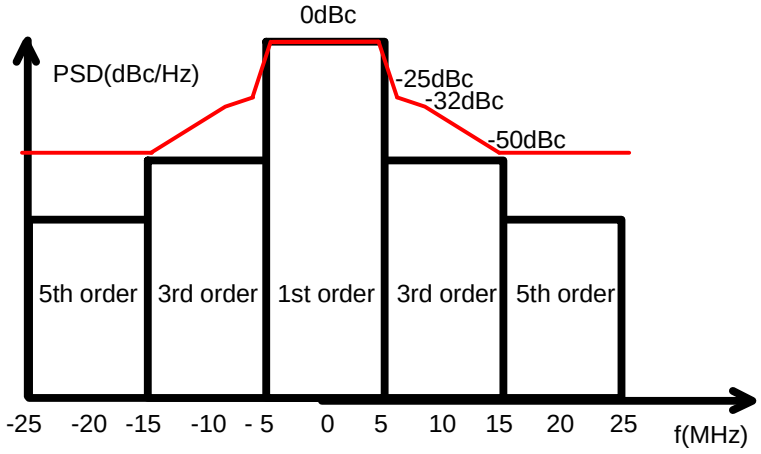

Figure 10 – Spectral regrowth

G_2 is output signal phase deviation vs. input power (AM/PM conversion) defined in [deg/dB]. As an example Figure 11 shows the impact of AM/PM distortion on QAM modulated signal, i.e. it rotates the received constellation.

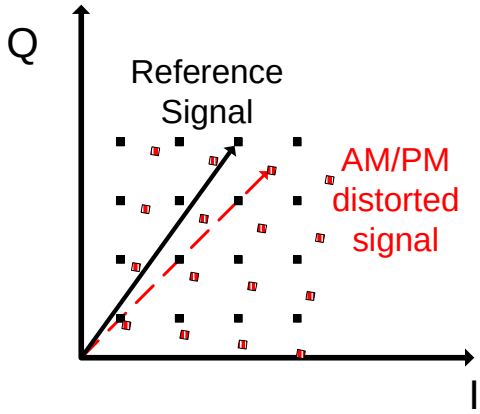

Figure 11 – AM/PM distortion impact on QAM modulated signal

1-3.4 Summary

High PAPR signals demand a large dynamic range which implies linearity within components of the RF architecture. To avoid overconsumption of linear low efficiency PA, many solutions were proposed in [13]. These solutions aim at growing PA efficiency, in a trade-off with signal distortion at the PA output.

1-4 PA linearization

The state-of-the-art linearization techniques can be classified into two major principles. The first one is based on nonlinear signal shaping; the second one is based on error suppression. Each method is more or less adapted to the used signal waveform, standard's specifications and fields of use. Clever compromises in combining these principles need to be carried out.

1-4.1 Nonlinear signal shaping

The first method of linearization relies on applying an inverse nonlinear function to the signal, as a digital multiplication of the signal amplitude (Figure 12) or by using hardware dynamic biasing. The former technique is well known as predistortion. The compensation can be applied in the transmitter or alternatively in the receiver.

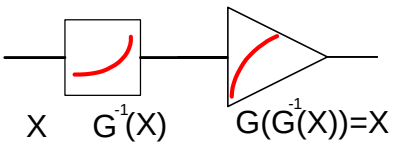

Figure 12 – Compensation by inverse function - Predistortion

1-4.2 Error suppression

The second method of linearization is the subtraction of an error function. Figure 13 shows an example of the error subtraction principle. The error signal is usually extracted from the signals

before and after PA. The error signal can be then propagated through Feedback or feed-forward architectures.

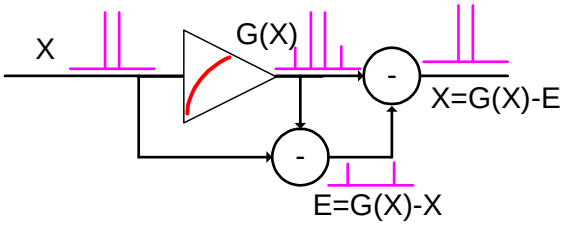

Figure 13 – Compensation by error suppression

1-4.3 Summary

A combination of techniques like error suppression or multiplication of the signal by the inverse function is used in the state-of-the-art in different forms, especially in architectures like polar loop, envelope tracking etc. If the signal is transformed into polar signal representation such as magnitude and phase, bandwidth limitation appears. Hence the solutions increasing bandwidth are only used for narrowband systems. If the signal is kept in the Cartesian domain, the linearization technique does not need to increase bandwidth, but the systems, such as Cartesian loops suffer from instability when the antenna has poor VSWR.

Linearization techniques applying nonlinear signal shaping, especially predistortion, are strongly dependent on the PA model used for signal shaping. A trade-off between PA model complexity and energy saving has to be found in order to reduce the overall consumption.

1-5 Scenarios of application

Figure 14 shows an example of different conditions of urban channel propagation. The green path channels correspond to Line Of Sight (LOS) paths, while channels in red correspond to Non Line of Sight Channels (NLOS) relying on reflections and subject to multipath propagation.

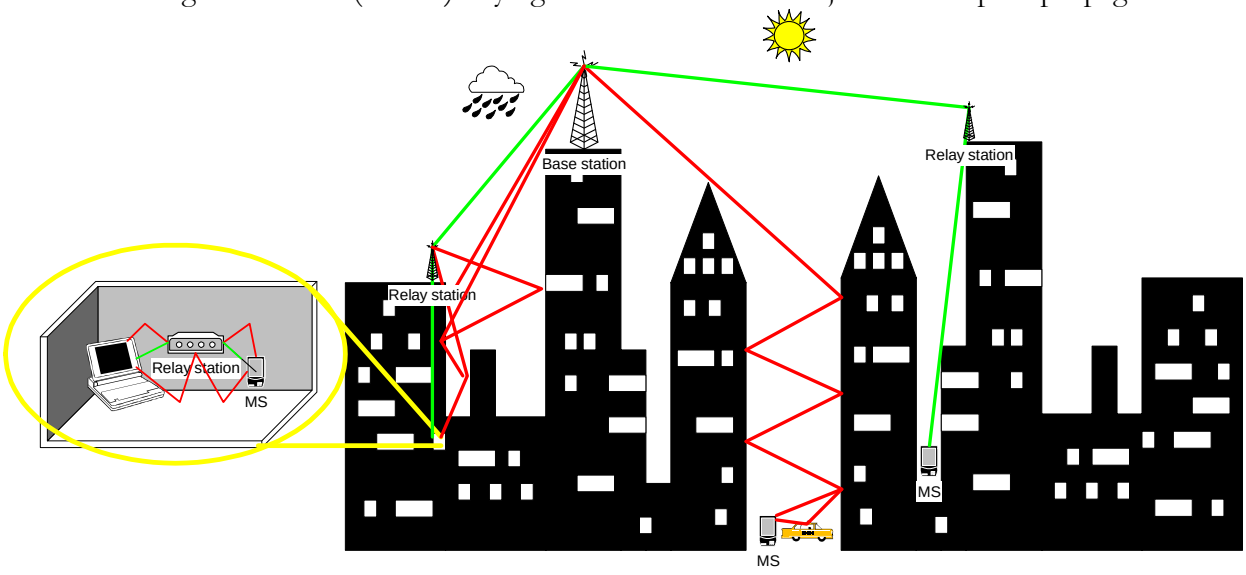

Figure 14 – Scenarios

1-5.1 Line-of-Sight channels

LOS link appears on scenario Figure 14 between outdoor relay stations and indoor relay stations, or between outdoor relay stations and mobile stations.

Directional antennas are often used between base station and outdoor relay stations. If the narrower Fresnel ellipsoid is not affected by obstacles, the AWGN channel might be used as a channel model. The channel is then only influenced by weather conditions.

If multipath propagation appears, but still with a direct visibility between receiver and transmitter, the statistical channel model becomes a Rician distribution, Eq. 12, where I_0 is the modified Bessel function of the first kind with order zero.

$$f\left(x|\nu\sigma\right)=\frac{x}{\sigma^2}\exp\left(\frac{-\left(x^2+\nu^2\right)}{2\sigma^2}\right)\cdot I_0\left(\frac{x\nu}{\sigma^2}\right) \qquad \text{Eq. 12}$$

1-5.2 Non-Line-of-Sight channels

Without direct visibility between emitter and receiver, the transmission is carried out through reflections of the multipath propagation. The amplitude is then Rayleigh distributed. Rayleigh distribution is a special case of Rice distribution where $\nu=0$, Eq. 13.

$$f\left(x,\sigma\right)=\frac{x}{\sigma^2}\exp\left(\frac{-x^2}{2\sigma^2}\right) \qquad \text{Eq. 13}$$

1-5.3 Scenarios summary

Figure 14 describes three representative channel conditions.

- The most favorable scenario for the estimation of parameters at the receiver is "LOS channel scenario". Within this channel the PA model parameters estimation is only affected by AWG noise. This scenario could be a BS-BS link in urban or rural area. Usually the distance between devices is bigger in rural areas than in urban areas. This link could also be outdoor RS/BS with direct visibility. Here the distance is several hundredths of meters. The output conducted power is set to 30dBm for this scenario.
- Second scenario is called "Rice channel scenario" with Rician channel model. In this scenario PA parameter estimation is slightly affected by multipath propagation in channel. This scenario could be an indoor RS/BS or MS/BS-RS link in rural area or in urban area, with direct visibility between communicating devices. The distances could reach hundredths of meters. The output conducted power for this scenario is set to 10dBm for MS and indoor RS. For outdoor RS or BS the conducted power is set to 30dBm.
- Finally when the multipath appears, the signal is more affected by channel propagation. The signal is then strongly distorted at the receiver side which affects the PA model parameters estimation. The scenario is called "Rayleigh channel scenario". This

scenario is between MS/indoor RS indoors where there is no direct visibility. The distance is from one to tenth of meters. The output conducted power for this scenario is fixed to 10dBm for MS and indoor RS.

1-6 Conclusion

The purpose of the following works is to reduce overall transmitter device consumption by PA predistortion in 802.16e and LTE standards. The compensation is aimed to save power within base stations, relay stations and even mobile stations within various scenarios of environment. For this purpose, we propose in the next chapters to estimate a model of nonlinearity at the receiver side, and feedback the estimated parameters to the emitter for predistortion. Thus the nonlinearity parameters shall be estimated from received signal experiencing multipath channel. A study is carried out to evaluate the robustness and the coupling of the different processing algorithms: PA nonlinearity estimation, gain control, channel estimation and equalization.

Chapter 2 : State of the Art

2-1 Power amplifiers - PA classes

The power amplifier is the key component of radio architecture, since it provides the data transmission range but consumes a great part of the emitter front-end power. In the following paragraph are presented the different PA operating classes, which determine the trade-off between power efficiency and linearity. Power amplifiers should be divided into two main families of subclasses as a continuous wave power amplifier, such as classes A, B and C, and switchmode power amplifiers, such as D, E and F.

2-1.1 Continuous wave power amplifier classes

In [13] the maximal power efficiency is formulated as the ratio between the emitted power and the delivered DC power (Eq. 14), where V_{DC} is the supply voltage and V_{OUT} is the output voltage. I_{DC} is given by Eq. 15 and I_1 is given by Eq. 16. α is the conduction angle, which determines the PA class.

- Class A PAs have a maximum efficiency equal to 50%, because the conduction angle is equal to 2π.
- Class B PA's maximum efficiency is given by $\pi/4$ = 78.5%, because the conduction angle $\alpha=\pi$.
- Class AB power amplifiers have a conduction angle α in the interval between π and 2π; hence its maximum efficiency is in the interval between 50% and $\pi/4$.
- Class C amplifiers have a conduction angle α smaller than π. The efficiency class C amplifier is more than $\pi/4$ according to conduction angle. Class C well-known modification is the Doherty amplifier which is composed of peaking amplifier and carried amplifier to enhance efficiency while keeping linearity.

$$\eta = \frac{P_{OUT}}{P_{DC}} = \frac{\frac{V_{OUT}}{\sqrt{2}} \cdot \frac{I_1}{\sqrt{2}}}{V_{DC} \cdot I_{DC}} \quad \text{Eq. 14}$$

$$I_{DC} = \frac{I_{MAX}}{2\pi} \frac{2\sin(\alpha/2) - \alpha\cos(\alpha/2)}{1-\cos(\alpha/2)} \quad \text{Eq. 15}$$

$$I_1 = \frac{I_{MAX}}{2\pi} \frac{\alpha - \sin(\alpha)}{1-\cos(\alpha/2)} \quad \text{Eq. 16}$$

For class A PAs, when a power back off is applied, the efficiency is given by Eq. 17, where IBO is the input back off defined as P_{1dB}-P_{IN} in dB. Because of the conduction angle, which is equal to 2π, the PA is active all the time ($I_{MAX}=V_{DC}/R$). Hence efficiency decreases linearly with IBO:

$$\eta(IBO) = IBO_{LIN} \cdot \eta_A \quad \text{Eq. 17}$$

For class B PAs, when power back off is applied, the efficiency is given by Eq. 18. The supply current, function on the conduction angle $\alpha=\pi$, is null half the time ($I_{MAX}=V_{OUT}/R$). Hence efficiency decreases as square root of IBO.

$$\eta(IBO) = \sqrt{IBO_{LIN}} \cdot \eta_B \qquad \text{Eq. 18}$$

Power efficiency from equations Eq. 17 (blue) and Eq. 18 (green) are drawn in Figure 15 for class A and class B power amplifiers. Class AB amplifier efficiency is between the blue and green curves depending on the conduction angle. Functions of the emitted signal dynamics, power back off highly reduces the power efficiency. For instance for an IBO of 3dB to 10dB the PA efficiency is reduced by 20% or 50%. This means that reducing IBO is the key objective within the linearization approaches.

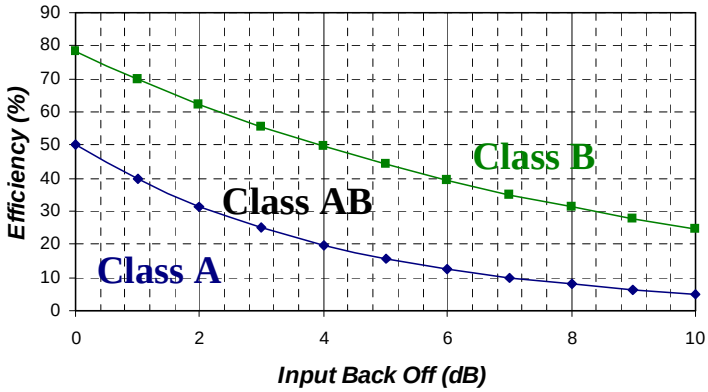

Figure 15 - power amplifier efficiency function of back-off

2-1.2 Switchmode power amplifier classes

Switchmode amplifiers, amplifier classes D, E and F, can theoretically reach 100% efficiency. Due to imperfections and on-chip parasitics, the efficiency falls towards 30-50% in measurement of designed power amplifiers. Switchmode power amplifiers are based on harmonic suppression. Thanks to Fourier transform the distorted signal can be decomposed into harmonics frequencies. Function of the non-fundamental harmonics filtering or suppression, the classes D, E and F are recognized.

- Structure of class D power amplifier is given in Figure 16. The fundamental harmonic is filtered from a rectangular signal. Class D power amplifiers suffer from important limitations such as needed output power and input signal frequency. The main problem of rising in frequency is mentioned in [16]. The input capacitance of transistors limits this power amplifier to lower frequencies. To reach the power specification, the current is difficult to deliver with 1V technology. A smart solution of cascode is proposed in [17]. Cascoded transistors allow using higher voltage to increase output power. Class D amplifier has an opportunity as a driver in combination with cascaded power amplifiers of different classes.

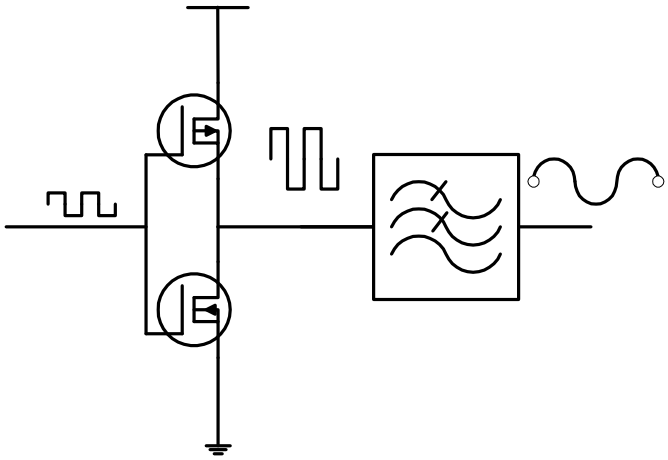

Figure 16 – Class D amplifier

- Class E power amplifier is based on principle of fundamental harmonics filtering by serial resonant circuit. The main problem of Class E power amplifiers is the quality factor of passive components. High quality factor passive components are in lumped version. With the integrated version it is difficult to reach the specifications. A method applying integration of lumped components is described in [16].

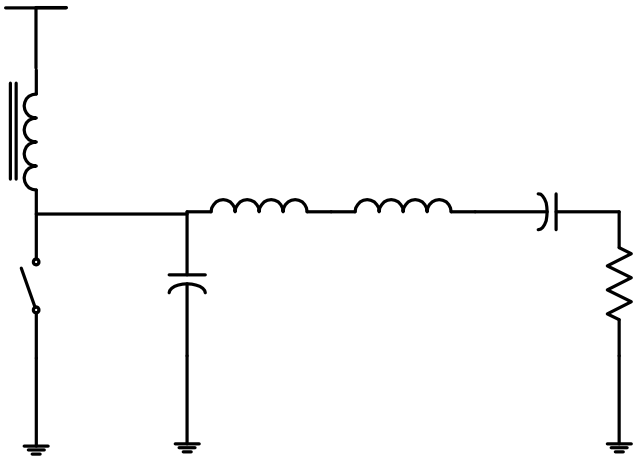

Figure 17 – Class E amplifier [18]

- Class F power amplifier is based on harmonics blocking by parallel resonant circuits. The article [53] shows class F power amplifier is integrated in technology of 180nm.

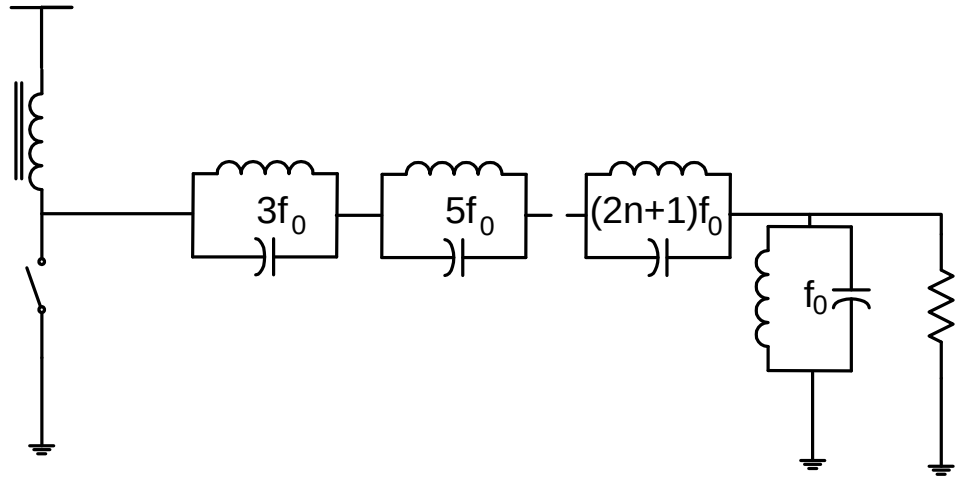

Figure 18 – Class F amplifier [18]

In the state of the art we can find cascaded power amplifiers of different classes. Figure 19 illustrates a combination of cascaded nonlinear devices can be described as a unique nonlinear device.

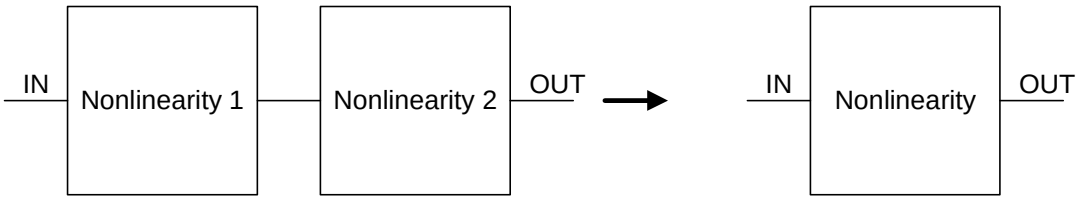

Figure 19 – transformation of combination of cascaded nonlinear devices illustration

The input signal to the first nonlinearity, where the nonlinearity function is given by Taylor expansion of a generic nonlinear function, in Eq. 19 is put into second nonlinearity Eq. 20 also given by Taylor expansion of a generic nonlinear function.

$$y = \sum_{i=0}^{\infty} a_i x^i \qquad \text{Eq. 19}$$

$$z = \sum_{n=0}^{\infty} b_n y^n \qquad \text{Eq. 20}$$

The output signal z=g(f(x)) is represent as a unique nonlinearity with coefficients of Taylor expansion of a generic nonlinear function given by Eq. 21. This property is valid for two cascaded nonlinearities in general.

$$z = \sum_{n=0}^{\infty} b_n \left(\sum_{i=0}^{\infty} a_i x^i \right)^n = \sum_{n=0}^{\infty} \sum_{i=0}^{\infty} b_n a_i^n x^{n+i} = \sum_{k=0}^{\infty} x^k \left(\sum_{l=0}^{\infty} b_l a_{k-l}^l \right) = \sum_{k=0}^{\infty} c_k x^k \qquad \text{Eq. 21}$$

2-1.3 Comparison of power amplifiers

Strongly nonlinear power amplifiers are defined in Table 3 as power amplifiers having a ripple in AM/AM conversion or power amplifiers similar to switches. Slightly nonlinear power amplifiers are defined in Table 3 as power amplifiers, where AM/AM conversion can be approximated by a monotonous function.

Slightly nonlinear power amplifiers	Strongly nonlinear power amplifiers
Class A, AB	Class AB, B, C, D, E, F

Table 3 - Power amplifiers classification

A consumption reduction technique for slightly nonlinear power amplifiers is based on efficiency enhancement. Strongly nonlinear amplifiers are efficient enough, but they need to enhance the linearity in order to meet EVM specifications of the transmitter.

2-2 Linearization Techniques

As illustrated in Figure 5, the goal of linearization techniques is to increase the operating zone within the AM/AM characteristics. The PA linearization techniques can be divided into analogue linearization techniques and digital baseband linearization techniques. An exhaustive summary of the analog methods might be found in [13]. Techniques such as polar loop, Cartesian loop, LINC, suffer from narrow linearization bandwidth. The feedforward technique needs two power amplifiers, where one needs to be linear to cancel the nonlinearity. EE&R and ET require a polar signal representation; hence a bandwidth limitation appears for wideband signals such as WiMAX [19]. As a result digital baseband predistortion is favored in [20] and [21] for its efficiency and stability. But for achieving a good precision throughout the linearization, adaptive algorithms are needed, based on the comparison of the signal before the PA and after the PA.

2-2.1 Analogue linearization techniques

A variety of analogue linearization techniques are based on non linear shaping or error suppression. Analogue linearization techniques can be applied on RF signal, IF signal or in the baseband. An important parameter is the bandwidth needed to keep the signal undistorted, or the bandwidth needed for signal transformation from quadrature into polar representation, which limit the linearizable signal bandwidth and data rate. Another important parameter is linearization complexity since software or hardware complexities can induce an extra consumption which is greater than the benefit of linearization on power amplifier. Some architecture suffers from additional issues, such as system stability. The last parameter is the performance or precision of the linearization technique.

2-2.1.1 Back-Off

Figure 20 shows the principle of power amplifier backing off. The mean power of distorted signal drawn as cyan color curve is lowered to the signal level drawn as magenta curve. As obvious from AM/AM conversion the area with signal dynamic range (pointers) is more linear than for cyan curve. As a drawback the power amplifier efficiency decreases with backing-off. The principle is to limit the signal to the linear portion of the nonlinear amplifier.

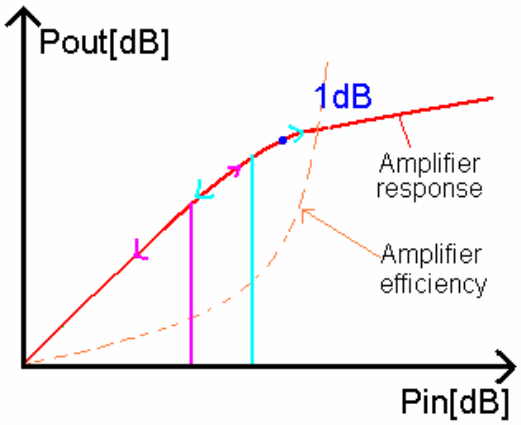

Figure 20 – Back-off principle

2-2.1.2 Feedback

Illustrated in Figure 21, the feedback principle is to suppress the distortions measured at the output of the power amplifier. Analogue feedback solutions such as Cartesian Feedback and Polar loops are described below.

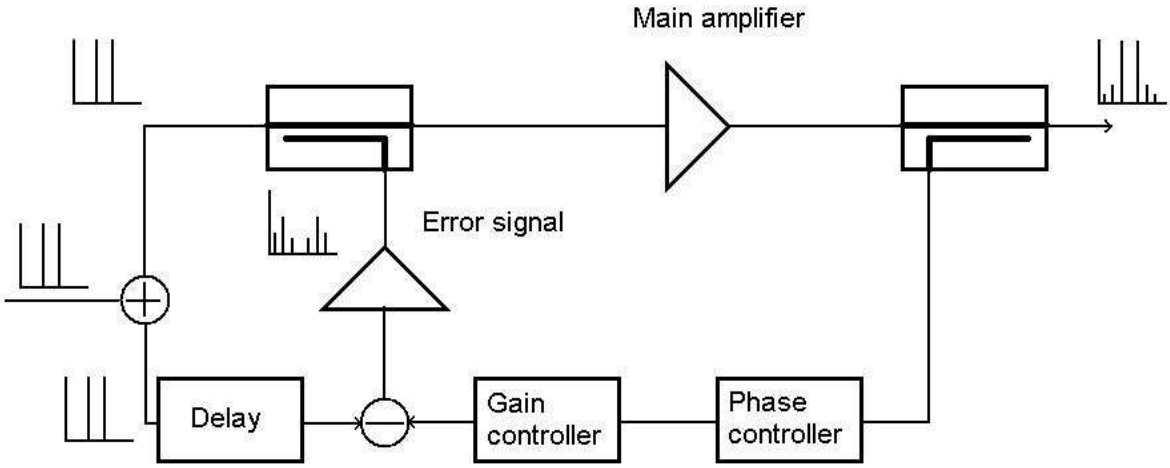

Figure 21 – Feedback techniques principle [13]

2-2.1.2.1 Cartesian Loop

The Cartesian feedback loop principle is depicted on Figure 22. The feedback signal is split into two branches in quadrature, and generates an error signal which is integrated by a loop filter to correct PA distortion.

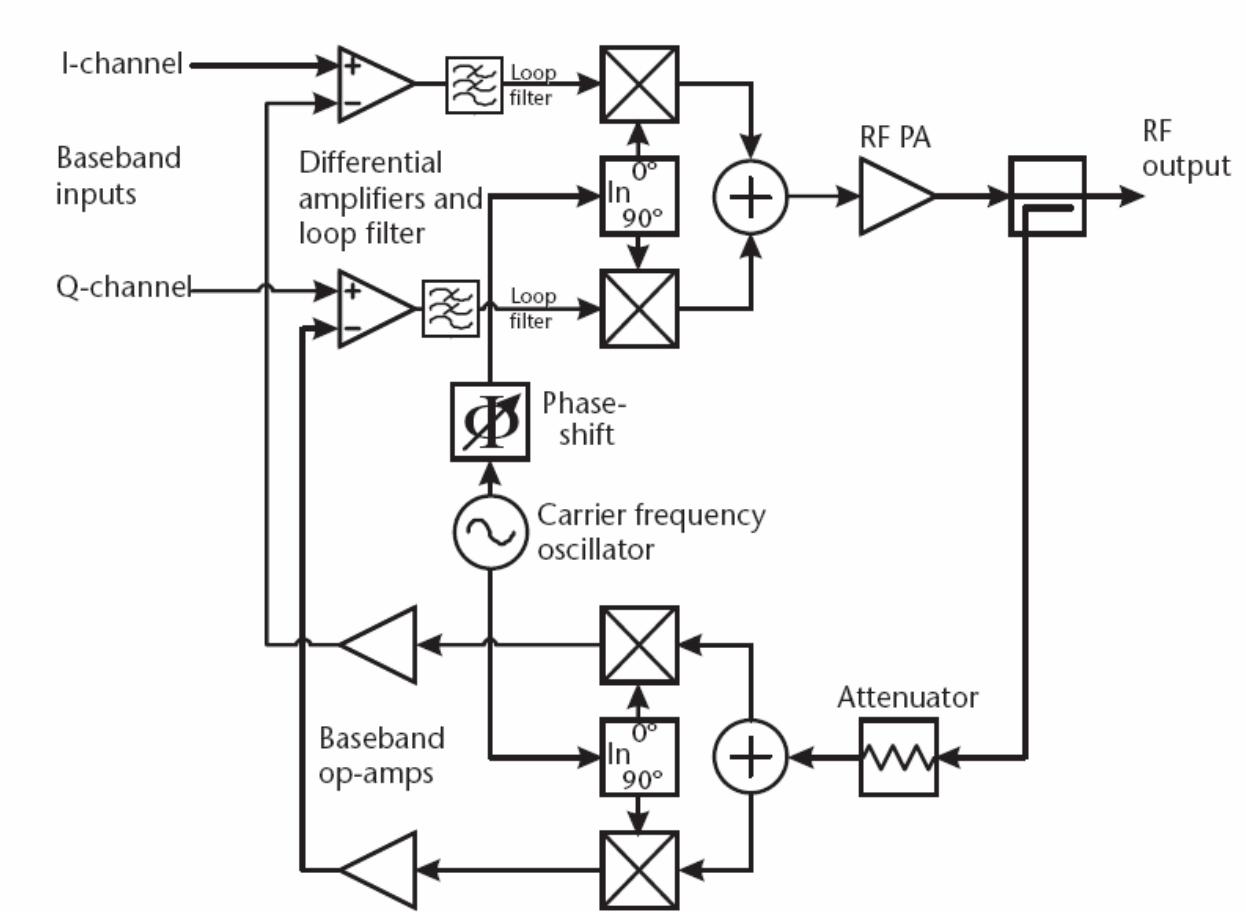

Figure 22 – Cartesian loop [13]

As an example of achievement, the article [22] implements a Cartesian feedback in the 800MHZ (TETRA) band. The measured RMS error vector is 8.99% for 800MHz, 9.55% for 806MHz, 3.81% for 815MHz and 4.01% for 824MHz with 10% specification limit.

In the article [23] the Cartesian feedback with a compact inverted Doherty amplifier has an ACLR of -51.1dBc.

Cartesian Loop works with signals I and Q. The spectrum is not enlarged with transformation to polar form. The major problem in Cartesian Loop is the management of the feedback delay and phase shift. When the antenna has a poor VSWR the loop might become instable. Like all feedback loops it achieves high power with low complexity but narrowband signal. According to [13] the Class-C amplifier should be used.

2-2.1.2.2 Polar Loop

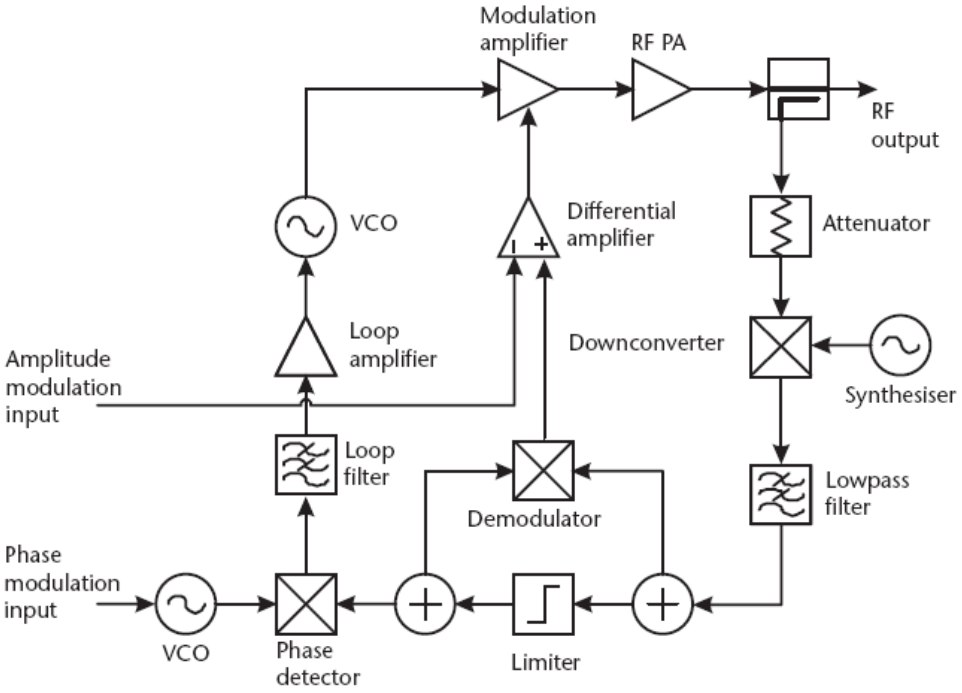

Figure 23 – Polar loop [13]

On Figure 23 is depicted the Polar loop scheme. The demodulator uses the feedback signal and input signal to detect the error signal. The error signal feeds modulation amplifier.

Nowadays the Polar Loop is mainly used in GSM/GPRS/EDGE applications [24],[25],[26] and [27] where the EVM_{RMS} is between 2.1% and 3.8%.

[24] Quad-Band GSM/GPRS/EDGE Polar Loop Transmitter	EVM 900MHz = 2.9% EVM 1800MHz = 3.8%	Modulation Spectrum 900MHz - -60dBc / -65dBc Modulation Spectrum 1800MHz - -60dBc/ -65dBc
[25] Optimized Closed Loop Polar GSM/GPRS/EDGE Transmitter	EVM 900MHz = 2.1%	Modulation Spectrum 900MHz - -59dBc / -69dBc
[26] Variable Gain Amplifier in Polar Loop Modulation Transmitter for EDGE	EVM 900MHz = 2.8% EVM 1900MHz= 3.4%	Modulation Spectrum 900MHz - -59.3dBc / -65.8dBc Modulation Spectrum 1900MHz - -60dBc/ -62.1dBc
[27] A Polar Loop Transmitter with Digital Interface including a Loop-Bandwidth Calibration System	EVM 900MHz = 3.1%	Modulation Spectrum 900MHz - -59dBc / -65dBc

Table 4 – Comparison of polar loop transmitters

Polar loop allows achieving linearization for high emitted power with low complexity, but the signal is narrowband only. The transformation from I and Q to polar enlarges the signal

bandwidth in the loop. The other problem is the feedback delay, which decreases the phase margin. According to [13] the Class-C amplifier should be used.

2-2.1.3 Linear Amplification with Nonlinear Components (LINC)

This architecture was invented by Cox in [28]. The principle of this technique is to perform linear amplification with nonlinear components. This technique is based on the cancellation the non linearities.

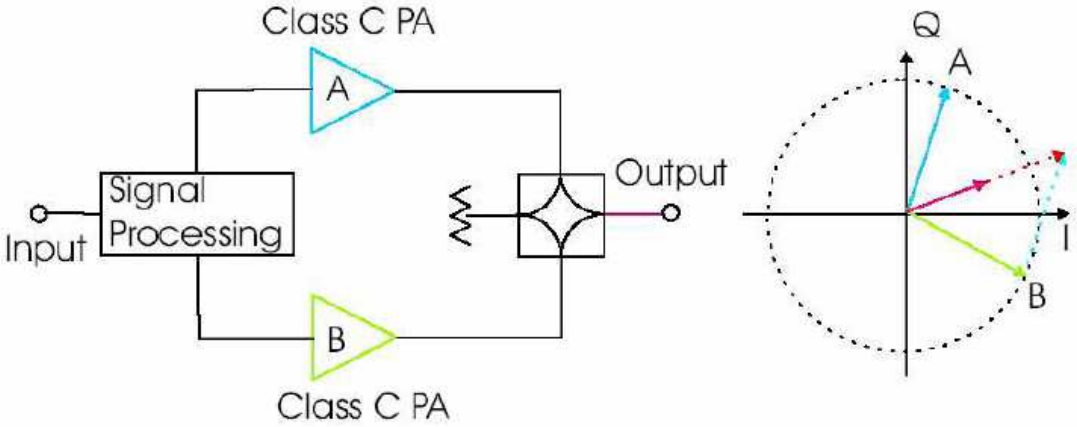

Figure 24 - LINC principle [10]

As we can see on Figure 24 the signal is split into two constant envelop signals which are amplified by identical power amplifiers. This technique could theoretically reach 100% efficiency but requires a complex computation to split the signal. Mathematical principle is well described in [13]. If the input signal in quadrature form is:

$$s(t) = s_I(t) + js_Q(t) \quad \text{Eq. 22}$$

The two constant envelop signals obtained from the LINC computation are:

$$s_1(t) = s(t) + e(t) \quad \text{Eq. 23}$$

$$s_2(t) = s(t) - e(t) \quad \text{Eq. 24}$$

Where e(t) is:

$$e(t) = -s_Q(t)\sqrt{\frac{1}{\left(s_I^2(t)+s_Q^2(t)\right)}-1} + js_I(t)\sqrt{\frac{1}{\left(s_I^2(t)+s_Q^2(t)\right)}-1} \quad \text{Eq. 25}$$

In the article [29] the LINC technique is used. Two different cases for ρ normalized threshold driving the power amplifier performances, see Table 5 for more info, were described, MM-LINC ρ=0.4 and LINC ρ=1. MM-LINC technique gives a best trade-off between efficiency and EVM. In the Table 4 we can see that EVM for LINC was 2.5% and for MM-LINC 8% for 1.7GHz WiMAX.

	ρ	EVM[%]	PAE[%]	P_{OUT}[dBm]
Balanced Class B	0	14	26	32
MM-LINC	0,4	8	21	33,4
LINC	1	2,5	6	31,5

Table 5 - 3 amplifiers from [29]

In the second article [30] we can find a 64-QAM LINC transmitter for 802.11. In the first part the signal is recombined in baseband. The EVM was -37.6dB (1.32%). In the second part, the signal was firstly upconverted and after combined by Wilkinson power combiner, EVM was -34dB (1.97%). This architecture dissipates 18mA with 2.5V supply.

According to book [13] this architecture allows the use of high distorting PA's. The implementation is easy, but the component bandwidth has to be very large [19], 10x more than channel bandwidth. The two amplifiers have to be almost identical. Also, the correction of the amplitude distortion can introduce a phase distortion. A method used in [31], [32] (which study different combiners for LINC architecture) combines the LINC architecture and phase-only predistortion.

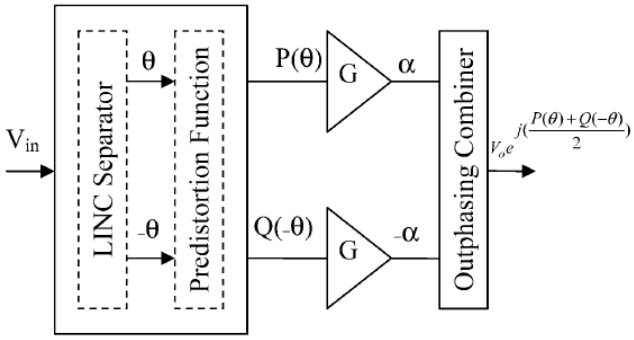

Figure 25 - Chireix-outphasing system with predistortion functions [31]

Figure 25 shows the predistortion scheme used in [10]. The input signal is separated for LINC and after predistorted with two proposed methods. The first one, constant phase-imbalance predistortion and the second one is variable phase predistortion. Both methods can lower the signal spectrum distortions by 40dB.

Combining phase only predistortion with LINC architecture is a smart approach. LINC corrects for amplitude and phase through linearization of the transmitter phase; hence the complexity needed for linearization is lower than for amplitude and phase predistortion.

An interesting architecture using modified LINC is used in the article [33]. The LINC signals S1 and S2 are transmitted separately and its combination occurs on receiver antenna. Figure 26 shows the architecture scheme.

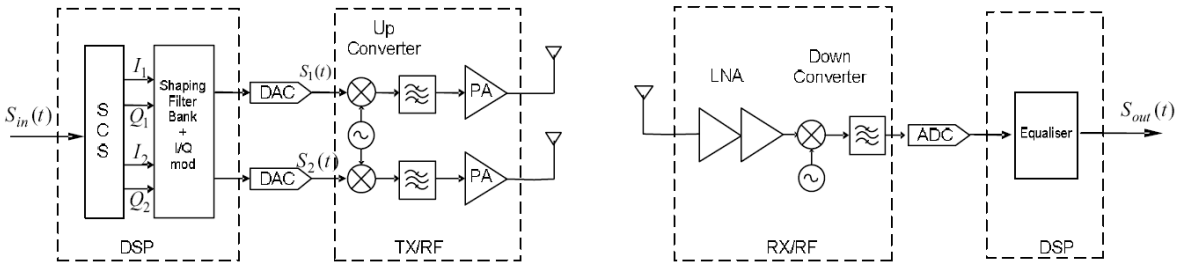

Figure 26 - Modified LINC architecture [33]

This architecture improves PAE from 1.43% for normal power amplifier to 16.3% for modified LINC architecture and having EVM 1.86%, which is lower than 802.11g specification 5.6%.

The second LINC architecture is marked in the article [34]. This architecture consists of LINC with bias control, shown on Figure 27.

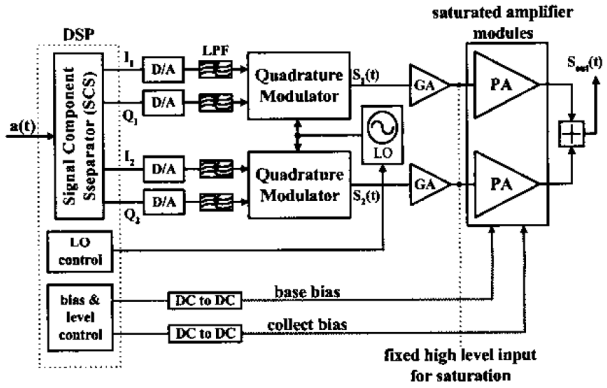

Figure 27 - LINC Amplifier with Bias Control [34]

The efficiency of this architecture is 24.75% @30dBm POUT, 17.9% @16dBm POUT and 11.5% @0dBm POUT. The ACPR is -52.8 @ 885 kHz offset for all the range from 16dBm to 30dBm POUT. The frequency band is 1.71GHz.

In the article [35] an outphasing power amplifier is proposed for WCDMA. This architecture is designed for base stations. In the baseband part, four direct digital synthesizers (DDS) are used. The signal is upconverted in the analog domain. The gain between non-predistorted and predistorted signal, when the branches were adjusted, was 5dB. This architecture shows that the DDS should be intricately envisaged in low-power radio architecture.

Figure 28, from the article [36], shows the All-digital radio transmitter architecture

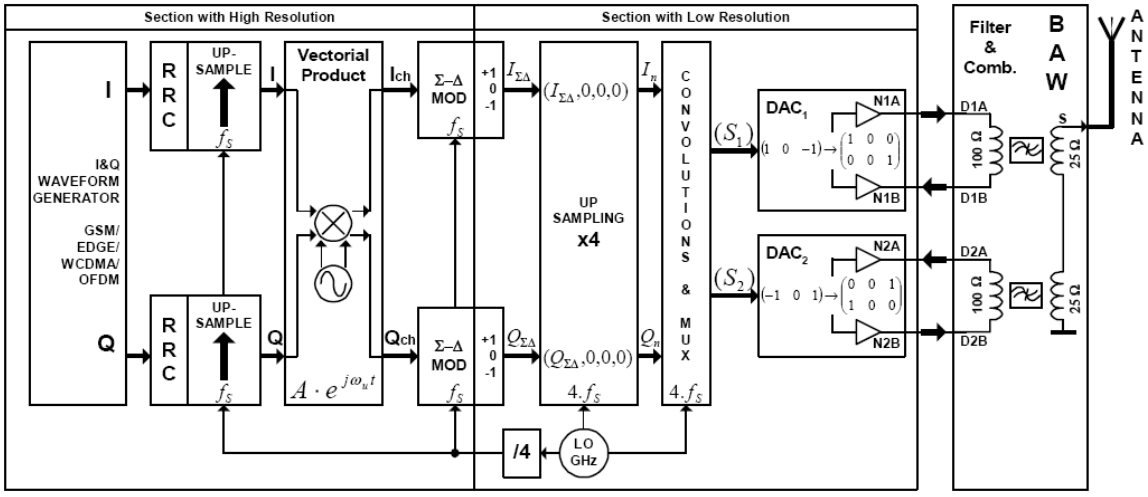

Figure 28 - All-digital radio transmitter architecture based on sigma delta modulation [36]

This opportunistic radio architecture has been tested with WCDMA signal with EVM_{RMS}=2.45% and $EVM_{PEAKtoPEAK}$=6.39%.

The input signal is shaped if necessary, after the signal is upconverted, and modulated by sigma-delta modulator with 3 stages. The signal is upsampled. ADPLL is envisaged as a local

oscillator at frequencies from 4GHz up to 8GHz. Finally the signal is convoluted and filtered by BAW-CRF filters. This solution doesn't contain a power amplifier.

2-2.1.4 ET&EER

The polar RF synthesis is known as EE&R envelope elimination and restoration technique. The scheme of polar RF synthesizer is on Figure 29. The signal is divided into two parts: amplitude part and constant envelop phase part. Polar signal representation needs more bandwidth than I and Q signal representation to reach the same linearity requirements. The signal is combined in power amplifier afterwards.

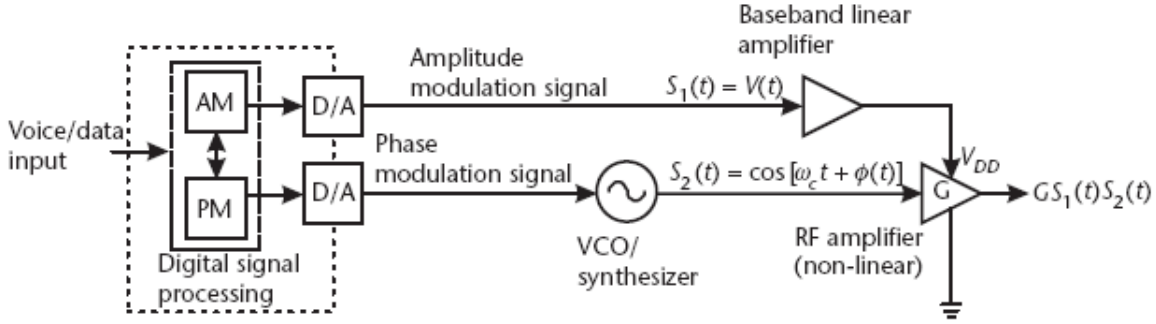

Figure 29 - Envelope restoration transmitter [13]

One solution with EVM = 1.2% for GSM is on Figure 30 from the article [37]. The GSM EVM specification limit is 9%.

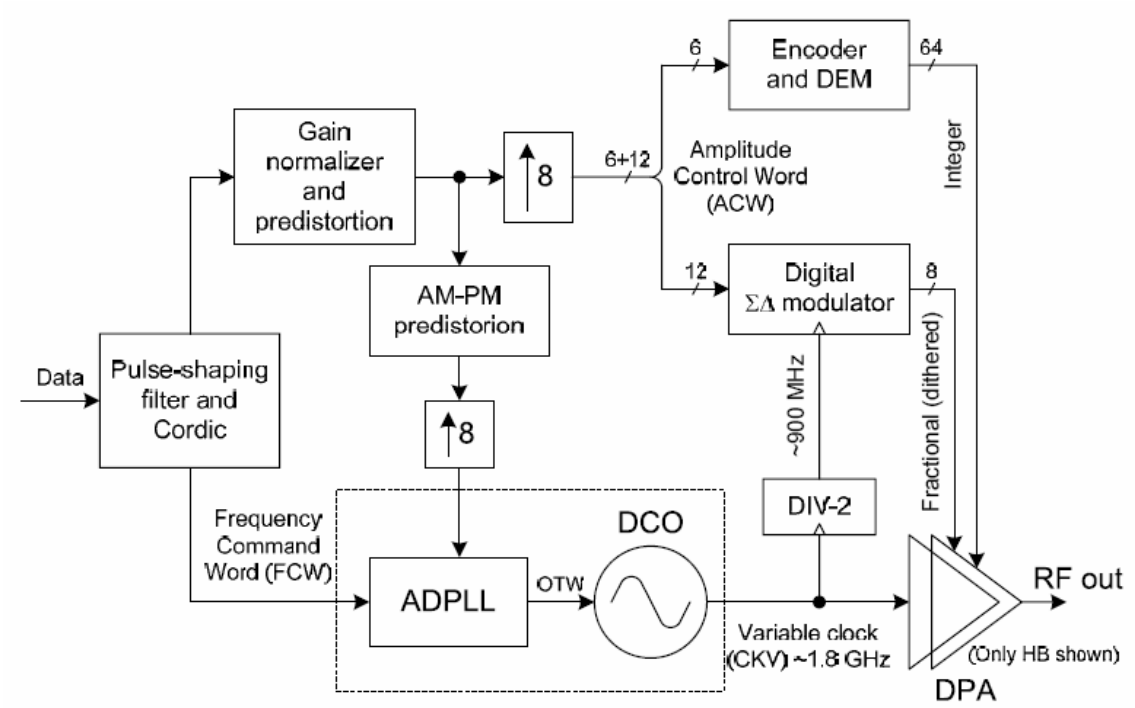

Figure 30 - Amplitude modulation path of polar transmitter [37]

The second usage of Polar Loop transmitters is in ultra wideband OFDM. In the article [38] an array of amplifier is used in polar transmitter, see Figure 31.

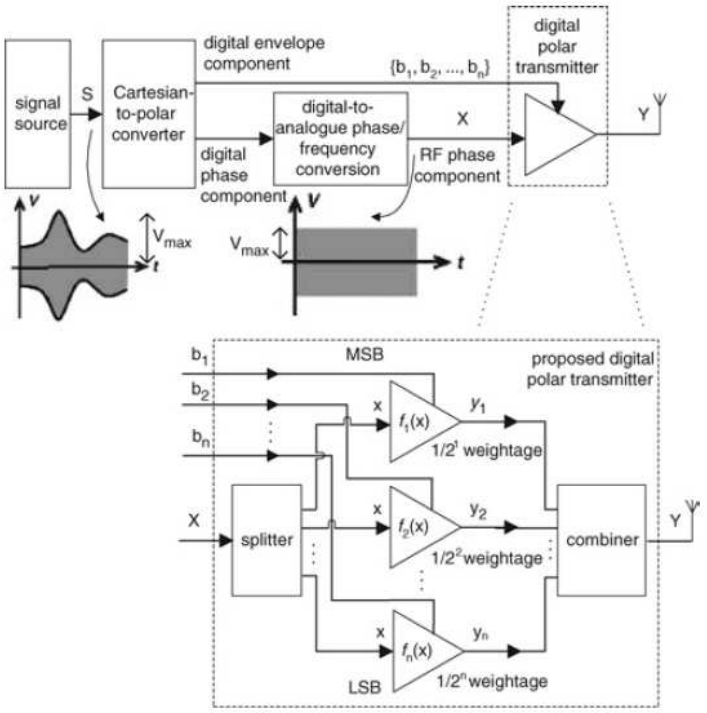

Figure 31 - Polar transmitter used in [38]

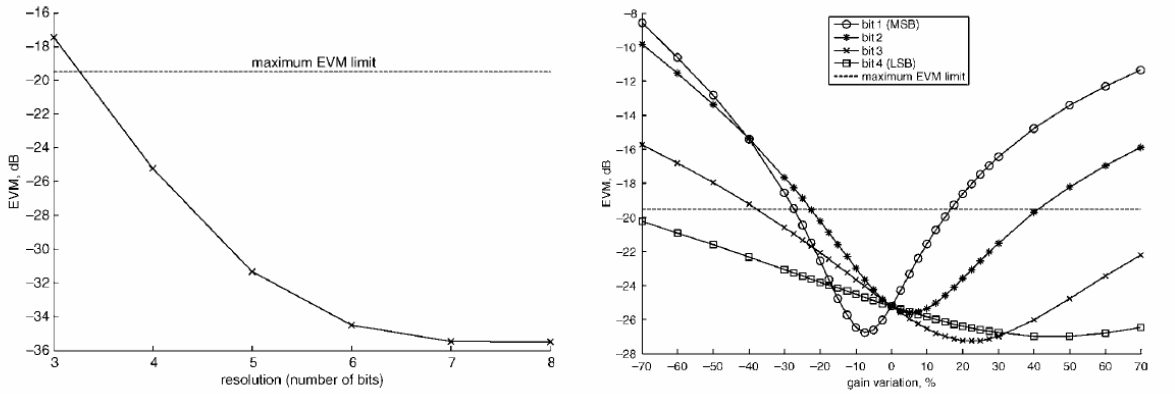

Figure 32 - a) EVM on number of parallel amplifiers b) EVM on gain variation [38]

On Figure 32 a) there are the EVM dependencies on the number of parallel amplifiers and on Figure 32 b) there are EVM dependencies on gain variation for each parallel amplifier.

In the article [39] a hybrid Polar transmitter is proposed for CDMA2000.

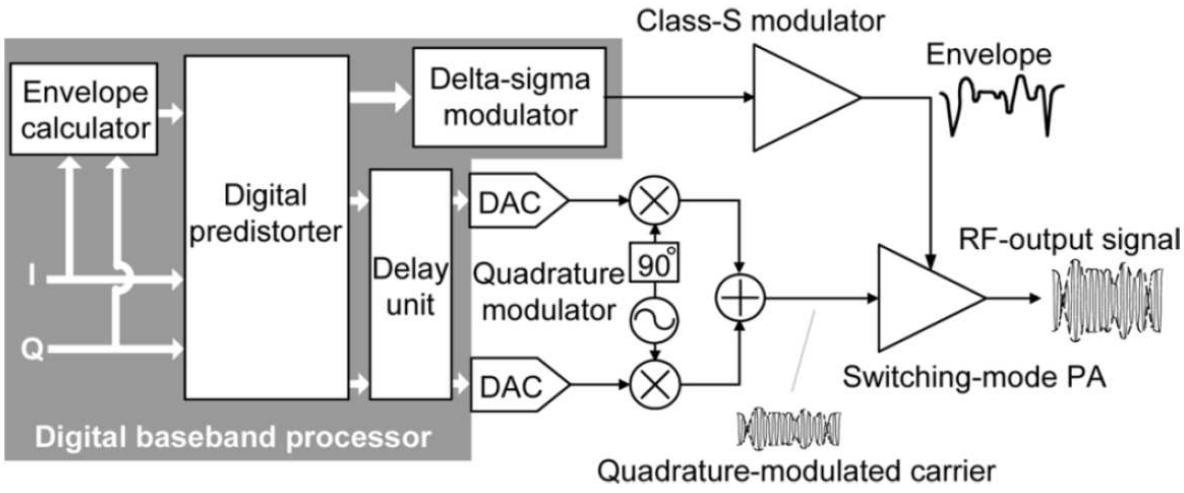

Figure 33 - Block diagram of the HQPM-based transmitter [39]

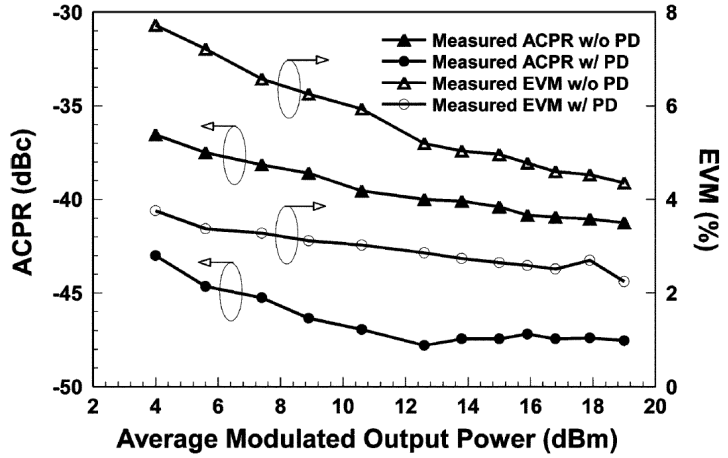

Figure 34 - Comparison of measured ACPRs and EVMs for HQPM-based transmitter with and without predistortion [39]

The HQPM-based transmitter has EVM from 2% up to 4% for predistorted signal and from 4% up to 8% for signal without predistortion. The EVM improvement is from 2% up to 4% and PAE varies from 18% to 35% for 4-19dBm output power.

Suite to [13] the advantage of this architecture is that the strong nonlinear amplifiers should be used. This architecture contains the same problem of signal transformation from Cartesian form to polar form, i.e. that the bandwidth of components has to be enlarged.

2-2.1.5 Analogue predistortion

In the article [40] we can find a system architecture with analogue predistortion for CDMA, Figure 35. The signal is taken before PA and after PA by directional coupler. The control circuit adapts the analogue predistorter using the error signal processed from two signals before and after PA. The signal vector error was 4.4% for linearized system and 8.2% for unlinearized system; therefore the improvement was 46%. Efficiency increased from 22% unlinearized to 29% linearized.

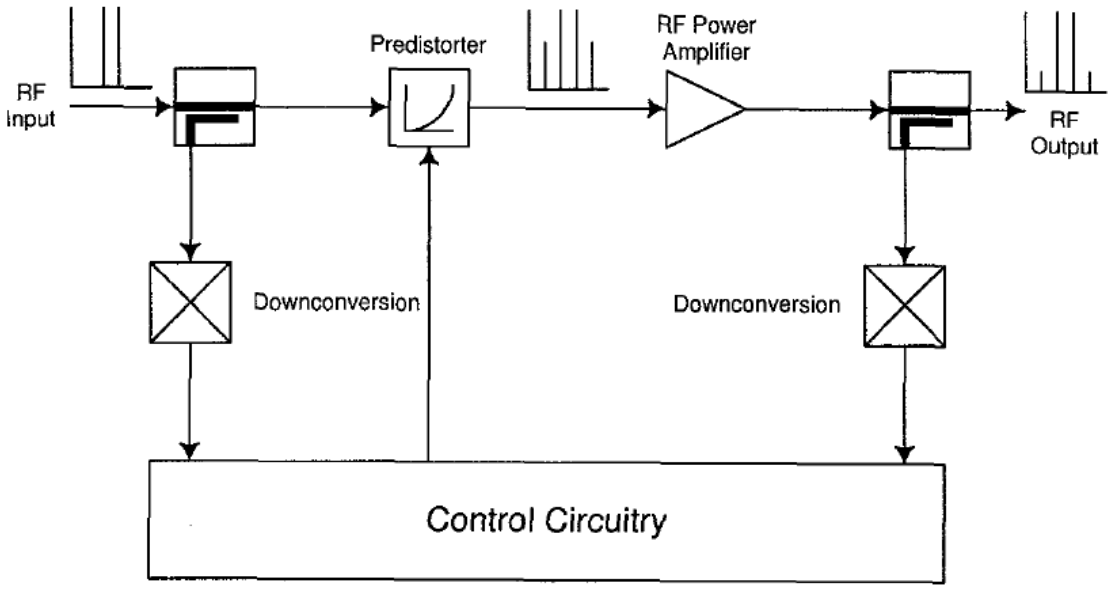

Figure 35 - Basic outline of an RF predistortion system [40]

2-2.1.6 Feedforward

Figure 36 shows the schematic of feed-forward architecture used in compensation of base stations [41]. This technique theoretically cancels all distortions. The main drawback of feedforward technique is the necessity of two power amplifiers. The error amplifier needs to be linear in order that the error signal stays undistorted.

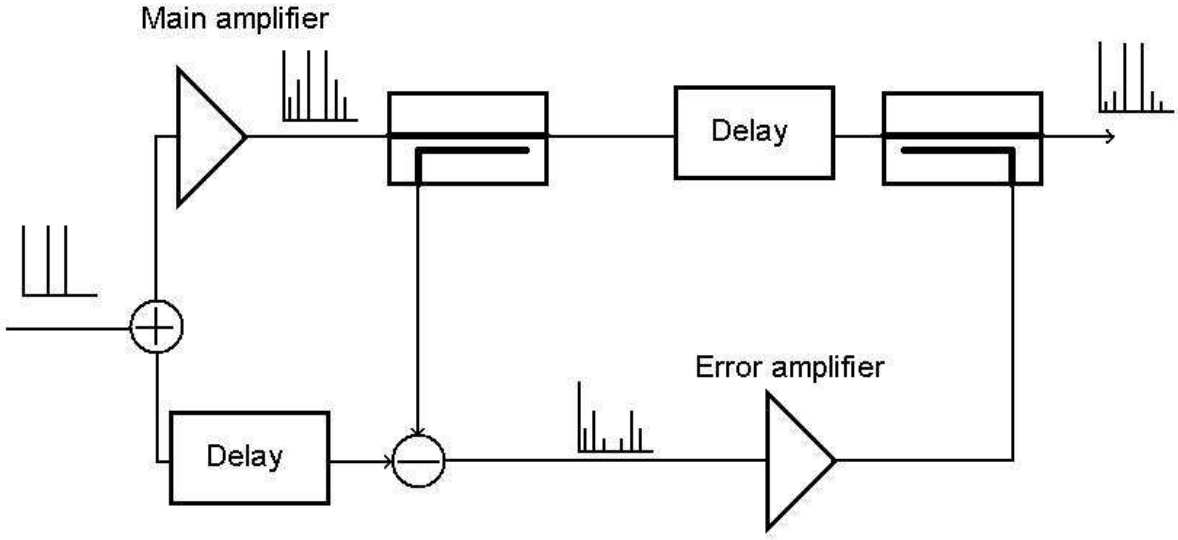

Figure 36 - Feedforward linearization technique [13]

2-2.1.7 Summary on analogue linearization techniques

As a conclusion the analogue linearization techniques suffer from deep limitations summarized in Table 6.

Architecture \ Parameter	Power efficiency	Linearization bandwidth	Stability	SW & HW complexity
Back off	-	+	+	+
Cartesian Loop	+	-	-	0
Polar loop	+	-	0	0
LINC	+	-	0	-
ET&EER	+	-	0	0
Analogue predistortion	0	+	+	-
Feedforward	-	+	0	-

Table 6 - Analogue linearization techniques summary

The techniques such as polar loop, Cartesian loop, LINC, suffer from narrow linearization bandwidth. Feedforward technique needs two power amplifiers, where one needs to be linear to cancel the nonlinearity. EE&R and ET require a polar signal representation; hence the bandwidth limitation appears for wideband signals such as WiMAX. A power backoff applied to PA is rather inefficient and there is big heat dissipation. Analogue RF predistortion needs to be complex to compensate precisely for the PA nonlinearities. Alternatively digital predistortion brings an interesting alternative.

2-2.2 Digital compensation

Digital baseband predistortion and postcompensation techniques are favored for their efficiency and stability. In the state of the art the compensation is applied in transmitters as predistortion or post compensation in the receivers. The digital approach is favored for its stability and reconfigurability. The computation part is done in Field Programmable Gate Array (FPGA) or Digital Signal Processors (DSP). Naturally integration is possible in Application Specific Integrated Circuit (ASIC). In [45] there is a complete predistortion methodology summary. According to [45] the compensation can be performed in two domains. The first one is the compensation in data subspace, which consists of compensating the constellation diagram. This compensation is allegedly [45] not able to eliminate adjacent channel spectral regrowth. A second set of methods consist of compensating the nonlinearity in the signal subspace. These methods are modulation independent, but slower than compensation in data subspace.

[45] divides the nonlinearity compensation into two other cases. The first case of compensation uses Look Up Tables. These LUTs are realized by memories, which have usually lower power consumption than signal processing units. The second case of compensation uses parametrical functions to process the signal in order to compensate for the PA nonlinearities.

2-2.2.1 Model-based estimation of nonlinearity

Mathematical properties of approximation functions open choices in estimation strategies. A first approach is to estimate first a nonlinearity model and then apply the inversed model function as predistortion. A special property of Lagrange polynomials allows the direct inversion of the estimated polynomial model.

2-2.2.1.1 Model estimation, inversion and application

Widely used numerical method of least squares (LS) is used in [46] for the estimation of polynomial models and in [47] for augmented Hammerstein models. [51] and [47] present a method of model estimation. The model is estimated and inversed though the flowchart in Figure 37. A WCDMA power amplifier is firstly measured and the measurement is treated for estimate an augmented wiener model using recursive Least Square. It is illustrated as forward modeling step from Figure 37 from [51]. The inverse model is estimated in the reverse modeling step. The inverse model has the form of an augmented Hammerstein nonlinearity model. Finally the augmented Hammerstein model is applied on signal.

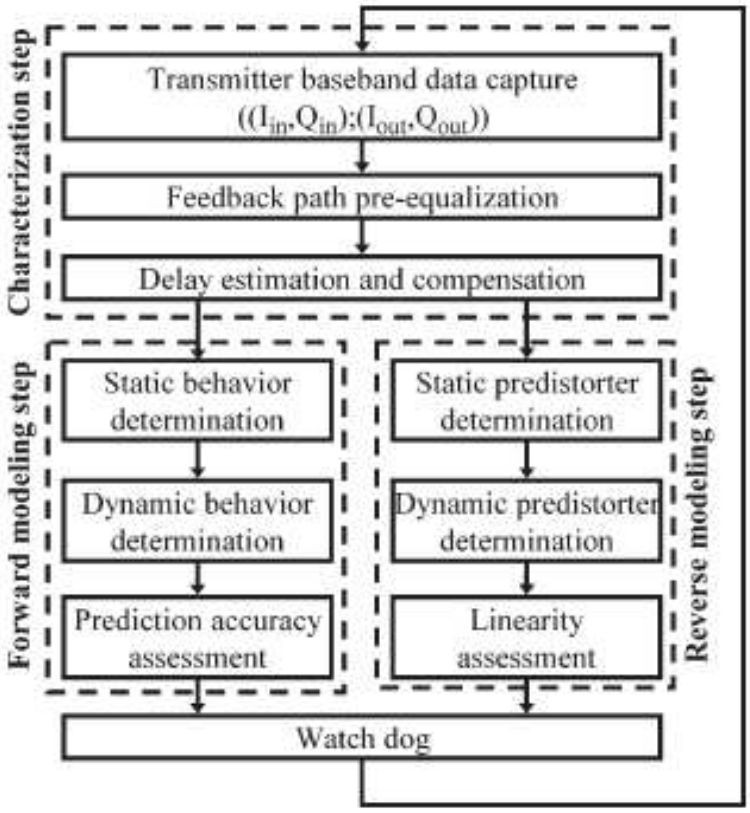

Figure 37 – Flowchart of nonlinear model estimation [51]

In the article [42] a robust memory polynomial model is developed. As each power amplifier has a really different characteristic, therefore the necessity of having a universal model. The universality is being done by indirect learning architecture, show on Figure 38.

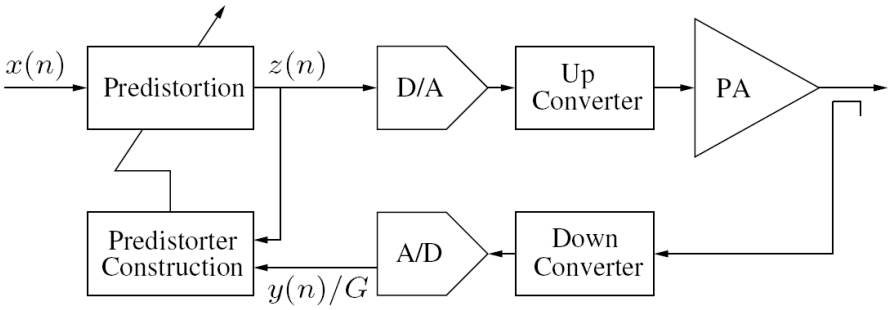

Figure 38 - Predistortion system diagram - indirect learning architecture [44]

Many models can be implemented in a predistorter, as shown on Figure 39. All the implemented models are special cases of polynomial Volterra models. Hammerstein model and Wiener model are two-box models with static nonlinearity and dynamic linearity. The parallel Wiener model takes single branch wiener models and parallelizes them. The Volterra model of causal systems with finite memory can be modeled by parallel Wiener models. The most general model is the Volterra model, where the linear filter is multidimensional for each branch, the nonlinearity can not be separated. This model has the highest complexity.

The polynomial functions are projected into orthogonal polynomial functions. Model parameters are found numerically by LS method from measured samples.

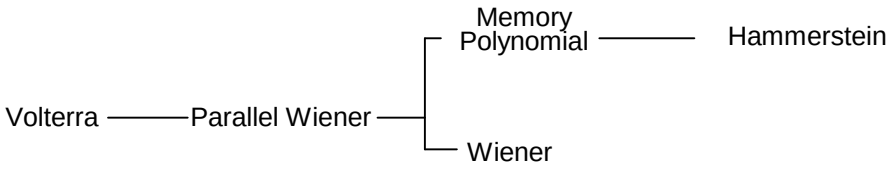

Figure 39 - Relation between nonlinear models with memory [42]

The predistortion implementation can be found in the patent [43]. This implementation is applied to baseband signals as a complex multiplication. The method is based on coefficient memory address calculation, allowing the compensation of AM/AM and AM/PM distortion.

If the nonlinearity is strong, piecewise predistortion can be used to split the PA behavior into pieces of models as in [49] for satellite communication in L-band.

2-2.2.1.2 Direct inversion of the estimation function

Articles [50] and [52] use the special property of Lagrange polynomial function construction. Lagrange polynomial interpolation is given by Eq. 2.

$$L_{\text{Lagrange}}\{a,b\}(x) = \sum_{i=1}^{L} a_i \prod_{k\neq i}^{L} \frac{x-b_k}{b_i-b_k} \qquad \text{Eq. 26}$$

Lagrange polynomial is used to interpolate the points {ai,bi} of a given function. As a result, the Lagrange interpolation of the points {bi,ai} gives an approximation of the corresponding inverse function.

The estimated inverse function is given by using inverse Lagrange polynomial interpolation Eq. 27.

$$|w(t)| = L\{b,a\}(|y(t)|) \qquad \text{Eq. 27}$$

Where w(t) is AM/AM distortion corrected signal. The advantage of direct estimation of nonlinear function is that it lowers the complexity on the model inversion.

An example using direct inverse function estimation is given by digital baseband post compensation architecture for 60GHz systems with 16QAM OFDM modulation [50].

2-2.2.2 Algorithm adaptation

A great property of all digital compensation methods is reconfigurability. Adaptive predistortion needs to add a feedback path after the PA to adjust the predistortion function. Despite the good precision and stability in its loop, the predistortion architecture suffers from the hardware implementation of the analog feedback (down-conversion mixer and ADC). Indeed this feedback loop requires usually three to five times the channel signal bandwidth to deal with the out of band nonlinearities. Nowadays the extra consumption of the feedback path (ADC) makes the digital predistortion only suitable for high power PA in base stations or relay stations.

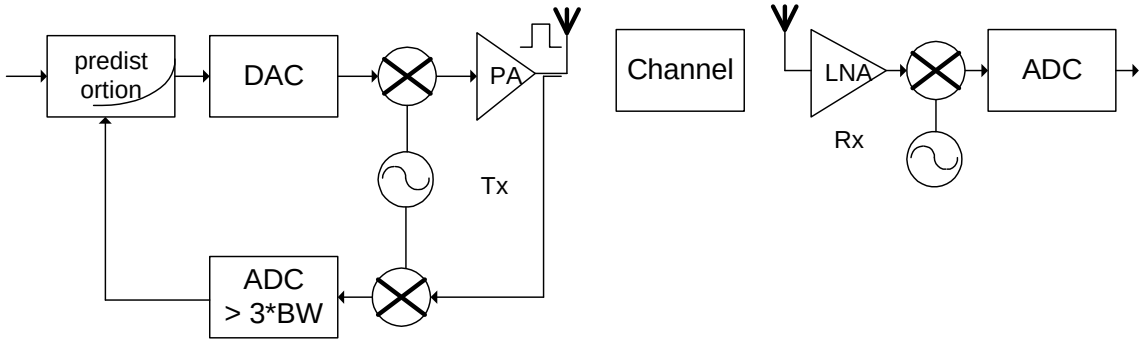

Figure 40 – Generic adaptative predistortion schematic

Kusonoki in [48] presents a solution for cellular PA in band 832-870 MHz, i.e. a replacement of a broadband ADC in the feedback path by a simple diode to detect the signal power. PAE is then improved by about 48% in comparison with conventional PAs. However this broadband ADCfree feedback path still needs two DA converters and one ADC to pilot analogue phase shifter and analogue gain controlling blocks. This architecture demands to change a PA block in each already installed network operator's base station.

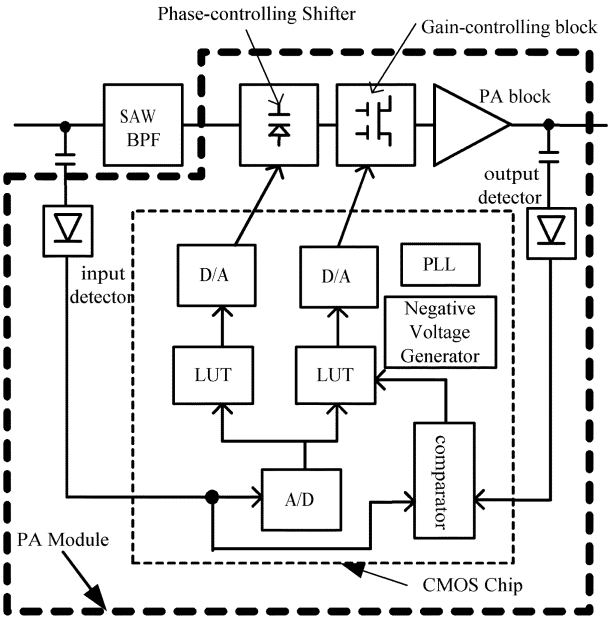

Figure 41 – PA module with adaptative predistortion [48]

Instead of classical adaptive pre-distortion technique (Figure 40) which requires wideband feedback loop and A/D conversion, an adaptive post-distortion is depicted on Figure 42, based on the compensation of the nonlinearity at the receiver side. This scheme is relevant for the uplink transmission from mobile stations, because the extra computations are being done in the receiver base stations. No hardware changes in the RF front-end of the network operator's base stations are needed.

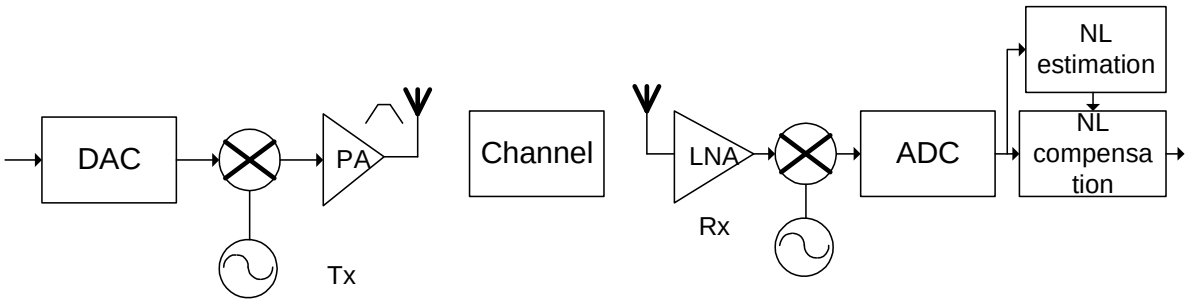

Figure 42 – Adaptative Receiver Aided Postcompensation

The estimation of the nonlinearity is carried out thanks to the use of training sequence, as channel estimation process. Figure 43 shows the flowchart of channel and nonlinearity estimation. The first training sequence q_1 with low PAPR is used for channel estimation while the second training sequence q_2 with high PAPR is used for PA nonlinearity estimation. The equalization and nonlinearity estimation are applied before decision.

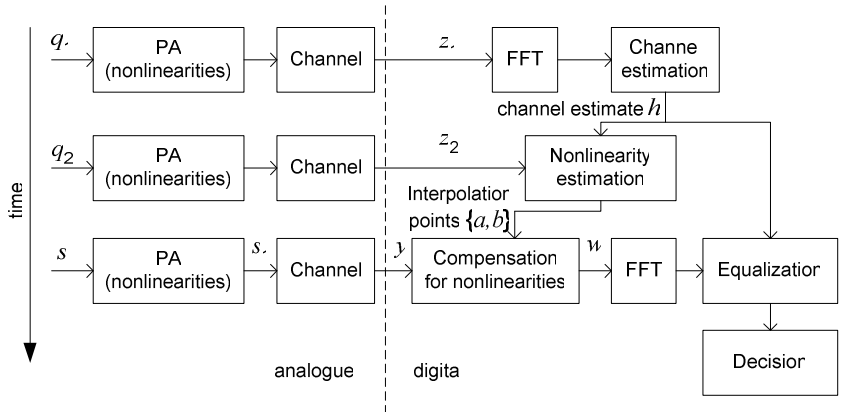

Figure 43 - Strategy for the estimation and compensation of nonlinearities in the receiver of an OFDM system [50]

Figure 44 shows the results of the post compensation. MSE and BER of the compensated signal reach the properties of a linear signal. The post compensation does not need any supplementary hardware implementation into base or mobile stations. The drawback of this architecture is that the PA is not compensated before emission; hence the spectral mask specification reaching might be tricky.

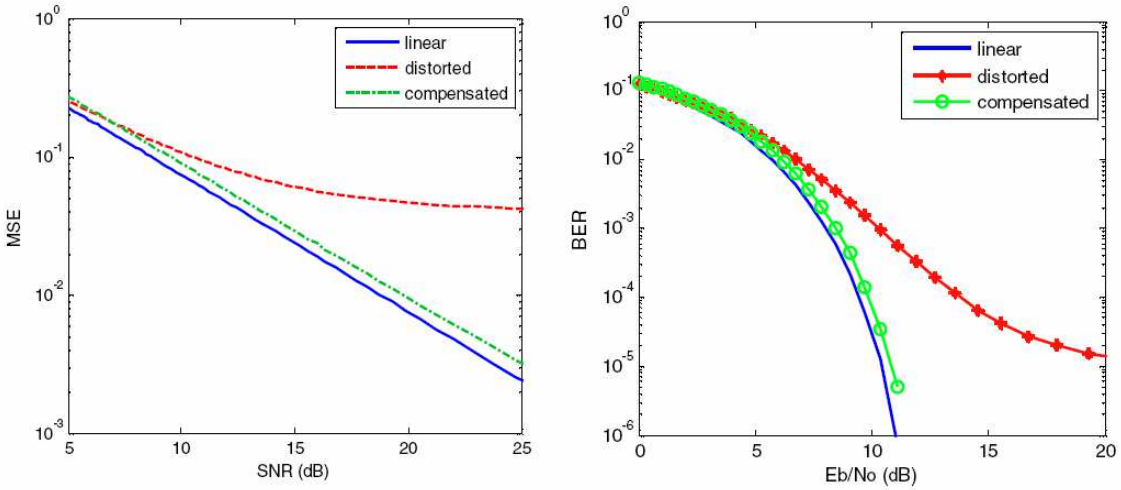

Figure 44 – a) Mean square error /SNR b) BER/ Eb/No [50]

2-2.3 Conclusion on linearization techniques and perspectives

Analogue linearization techniques are not always suitable for wideband signals such as WiMAX or 3GPP LTE. They are suffering either from narrow linearization bandwidth or efficiency. Digital linearization techniques have better wide-band linearization ability. Digital adaptive predistortion with feedback loop is favored for its robustness. The emitted signal is compensated before being emitted. However its drawback is the feedback loop broadband ADC drawn on Figure 40. This broadband ADC might consume more than the PA power gained thanks to the predestortion.

A light architecture from Figure 42 with nonlinearity compensation in receiver does not add any extra hardware. So it does not suffer from broadband ADC extra consumption. The

drawback of this architecture is that the power amplifier nonlinearities are not compensated before the distorted signal is being emitted, which can raise the problem of spectrum mask limitation.

Hence we propose in Figure 45 an architecture combining the advantages of both post-compensation and predistortion approaches. Here the nonlinearity is estimated at the receiver side, nonlinearity parameters are fed back in the protocol layers, and predistortion is carried out with those parameters at the emitter side. Then no over consuming broadband ADC or additional hardware is required by the feedback loops. Thanks to software feedback the predistortion algorithm is regularly refreshed.

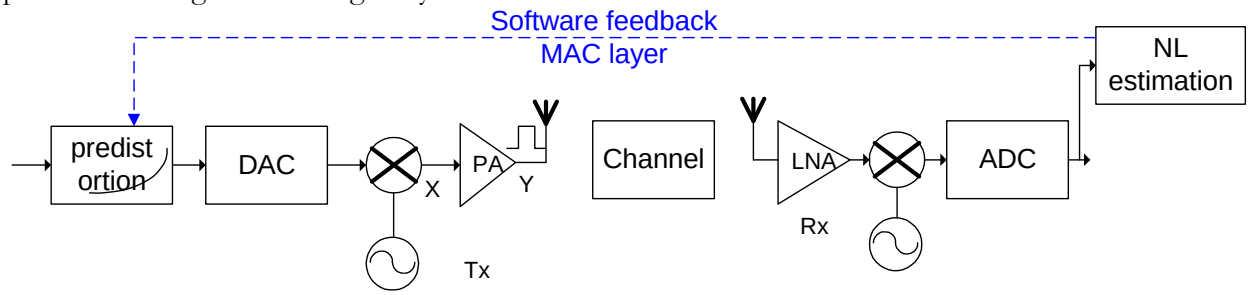

Figure 45 – Suggested architecture with software feedback

Chapter 3 : PA non-linearity modeling and model parameter estimation

3-1 Power Amplifier Models

Power amplifier effects on the signal can be seen as a tricky combination of nonlinear distortion and memory effects [54]. Indeed Figure 46 shows the power amplifier nonlinearity deployment. Amplitude function of amplitude (AM/AM) distortions is subset of memoryless nonlinear systems while phase function of amplitude (AM/PM) distortions and memory effects belong to nonlinear systems with memory. Memory in circuits is caused by energy storing elements such as inductance and capacitance in matching networks and other parts of circuits. The amounts of each kind of distortion vary from one power amplifier to another, depending on its structure and environment. As a result the behavioral model of a power amplifier has to be adapted to a particular amplifier.

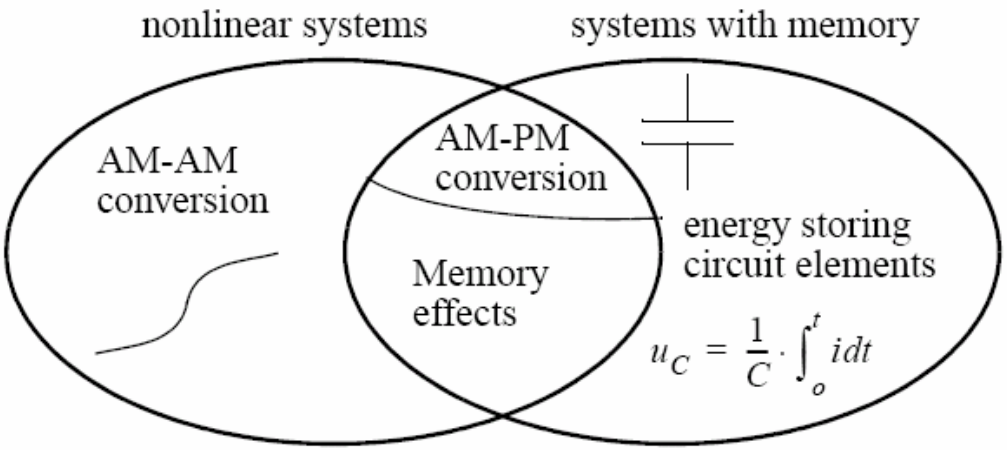

Figure 46 – Power amplifier nonlinearity deployment [54]

3-1.1 PA models

An exhaustive summary of power amplifiers is described in [55]. Figure 5 shows a power amplifier's AM/AM distortion relevant of many PA's behavior. The AM/AM characteristics can be split into three operating zones:

- the linear zone where linearization is useless (linearized PA (green) curve and PA's AM/AM conversion is superposed)
- the saturation zone where linearization is impossible
- the nonlinear zone where linearization is possible

This zone can be linearized partially or entirely depending on the application and trade-off between the model accuracy, model fitting and model complexity. Hence the models can be divided into high complexity models families, which are able to compensate all linearized zone, or low complexity models which are able to compensate only a part of linearized zone. The complexity is directly related to baseband consumption unit. For having positive consumption

budget the trade-off between model accuracy, model fitting and hardware complexity has to be carried out.

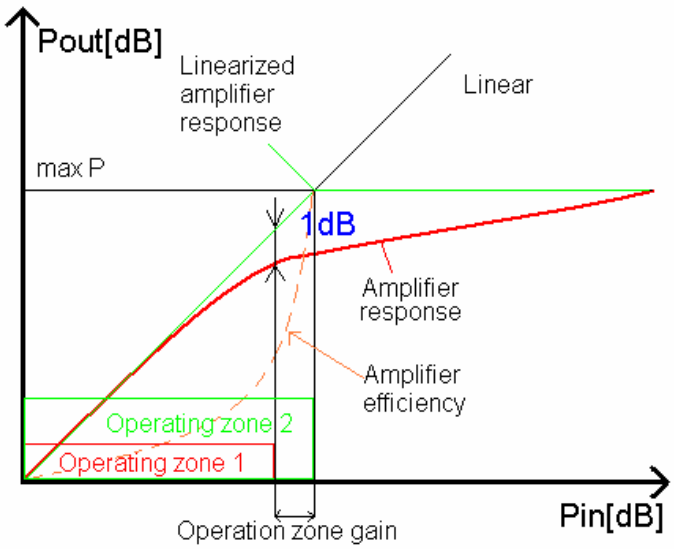

Figure 47 –Nonlinear power amplifier AM/AM conversion

3-1.1.1 High complexity models

High complexity models are theoretically able to handle for all kind of nonlinearities including AM/AM distortions, AM/PM distortions and memory effects. If those models are exhaustive, their complexity of formulation is not suitable for estimation or compensation of nonlinearities in the linearization of power amplifiers in mobile stations. However the models presented below helps understanding the behavior of active components.

3-1.1.1.1 Volterra model

The Volterra model describes nonlinearities with infinite memory through non-recursive polynomial models [3]. In [56], the Volterra model for a discrete system is given by Eq. 28 where the Volterra kernels h might be interpreted as multidimensional impulse responses.

$$y(n)=\sum_{p=1}^{\infty}\sum_{n_1=0}^{\infty}\sum_{n_2=0}^{\infty}\cdots\sum_{n_p=0}^{\infty}h_p(n_1,\cdots,n_p)\prod_{j=1}^{P}u(n-n_j) \qquad \text{Eq. 28}$$

If the nonlinearity is causal, time invariant and with finite memory its model corresponds to a finite Volterra model:

$$y(n)=\sum_{p=1}^{P}\sum_{n_1=0}^{M-1}\sum_{n_2=0}^{M-1}\cdots\sum_{n_p=0}^{M-1}h_p(n_1,\cdots,n_p)\prod_{j=1}^{P}u(n-n_j) \qquad \text{Eq. 29}$$

The amplifier generates also thermal noise, which has to be separated from long-term memory terms.

In [56], there is demonstrated that Wiener model is a Volterra model with separable one-dimensional kernels, such as:

$$h_p(n_1,\cdots,n_p)=\prod_{j=1}^{P}h_1(n_j) \qquad \text{Eq. 30}$$

By extension [3], a parallel-cascaded Wiener model is equivalent to a truncated Volterra model with finite memory, as depicted in Figure 48, where H are linear dynamic kernels and g are static nonlinear kernels.

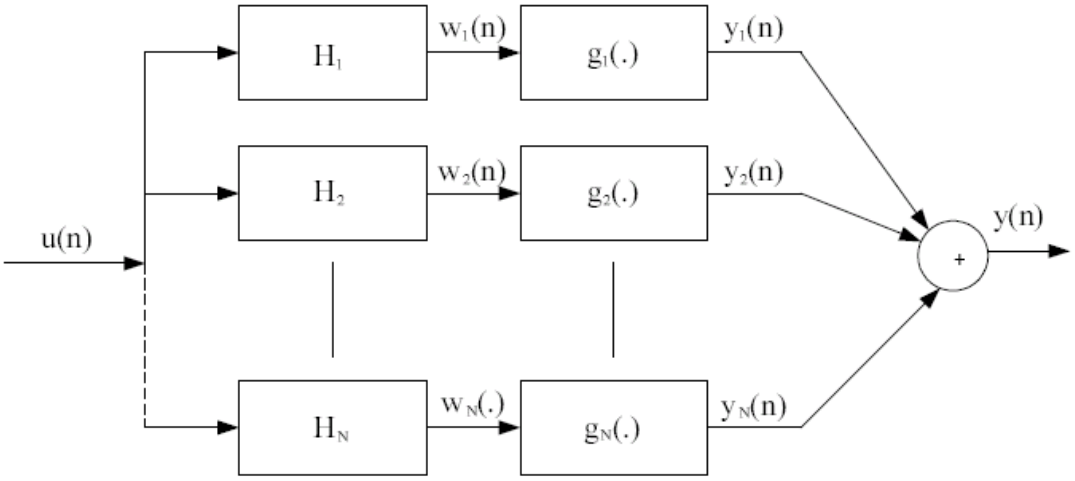

Figure 48 - Parallel Wiener model [56]

3-1.1.1.2 Wiener Hammerstein model

A PA behavioral model derived from Volterra's model is described in [56] through Wiener and Hammerstein filter model. The base of this model is to separate the static nonlinear behavior from the memory effects as in Figure 49.

For the monotonous increasing distortions the number of branches of parallel Wiener model is reduced to one. This type of modeling is called a "box model" approach. This approach allows passing from memory-less model to a model with memory including a box with Finite Impulse Response (FIR) filter.

This model is often used in system simulations and it is suitable for narrowband signals. We can find, "two-box model" and "three-box model" as described in [55], Figure 49.

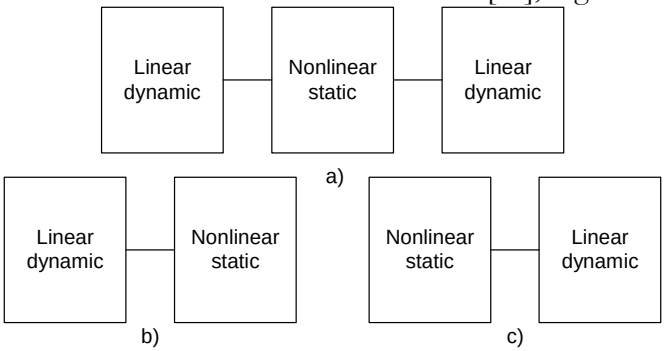

Figure 49 - a) Three-box model Wiener-Hammerstein b) Two box model Wiener c) Two box model Hammerstein

3-1.1.1.3 Neural Networks

In [57] a nonlinear behavior with memory is modeled though a neural network as depicted in Figure 50. The article shows that the adaptation of the neural network (AM/AM and AM/PM convergence) is more accurate with non-uniform delays.

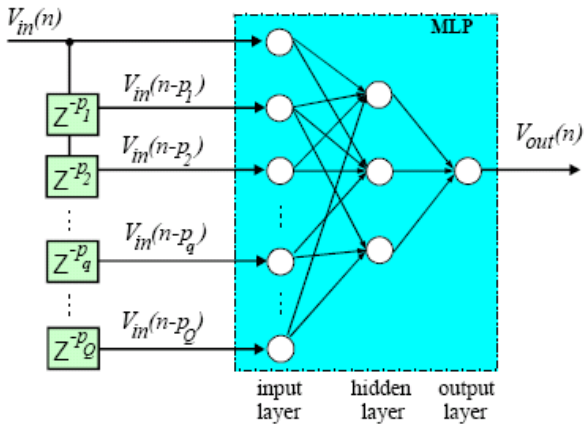

Figure 50 - Nonlinearity model with non uniform memory [57]

3-1.1.1.4 NARMA model

Another model, also proven by measurement, described in [55] is NARMA model (Nonlinear Autoregressive Moving-Average Model). Instead of FIR filter structure, NARMA model is based on IIR filter structure, Figure 51.

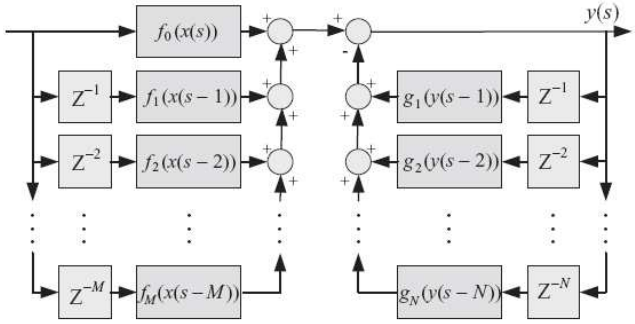

Figure 51 - NARMA model [55]

3-1.1.1.5 Laguerre – Volterra model

The Laguerre-Volterra model is an extension of Volterra's model, based on Laguerre filter, Figure 52 [55].

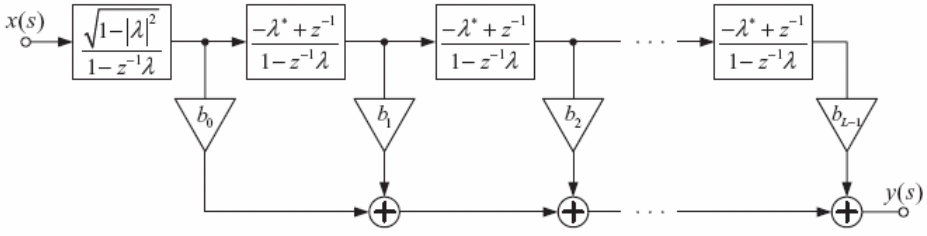

Figure 52 - Laguerre filter [55]

This model exploits the special property of orthogonal Laguerre polynomials. The duration on memory effect is kept by Laguerre polynomial functions; hence the Dirac impulses in the Volterra model are changed by Laguerre orthonormal basis functions, which reduce the number of parameters to estimate.

3-1.1.1.6 Augmented Wiener model

Another non linear model, used in predistortion algorithms, is described in [51]. This augmented wiener model, Figure 53, contains a first 64 tap FIR filter, which is applied on the signal and a second FIR applied on the signal multiplied by its module. This gives non-uniformity to the memory effects; hence the model complexity is reduced. Usually the number of branches of a parallel wiener model, which is suitable to describe causal Volterra polynomials with finite memory, is still significant. When randomizing the memory effects the number of branches is reduced significantly.

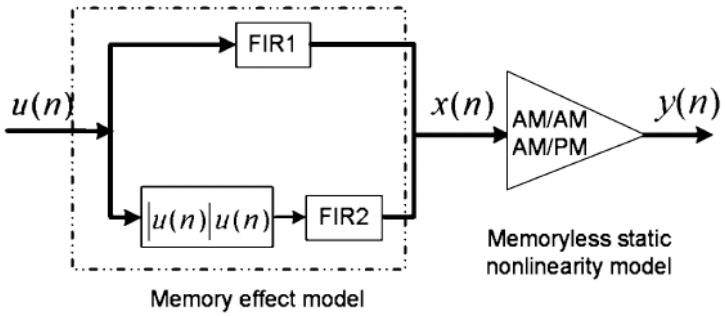

Figure 53 - Augmented Wiener model [51]

3-1.1.1.7 State-space-based-model

A last model presented in [55] is the state-space-based-model given by Eq. 31.

$$X'(t) = F_a(X(t), U(t))$$
$$Y(t) = F_b(X(t), U(t)) \qquad \text{Eq. 31}$$

Where X is the vector of state variables, U is the vector of input variables, Y is the vector of output variables and X' is the time derivative of state variables. This model is a circuit-based model. It is not restricted to weakly nonlinear phenomena as Volterra series. This model has to be characterized along with circuit design.

3-1.1.1.8 High complexity model summary

This chapter relates nonlinearity with memory effect modeling. Among the described models, only a few are definitely suitable for a low complexity implementation. Indeed the number of parameters to estimate is often too high to characterize amplitude and phase distortion of a power amplifier. A trade-off between the model's complexity, the number of parameters to estimate and the modeling accuracy has to be found while selecting a model for identification and correction of PA nonlinearities. High complexity models are used mostly for compensating the PAs of base stations.

3-1.1.2 High complexity model fitting

The difficulty of characterization of those models lies in the estimation of the memory effects. Some methods are depicted in the following chapter, divided into time domain, frequency domain and time-frequency domain methods.

3-1.1.2.1 Time domain methods

A time-based method was presented in [58], where the amplifier behavior is given by

$$X_{OUT}(t) = G(X_{IN}(t), Z(t))X_{IN}(t) \quad \text{Eq. 32}$$

where X_{OUT} is the output signal X_{IN} is the input signal and Z is the function of the historical input signal. This equation can be taylorized into linear terms and Z(t) approximated as Linear Time Invariant response of the input signal. Finally, the memory effects are extracted from the system's step response.

The input signal used can be RF rectangular pulses with different initial and final levels. The memory effects response h_Z is extracted from the output signal.

This method is also valid with triangular signals (memory effects as AM/AM hysteresis), two tone signals (as a Δf difference and the intermodulation products asymmetry) and CDMA signals as a product of cross correlation between $x_{IN}(t)$ and $x_{OUT}(t)$, where the normalized gain residue $\gamma_{IN}(t)$ is given by Eq. 33:

$$\gamma(t) = \frac{\left|\frac{x_{OUT}}{x_{IN}}\right|}{G_{AVERGAGED}(x_{IN})} - 1 \quad \text{Eq. 33}$$

Two articles are alternatively using modulated or multi-tone signals for the identification of two box wiener models. The first one uses a NARMA model characterized by matching the model with measurements though normalized error [60]. The other one uses a 3rd order Chebyshev filter in a two-box model with RMS adaptation.

3-1.1.2.2 Frequency domain methods

The frequency domain methods for nonlinearity and memory effect measurement usually use the 3rd intermodulation product (IM3). In [61] a multi-tone signal is injected into the system using an automatic measurement system. Finally a neural network is trained by asymmetry of 3rd order intermodulation products and applied.

The principle of the method using IM3 is shown in Figure 54. The input intercept point of fundamental and 3rd harmonics is calculated and P_{1dB} point is situated 9,6dB lower. An improved method with calibration based on the IM3 measurement was presented in [54]. The advantage of this method is that the sources do not need to achieve the high power (a power close to saturation) to measure the nonlinearity

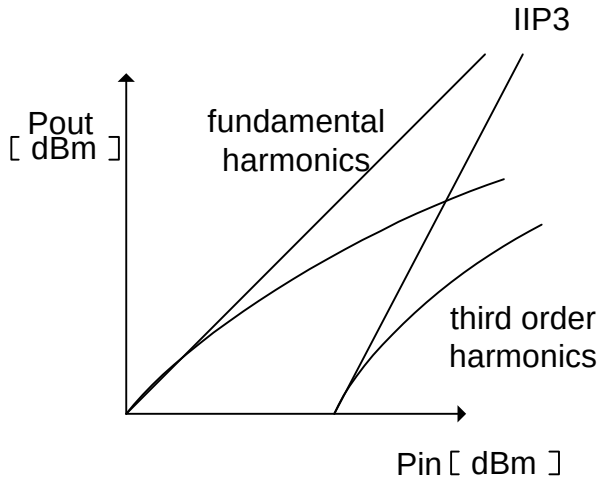

Figure 54 – Principle of two tone signal nonlinearity measurement

3-1.1.3 Low complexity models

Low complexity models only deal with the remarkable memoryless part of distortion caused by power amplifiers. Indeed the estimation of these models should require low complexity computation.

3-1.1.3.1 Cubic polynomial model

The cubic model represents the AM/AM conversion through Eq. 34 where x is the magnitude of input signal.

$$y = G(x) = x(1 - bx^2) \quad \text{Eq. 34}$$

3-1.1.3.2 TWT model

Saleh model was developed for TWT in [62]. The AM/AM conversion is given by Eq. 35:

$$|y| = G(x) = \frac{\alpha x}{1 + \beta x^2} \quad \text{Eq. 35}$$

The AM/PM conversion is given by Eq. 36:

$$\angle y = F(x) = \frac{\alpha x^2}{1 + \beta x^2} \quad \text{Eq. 36}$$

3-1.1.3.3 SSPA model

The SSPA Rapp's model introduced in [63] is given in the power domain by Eq. 37.

$$Y_{POWER} = \frac{X_{power}}{\left(1 + \left(\frac{X_{power}}{A_s^{\,2}}\right)^p\right)^{\frac{1}{p}}} \quad \text{Eq. 37}$$

Where A_s is output saturation level and p is smooth factor.

3-1.1.3.4 Polynomial interpolation model

This model is based on the interpolation of characteristic points of AM/AM and/or AM/PM functions to fit on mentioned amplifiers behavior. Polynomial functions can be chosen to interpolate theses point for their low complexity. For instance, the polynomial coefficients can be calculated thanks to the Lagrange's polynomial interpolation function:

$$y(x) = \sum_{j<n} y_j \psi_j \quad \text{Eq. 38}$$

Where

$$\psi_j(t) = \frac{\prod_{i<n, i\neq j} (x - x_i)}{\prod_{i<n, i\neq j} (x_j - x_i)} \quad \text{Eq. 39}$$

Where x_i and y_i abscise and ordinate points of the AM/AM or AM/PM, y is the output signal and x is the input signal.

3-1.1.4 Low complexity models fitting

On Figure 55, four low complexity power amplifier AM/AM models are compared after fitting to AM/AM measurements of a SiGe technology PA (Atmel T7023) on a network analyzer Agilent E8358A. We observed on this example that the SSPA Rapp model [63] gives a good physical description of the PA behavior up to the saturation.

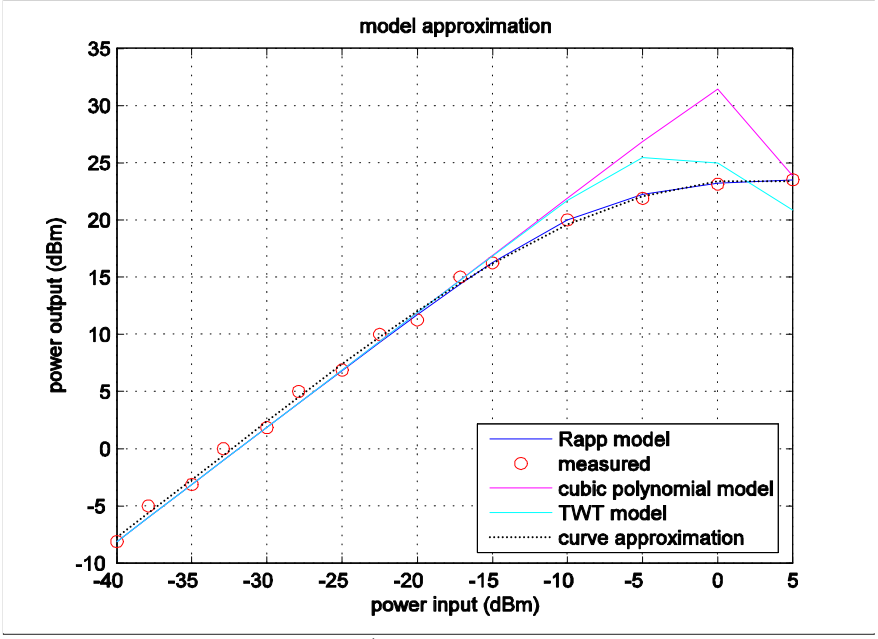

Figure 55 - AM/AM conversion model fitting

Moreover Rapp's model is fully described by only two parameters A_s and p, giving the saturation limit (A_s) and the saturation speed (p). Therefore this model is suitable for a fast and low complexity characterization of the amplitude distortion of a power amplifier. For this reason it has been widely used in the following developments.

Model	Rapp	p_opt	0,568	Error RMS	3,84
Model	Cubic polynomial	b_opt	0,096	Error RMS	366
Model	Saleh model	β_opt	4,61	Error RMS	71,3
Model	Polynomial fitting	Order	3	Error RMS	4,94

Table 7 – Model performances

Table 7 shows the precision on the approximation of AM/AM measurements with low complexity models.

AM/AM conversion has a major impact on EVM. In simulations with measured data from real power amplifier the AM/AM distortion causes an EVM of 9% in the same conditions AM/PM conversion causes only 0,2%. AM/AM and AM/PM distortion together cause an EVM=9%; hence the impact of AM/PM distortion is further neglected in the condition of having $\Delta\phi$ lower than 7°.

3-1.2 Relevance of the models for the linearization purpose

The relevance of the previously defined models for the linearization purpose can be estimated through several parameters: the number of variables to estimate, the obtained precision for the kind of PA used, the bijective properties for model inversion, etc.

The main one is the number of variables to estimate. Among low complexity models the number of parameters is one for cubic polynomial model, two for TWT model and Rapp model and n+1 for the canonical form of interpolation polynomial function (where n is the polynomial function order).

The precision of the cubic and Saleh model and the number of coefficients of the polynomial fitting limit their use in a linearization scheme. At the opposite the Rapp's model seems to be a good candidate for this purpose.

However the inversion of the models has also to be checked carefully.

By its construction, the Lagrange polynomial function inversion is achieved simply by swapping input and output signal interpolation points [52]. Rapp model inverse function is calculated analytically in Eq. 40.

$$X_{POWER} = \frac{Y_{power}}{\left(1 - \left(\frac{Y_{power}}{As^2}\right)^p\right)^{\frac{1}{p}}} \qquad \text{Eq. 40}$$

Such bijective models need little computation to approximate the inverse PA nonlinearity function in a linearization scheme. In the mean time the model function can be not invertible. It usually happens when the slope of the inverse function goes to infinity at saturation. According to [64], the piecewise cubic hermite polynomial function can be an alternative to cope with a nonbijective function issue. This polynomial function is constructed in this manner:

$$\begin{aligned} H(x_1) &= f(x_1) \\ H(x_2) &= f(x_2) \\ H'(x_1) &= f'(x_1) \\ H'(x_2) &= f'(x_2) \end{aligned} \qquad \text{Eq. 41}$$

Where f is the nonbijective function to inverse and H(x) is a cubic polynomial function of the form:

$$H(x) = a_1 + a_2 x + a_3 x^2 + a_4 x^3 \qquad \text{Eq. 42}$$

Finally the piecewise polynomial function is given by switching the cubic polynomial functions according to intervals:

$$H(x) = \begin{cases} H_1(x) & x_1 \le x < x_2 \\ H_2(x) & x_2 \le x < x_3 \\ & \cdots \\ H_{n-1}(x) & x_{n-1} \le x < x_n \end{cases} \qquad \text{Eq. 43}$$

Where Hi(x) is the cubic polynomial function:

$$H_i(x) = a_1 + b_i(x - x_i) + c_i(x - x_i)^2 + d_i(x - x_i)^2(x - x_{i+1}) \qquad \text{Eq. 44}$$

In the case of AM/AM predistortion the goal of this method is to find a function ***F*** of predistortion where P_{IN} is the input signal and P_{IN}' is the predistorted signal. The equations is $P_{IN}'=\boldsymbol{F}(P_{IN})$ with ***F*** such that P_{OUT} is linear.

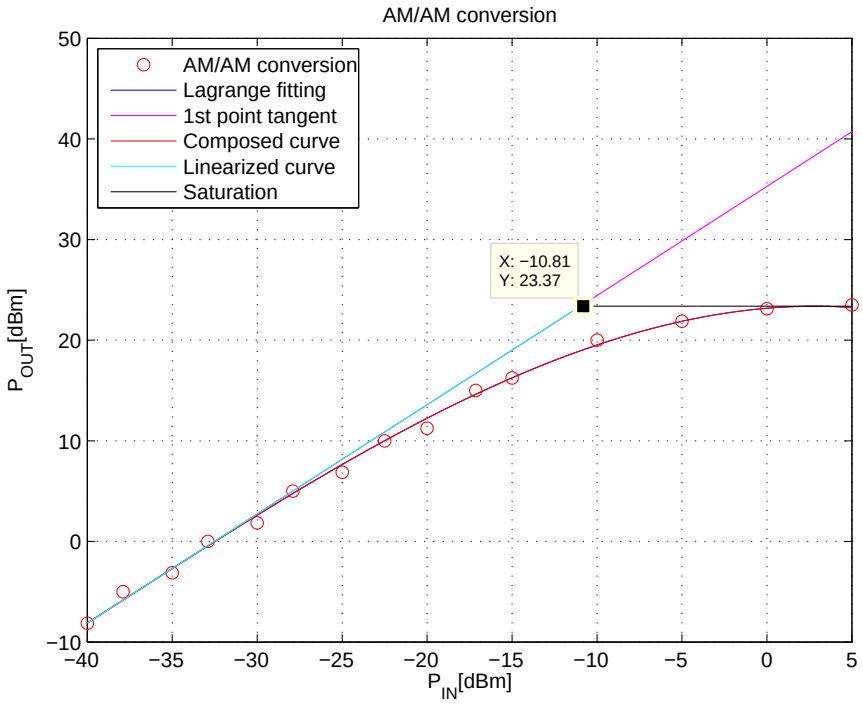

Figure 56 - Predistortion simulation

Figure 56 shows the applied predistortion. The red circles are AM/AM conversion given by measurements. The blue curve is Lagrange's polynomial function fitted AM/AM conversion (covered by the red curve). The magenta curve is the tangential to the first point of Lagrange's approximation. The red curve is a curve composed from the tangential curve in linear zone and by Lagrange's approximation in the rest. The cyan curve is predistorted signal P_{IN}', which passed through a nonlinearity ***G***. Output power P_{OUT} is hence given by $P_{OUT}=\boldsymbol{G}(P_{IN}')$. The black curve is the amplifiers saturation P_{SAT}=23.37 dBm.

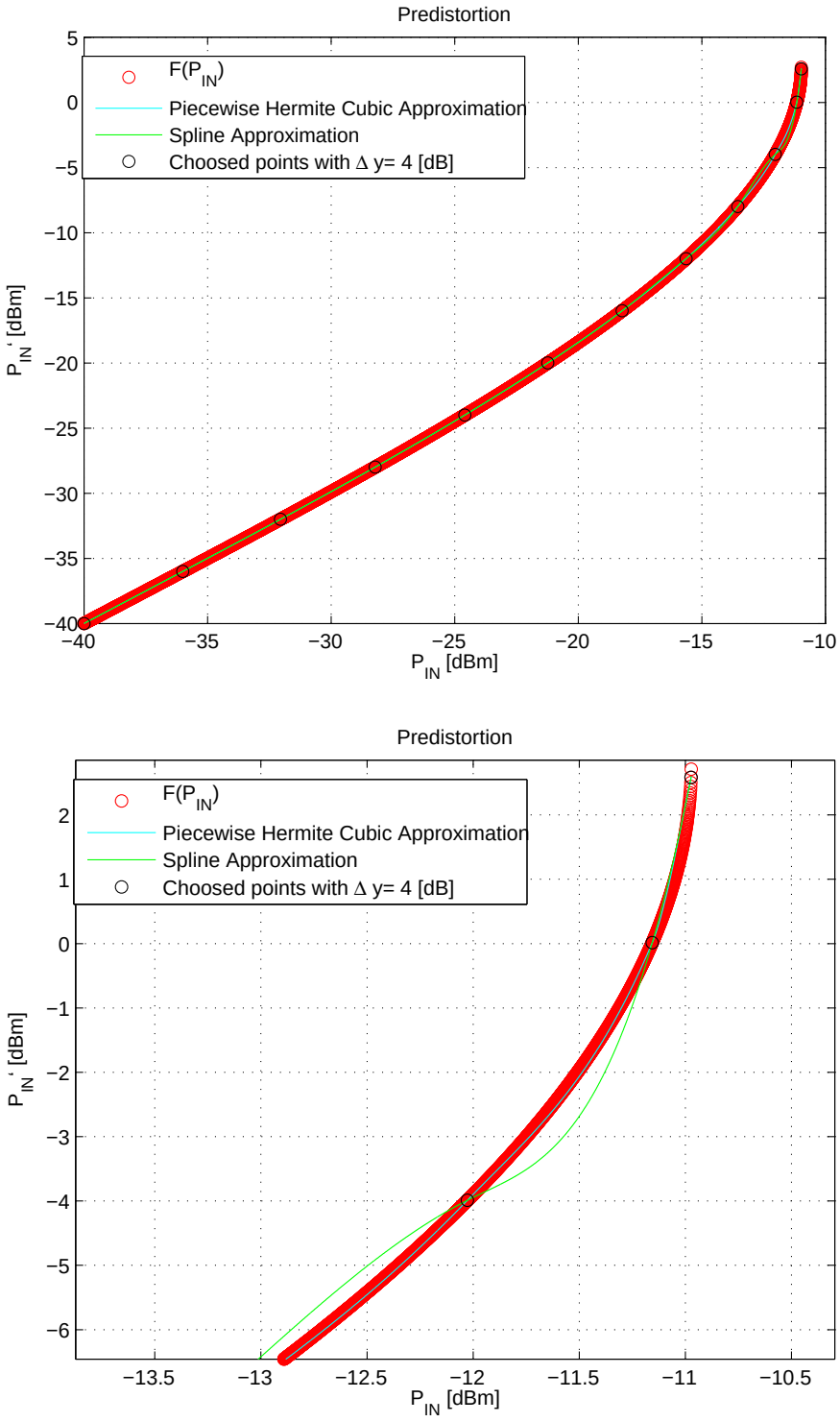

Figure 57 - Predistortion spline and Cubic Hermit polynomial fitting for Δy=4dB a) all curve b) zoom near to saturation

Δy[dB]	Error RMS Hermit [mW]	Error RMS Spline [mW]
0.5	0.000243	0.000320
1	0.000324	0.00166
2	0.000699	0.0102
3	0.00154	0.0280

4	0.00766	0.0150
8	0.00849	0.0447
16	0.0721	0.0744

Table 8 – Inverse function approximation

Figure 57 shows the spline and piecewise cubic Hermit polynomial fitting on predistortion function $\boldsymbol{F}$ by $P_{IN}'=\boldsymbol{F}(P_{IN})$. As we can see on Figure 57 b) and in Table 8, piecewise Hermit polynomial fitting has better performances than spline. Using spline, there might be a risk of loosing monotonicity.

3-1.3 Conclusion on nonlinearity models

High complexity models were rejected for our application because of the number of parameters to estimate. If the estimation function is not estimated directly or the inverse function is not able to be expressed analytically, the high complexity hermit approximation of inverse function becomes necessary.

For the proposed architecture on Figure 45, there is a field of only a few bits in MAC messages. Hence the low complexity models having only one or two parameters are favored. Cubic polynomial model diverges from measurements for the region near to saturation, while TWT model has poor precision. Polynomial fitting has a really good performance, but it is defined only in node points. Outside of the interval given by node points the polynomial curve fitting might diverge and between node points it might oscillate especially for high order polynomial functions. Also for high order polynomials, more than two parameters are needed. As a result Rapp's model appears has the best trade-off between precision and complexity. The main advantage of Rapp's model is that only two parameters are needed to describe the power amplifier. The physical reality is well described by this model up to the PA's saturation. The model is given by a monotonous function; hence there are no oscillations between node points in case of polynomial interpolation of its inverse function. Due to its exponential form, the disadvantage of this model is that the Rapp's model is more complex in hardware implementation than polynomial fitting. However we'll see that the use of Look-Up Table helps reducing this complexity. For this reasons, the Rapp's model is used for PA linearization in the further parts of the thesis.

3-2 System modeling

In this paragraph the system modeling is described. Firstly the OFDM signal is approximated by a random process. The proposed architecture is put into bloc schematics, where the blocks are given by equations, and the predistortion function is implemented for ideal parameters.

3-2.1 Signal approximation

Assuming signal ergodicity, the OFDM-based 802.16 signals have such similarities with complex random signals that they might be approximated by a generalized random signal. Firstly the distribution was analyzed.

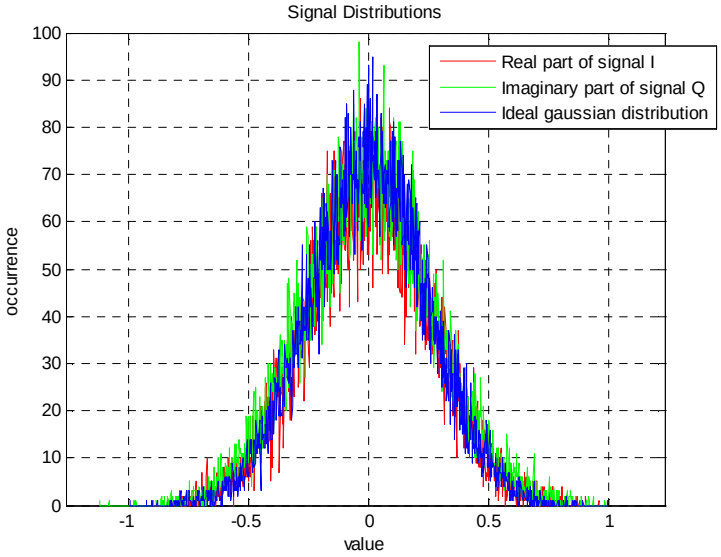

Figure 58 - OFDM signal from standard 802.16 and AWGN distributions

Figure 58 shows that the input signal real part (red) and imaginary part (green) have distributions similar to the one of an ideal Gaussian distributed signal (blue).

.

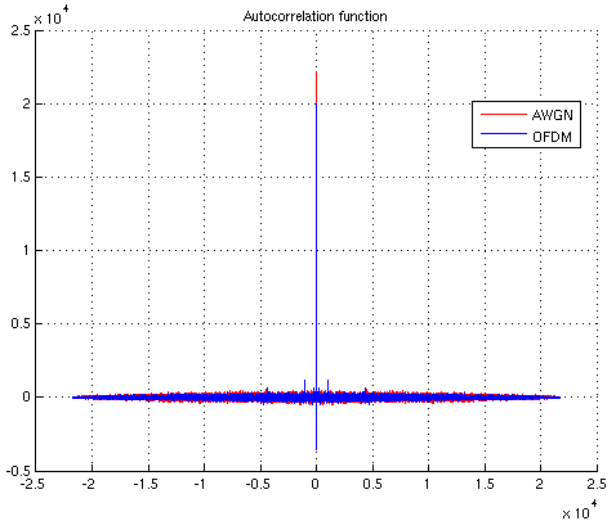

Figure 59 - OFDM signal from standard 802.16 and AWGN autocorrelation functions

Figure 59 shows the autocorrelation function of a real part of 802.16 signals with parameters in Table 9 and a Gaussian distributed signal.

Type	Parameter	Value
RF	Central frequency	3.5GHz
	Bandwidth	10MHz
PHY	Access mode	TDD/OFDMA/PUSC
	DL/UL	Downlink only
	FFT + CP sizes	1024 + 64
	Modulation order	64 QAM
	Frame period	2 ms

Table 9 - 802.16 signal parameters

The time complex OFDM signal is composed of real part I and imaginary part Q. Each part has centered Gaussian signal distribution. Their probability density function is given by Eq. 45, where σ is standard deviation and μ is mean value.

$$f_X(t) = \frac{1}{\sqrt{2\pi\sigma^2}} e^{\frac{-(x-\mu)^2}{2\sigma^2}} \qquad \text{Eq. 45}$$

When passing to the power mode (I^2+Q^2), the distribution changes to centered $\chi 2$ with two degrees of freedom.

For normalized signal, the probability density function is given by Eq. 46. The input signal has this distribution.

$$f_X(x) = \begin{cases} 0 & x < 0 \\ \frac{1}{2}\exp\left(-\frac{1}{2}x\right) & 0 \le x \end{cases} \qquad \text{Eq. 46}$$

3-2.2 Transmission link

Figure 60 shows the schematics of classical predistortion. The signal is generated as a complex Gaussian distributed random signals. When passing to the power domain, the distribution changes to χ^2 with two degrees of freedom. The signal is optionally predistorted depending on the frame. The signal is distorted by power amplifier before being emitted through the channel. At the receiver only LNA nonlinearities which affect the signal are considered. Optionally the nonlinearity parameters are estimated and transmitted back to Tx by software feedback loop with limited information volume.

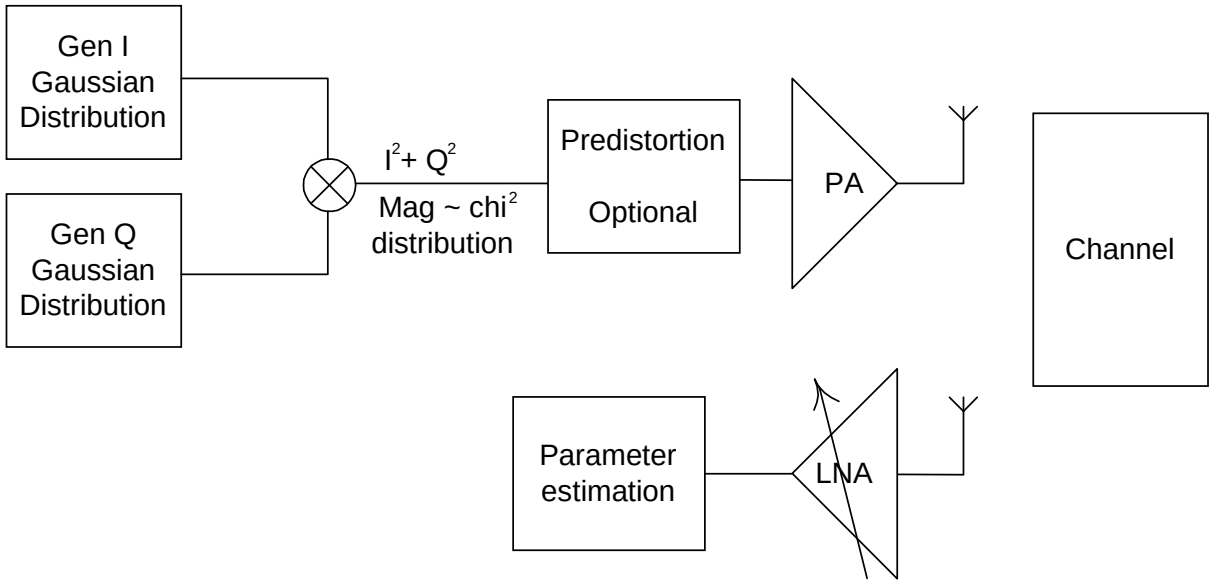

Figure 60 - Architecture diagram

This chain might be described by Eq. 47.

$$V_{LNA} = K \cdot \left(L\left(H * \left(G \cdot F\left(P\left(V_{IN}\right)\right)\right)\right)\right) + w(t) \qquad \text{Eq. 47}$$

Where:

- *K denotes LNA gain*
- *L denotes LNA nonlinear function*
- *H denotes channel impulse response*
- *G denotes PA gain*
- *F denotes PA nonlinear function*
- *P denotes Predistortion function – if disabled y=x*
- *w(t) denotes Gaussian white noise*

For an ideal case where L is a linear function, perfect channel H=1 with negligible noise the V_{LNA} is equal to V_{IN} only if predistortion function is the inverse function of the PA nonlinear function $P=F^{-1}$. When estimating the nonlinearity at the receiver, the algorithm has to cope with the composition of all these nonlinear functions and channel convolution.

The power amplifier F is described by the monotonous Rapp's model given by Eq. 37, whose saturation is given by A_s. Its inverse function used as predistortion is given by Eq. 40. From the equation we can see that the function has a non trivial singularity for $Y_{POWER}=As$.

3-2.3 Probability density function

When passing through the nonlinear components, such as power amplifier, the signal statistical properties change i.e. mean value and variance. Figure 61 shows how the histogram of I or Q signals are impacted after passing through power amplifier. The highest amplitudes are attenuated, while part of the signal is clipped at saturation. In this paragraph, the modification of the signal statistics is studied analytically.

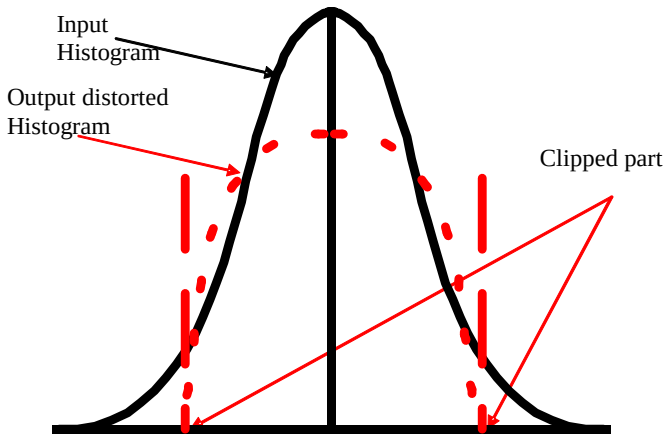

Figure 61 – Normal an distorted signal histogram

To compute the probability density function we used the definition of random variable transformation, Eq. 48.

$$F_Y(y) = \Pr(Y \le y) = \Pr(G(X) \le y) = \Pr(X \le g^{-1}(y)) = F_X(g^{-1}(y)) \qquad \text{Eq. 48}$$

Where $F_Y(Y)$ is the cumulative probability function of the output signal, $F_X(x)$ is the cumulative probability function for $F_X(y)$, G(X) is the nonlinearity function given by Rapp's model (Eq. 37) and $g^{-1}(y)$ is the real solution of inverse Rapp's model function (Eq. 40). The probability density function (Eq. 49) is given by the first derivation of the cumulative probability function, Eq. 48.

$$f_Y = \frac{dF_X\left(g^{-1}(y)\right)}{dy} \qquad \text{Eq. 49}$$

The probability density function is then given by Eq. 50.

$$f_Y(y) = \begin{cases} 0 & y < 0 \\ \dfrac{\exp\left(-\dfrac{1}{2}\dfrac{y}{\left(1-\left(\dfrac{y}{A_s^{\,2}}\right)^p\right)^{\frac{1}{p}}}\right)}{\left(1-\left(\dfrac{y}{A_s^{\,2}}\right)^p\right)^{\frac{1}{p}+1}} & 0 \le y < A_s^{\,2} \end{cases} \qquad \text{Eq. 50}$$

Figure 62 shows the probability density function obtained analytically for As=3 and p=1 for the distorted and the non-distorted case, along with probability density function obtained numerically from simulation.

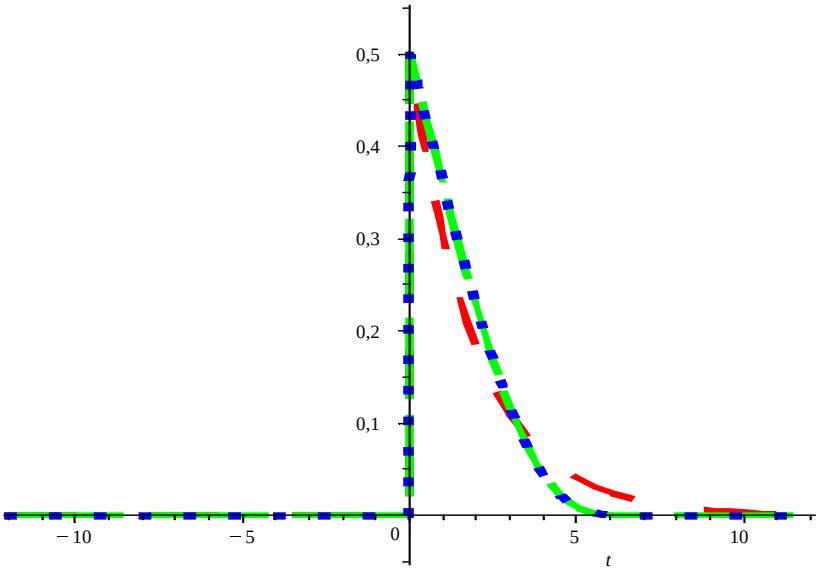

Figure 62 - Distorted PDF A_s=3 p=1 (blue) and input signal PDF for A_s=3 p=1 (red); model of distorted PDF A_s=3 p=1 (green)

3-2.3.1 Analytical solution of the mean value at the output of PA

The mean value is defined as the 1st order statistical moment through Eq. 51. Because of the singularity at the saturation point, this definition can not be solved at this point.

$$E[Y] = \int_{-\infty}^{\infty} u \cdot f_Y(u) du \qquad \text{Eq. 51}$$

Alternatively Eq. 52 allows the computation of the mean value after non linearity degradation without having the near-to-singularity issue.

$$E[Y] = \int_{-\infty}^{\infty} g(u) \cdot f_X(u) du \qquad \text{Eq. 52}$$

Where g(u) is given by Eq. 37. The analytical solution is computed for A_s positive and p a positive integer.

The solution for p=1 is given by Eq. 53, where Ei denotes Exponential Integral function.

$$E[Y] = 2 - 4 \cdot \exp\left(\frac{A_s^2}{2}\right) Ei\left(3, \frac{A_s^2}{2}\right) \qquad \text{Eq. 53}$$

The solution for p=2 is given by Eq. 54, where StruveH denotes Struve H function and BesselY denotes Bessel Y function. The difference between Struve H and Bessel Y function is that the Struve H is the solution of the inhomogeneous Bessel differential equation.

$$E[y] = \frac{1}{4} As^4 \left(-2 + \pi\left(StruveH\left(1, \frac{1}{2}A_s^2\right) - BesselY\left(1, \frac{1}{2}A_s^2\right)\right)\right) \qquad \text{Eq. 54}$$

The solution for p= {3..6;8,10,12…}odd numbers is given by Eq. 55.

$$E[Y] = \sin\left(\frac{\pi}{p}\right) \cdot \frac{\sqrt{p}}{2^{\frac{p-1}{2}}} \cdot \frac{\Gamma\left(1-\frac{1}{p}\right) \cdot A_s^2}{\pi^{\frac{p+1}{2}}} \cdot G_0^{2p+1\ 1}_{0}\left(\begin{matrix} 1-\frac{1}{p} \\ \frac{p+1-j}{p} \end{matrix} \middle| \left(\frac{A_s^2}{2p}\right)^p\right) \qquad \text{Eq. 55}$$

The solution for p= {7,9..23} even numbers is given by Eq. 56.

$$E[Y] = \frac{\sqrt{p}}{2^{\frac{p-1}{2}}} \cdot \frac{A_s^2}{\Gamma\left(\frac{1}{p}\right) \cdot \pi^{\frac{p+1}{2}}} \cdot G_0^{2p+1\ 1}_{0}\left(\begin{matrix} 1-\frac{1}{p} \\ \frac{p+1-j}{p} \end{matrix} \middle| \left(\frac{A_s^2}{2p}\right)^p\right) \qquad \text{Eq. 56}$$

Where G denotes a Meijer G function and Γ denotes Gamma function.

Figure 63 shows the graphical representation of analytical solution if distorted signal for p type positive integer. The solutions for non-integer values of p are situated between the curves.

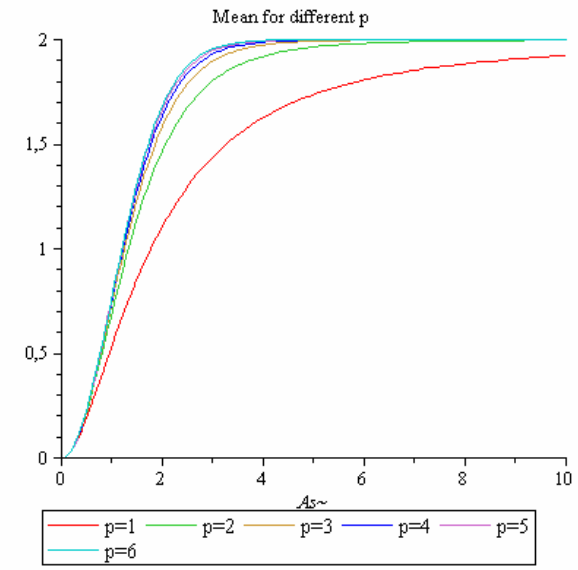

Figure 63 - Graphical representation of analytical solution of the distorted mean

This function predicts the mean gain reduction of signal having distribution χ^2 passing through a PA and it converges to the mean value of χ^2 distribution with 2 degrees of freedom; hence the mean value is equal to two. In the case of a non normalized signal with variance $2\sigma^2$, E[Y] is divided by σ^2.

This result is important since the gain reduction due to nonlinearity has to be separated from linear attenuation (e.g. channel path loss) in signal processing. Indeed, the Automatic gain Control Loop can be corrected or dissociated from the nonlinear reduction of gain.

3-2.3.2 Analytical solution of variance value

The variance is computed from its definition, as the second moment of centered random value Eq. 57.

$$E[Z] = \int_{-\infty}^{\infty} (g(u) - E[Y])^2 \cdot f_X(u) du \qquad \text{Eq. 57}$$

Figure 64 shows the graphical representation of distorted variance after power amplifier. For non integer values of "p", the curve is situated between the curves for integer values.

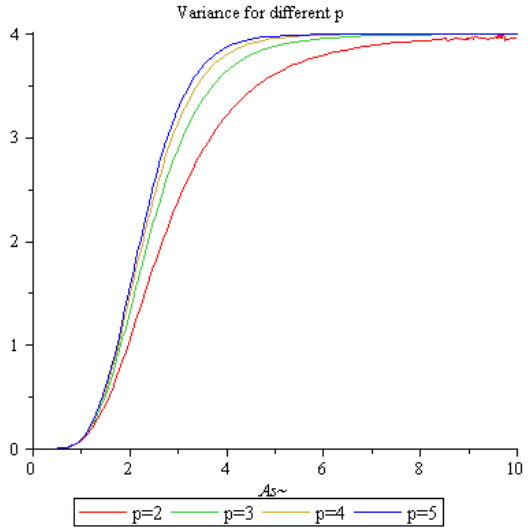

Figure 64 - Graphical representation of analytical solution of the distorted variance

3-2.3.3 Channel

The channel is modeled as a convolution of the nonlinear emitter output signal with an impulse response, Eq. 58.

$$E[Z] = \int_{-\infty}^{\infty} (g(u) * h) \cdot f_X(u) du \qquad \text{Eq. 58}$$

For a perfect channel $h=\delta(t)$, the equation became the same as Eq. 52. For a two-path channel $h=\delta(t)+\delta(t-\tau)$, the solution using the sampling property of Dirac pulse is in Eq. 59.

$$E[Z] = \int_{-\infty}^{\infty} (g(u) + g(u-\tau)) \cdot f_X(u) du \qquad \text{Eq. 59}$$

3-2.4 Parameter estimation

At the receiver several algorithms impact, or can be affected by a modification of, the signal dynamic. First Automatic Gain Control (AGC) has to be dissociated and corrected from nonlinearity impact, so that the parameters of nonlinearity are estimated without bias. Next channel estimation and equalization can also interact with nonlinearity estimation.

Using a dedicated algorithm for AGC and channel equalization, the nonlinearity effects can be separated from linear gain estimation, and linear channel estimation. Finally the PA nonlinearity is estimated without being biased by channel estimation.

3-2.5 Conclusion

In the first part of this chapter power amplifier models have been summarized and evaluated. Then a statistical model of the receiver input signal affected by the non-linear characteristic of the PA and the channel transfer function was introduced. This system analysis is the basis for the performance optimization described in the fifth chapter, where the tradeoff between performances and imperfections from predistortion is given.

Chapter 4 : Hybrid Receiver-aided Linearity Compensation

4-1 Introduction

In this chapter the concept of the hybrid receiver-aided linearity compensation architecture is proven by measurement. Firstly the measurement test bench is developed to proof the architecture of post-compensation. When the test-bed is valid for the known architecture, it is adapted to be used with new hybrid receiver aided architecture. Finally a test bed with synthetic channel is built for the new hybrid receiver aided architecture to evaluate its robustness and performances in more realistic conditions. In contrast to classical predistortion, which has been developed for base stations in cellular networks (2.5G, 3G), post-compensation and receiver-aided predistortion power amplifier nonlinearity compensation architectures can be applied for large band WiMAX and LTE networks, at base station, relay station or mobile station sides.

4-2 Architectures

4-2.1 Predistortion

In a predistortion architecture, the power amplifier nonlinearity is compensated before the signal is emitted. For a good precision it needs a feedback path to bring from the PA output to the predistorter the image of the remaining nonlinearities. An example of adaptive predistortion with feedback path using charge sampling is described in [65].

Usually the signal has a good SNR at emitter side, and so the precision of the adaptive predistortion is good. The architecture is often stable and robust to antenna VSWR. This architecture leads to good improvement both on error vector magnitude and spectral regrowth, allowing satisfying the most stringent standard requirements.

However the feedback path should have a large bandwidth (usually 3 to 5 times the signal bandwidth) to pass nonlinearity information (3^{rd} to 5^{th} order) to predistorter without overlapping. Thus broadband mixers and ADCs add extra power consumption. For instance for 50MHz signal bandwidth and discrete components, (Analog Devices ADC9211 ADCs at 300MSPS), the extra power consumption of the feedback path can reach 1W.

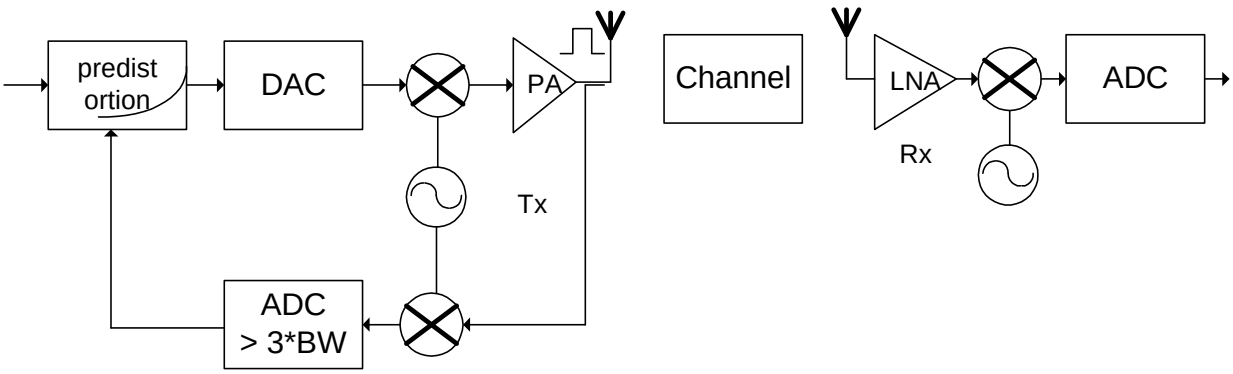

Figure 65 – Architecture based on predistortion feedback path

4-2.2 Post compensation in Rx

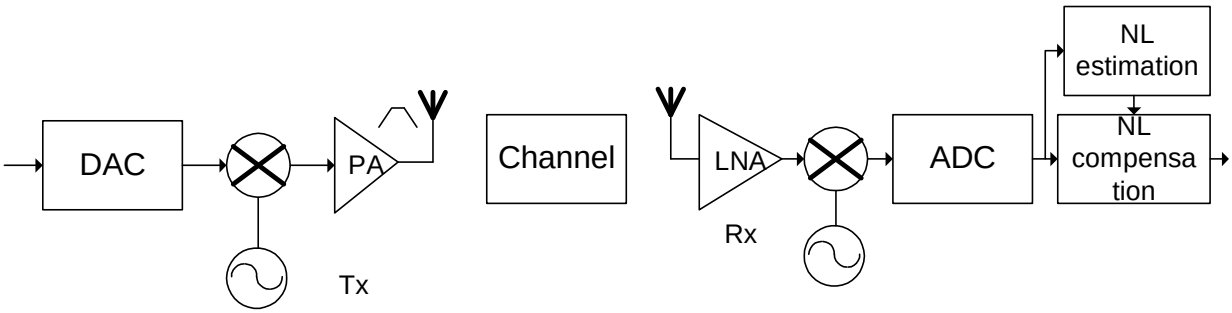

Figure 66 – Architecture with post compensation in Rx

As a second architecture, postcompensation, is shown in Figure 66. The non-linearities are corrected at the receiver side, after the analog-to-digital conversion. The pros of this architecture are that no extra hardware is required at the transmitter sided. The transmitter stays as light as possible, since complexity is pushed to the receiver. The con of this architecture is that the signal is not corrected at emitter while EVM and spectral regrowth shall stay within the standard requirements. Figure 67 shows the signal power spectral density (green curve) and the WiMAX's spectrum mask (red curve). The picture clearly highlights the drawback of this architecture: even if the nonlinearity is well compensated at the receiver, power has to be backed off at the emitter to meet the standard spectrum requirements..

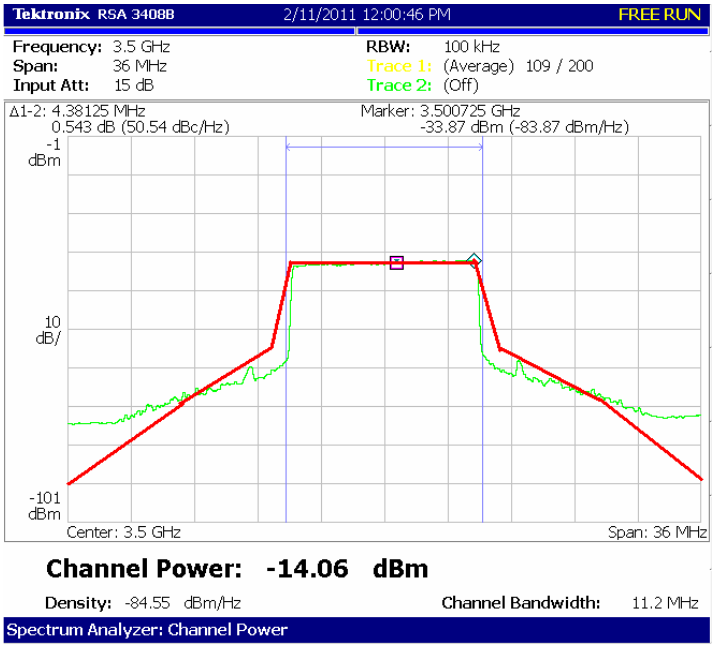

Figure 67 – Emitted signal and spectral mask

4-2.3 Receiver-aided hybrid compensation architecture

The receiver-aided hybrid architecture patented in [72] is a logical outcome of the state of the art. It combines in Figure 68 the advantages of the two former architectures: the signal is

predistorted before power amplifier with good precision and no supplementary hardware is needed. Here the PA is predistorted at the transmitter side, but the nonlinearity estimation is carried out at the receiver side. The information about PA nonlinearity is transmitted by the MAC layer from the receiver back to the transmitter; hence the additional hardware feedback path is not needed.

This information should be transmitted as a short sequence of bits to be included into the MAC data fields. For this reason the nonlinearity estimation at the receiver corresponds to an identification of a small set of parameters of a power amplifier model.

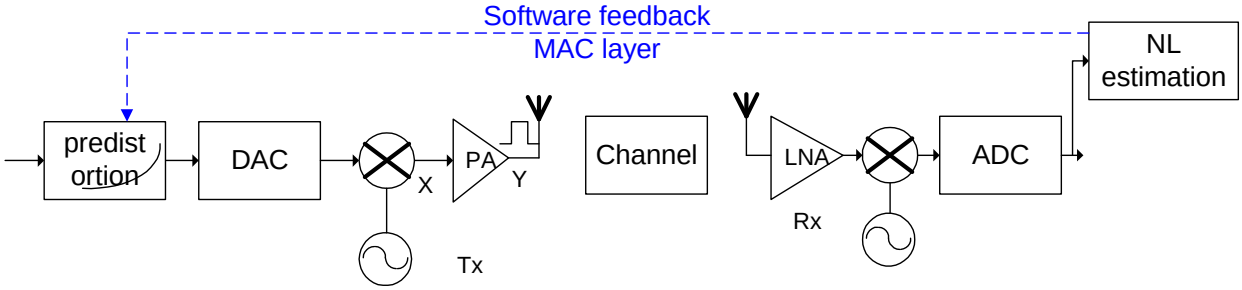

Figure 68 – Receiver aided architecture using a software feedback

4-3 Compensation methods

The different compensation methods are investigated and compared in this paragraph. First post compensation in the receiver uses an orthogonal polynomial base decomposition algorithm to estimate the nonlinearity parameters. It computes directly the inverse function and applies compensation. Differently the hybrid architecture uses a least mean square (LMS) algorithm to estimate at the receiver a model of nonlinearity. Thanks to Rapp's model properties, the inverse function is computed analytically at the emitter; and is directly applied on signal.

4-3.1 Common devices

In this paragraph the common devices used both by post compensation in Rx and hybrid receiver-aided compensation architecture are listed. The common power amplifier is measured; the common synchronization and equalization algorithms are described.

4-3.1.1 Power amplifier

For wire measurement of power amplifier, attenuators are often required to lower the signal before acquisition. According to [67], class-A amplifiers should be modeled by time-invariant Volterra series and that attenuators should be modeled by time varying Volterra series. When the nonlinearities are cascaded, it is not possible to distinguish which nonlinearity impact comes from the power amplifier and which part comes from the attenuator. Hence we took the decision to use a medium power amplifier in order to avoid the use of strong attenuation before measurement.

The PA S parameters were measured using a spectral analyzer from Rohde-Schwartz from 0dBm to 15dBm. The power amplifier has AM/AM and AM/PM conversion characteristics on Figure 69.

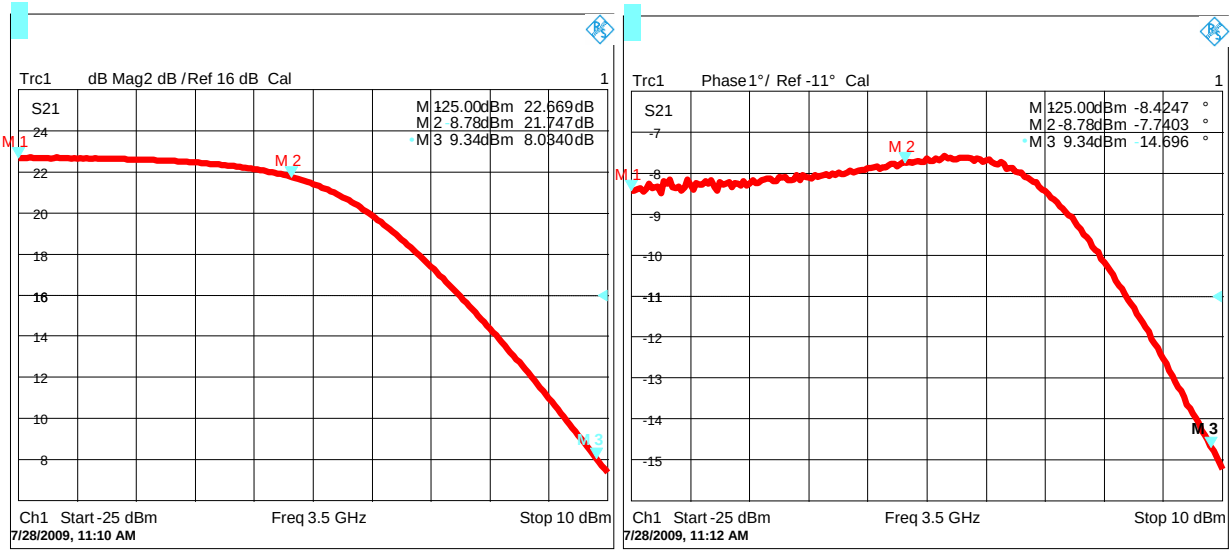

Figure 69 – a) amplifiers AM/AM characteristic b) amplifiers AM/PM characteristic

4-3.1.2 Signal waveform and algorithms

This analysis has been carried out in the framework of ICT-ROCKET [69], which aims at investigating the use of large constellation to increase the data rate. For this purpose a high dynamic WiMAX signal is considered in [69] with high modulation order and large number of OFDM subcarriers. Figure 70 shows the received WiMAX signal after the ADC with parameters in Table 10.

Type	Parameter	Value
RF	Central frequency	3.5GHz
	Bandwidth	10MHz
PHY	Access mode	TDD/OFDMA/PUSC
	DL/UL	Downlink only
	FFT + CP sizes	1024 + 64
	Modulation order	64 QAM
	Frame period	2 ms

Table 10 - Signal parameters

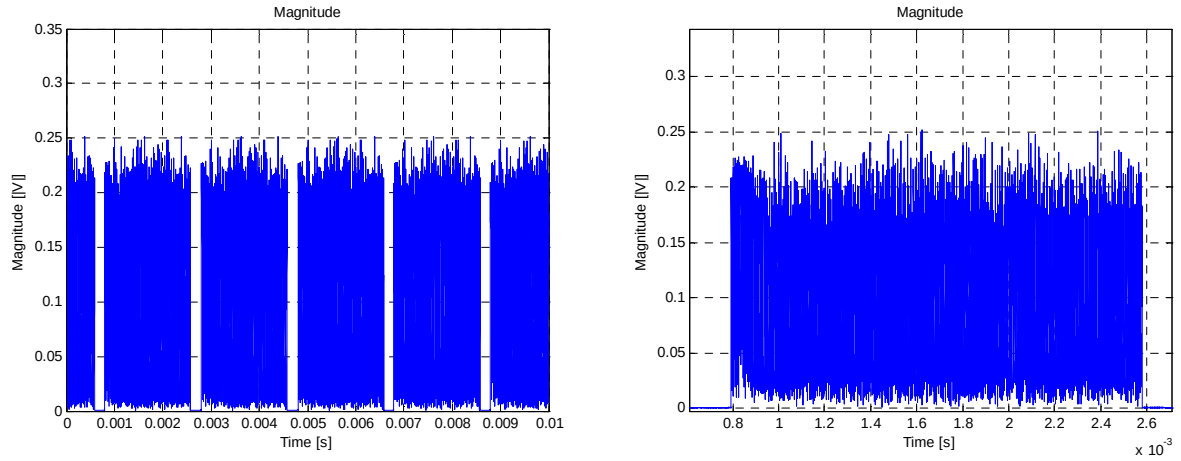

Figure 70 - Magnitude of real WiMAX signals (after the ADC)

The preamble mean power is greater than the payload power (3dB boosting), but in the same time, the peak average power ratio (PAPR) is greater during the payload than during the preamble. The preamble of the standard is well chosen to limit PAPR, in order not to bias channel estimation with a nonlinear power amplifier.

Figure 71 shows auto-correlation and cross-correlation mandatory for the time synchronization.

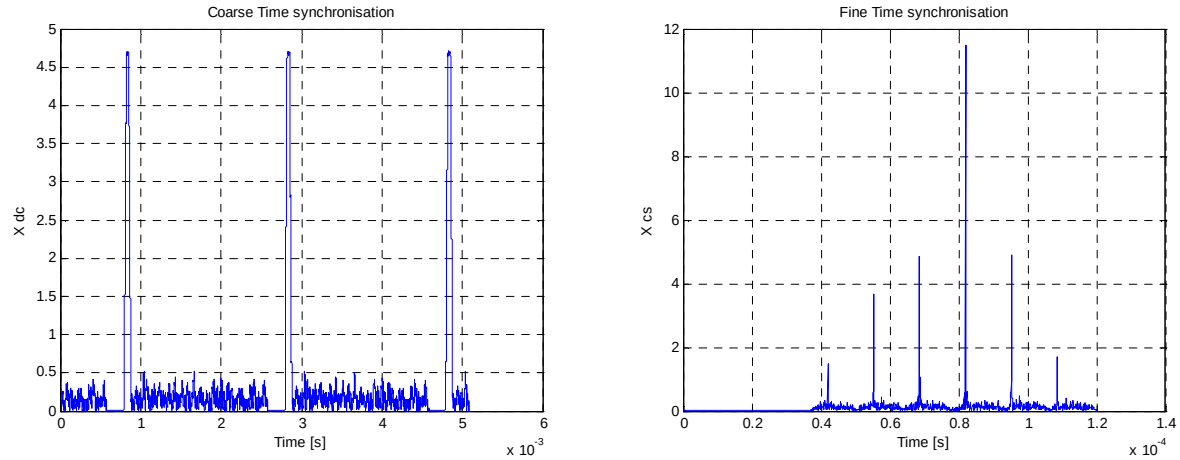

Figure 71 - Synchronization on measured WIMAX signals

In this example, the rough Carrier Frequency Offset is estimated (here to -107Hz) using the angle of the autocorrelation based on the CP repetition [68].

Figure 72 shows the constellation before equalization.

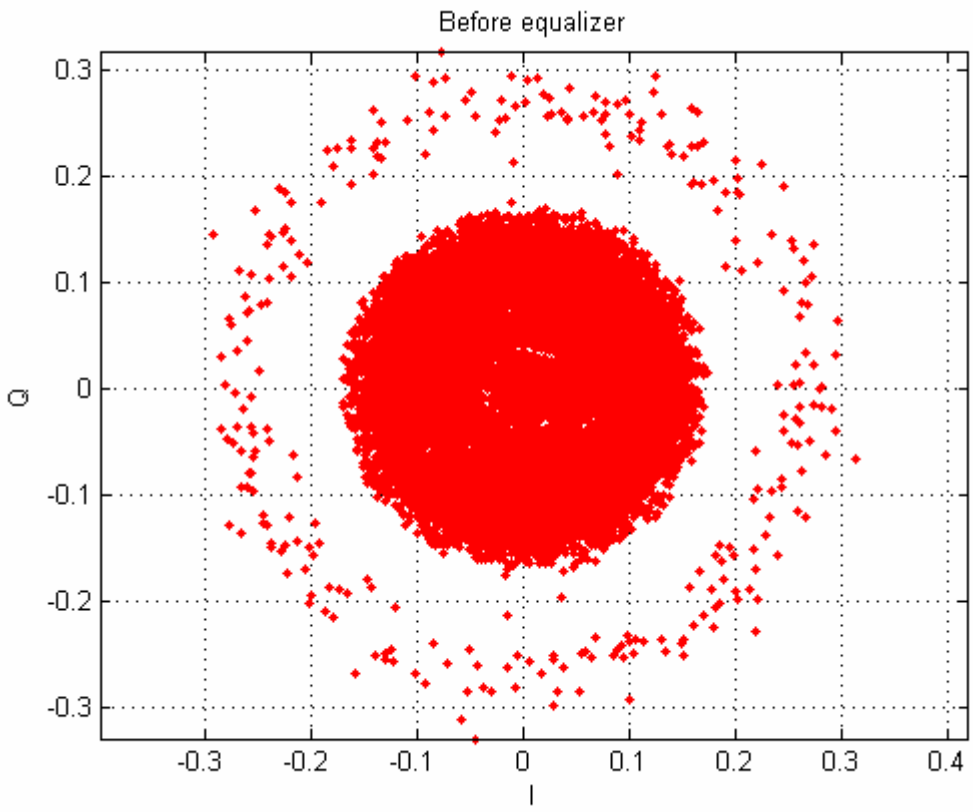

Figure 72 - Constellation before equalizer

After synchronization and equalization, the 64QAM constellation can be observed without and with the compensation on Figure 73.

$$y = y_C + y_D = \alpha \cdot x + (y - \alpha \cdot x) \qquad \text{Eq. 60}$$

A Bussgang theorem Eq. 60, which is explained in [81], stands for estimate signal to noise and distortion ratio SINAD. It says that for complex Gaussian distributed signals x the distorted signal y can be divided into a part y_C dependent on the input signal and a part y_D independent of the input signal. The dependent part is estimated by correlation, because two Gaussian distributed signals are uncorrelated when they are independent. This part is considered as output signal, with α as the gain. The independent part is estimated by removing the correlated part hence it remains only the uncorrelated part, which is considered as an additive noise that is found in the constellations.

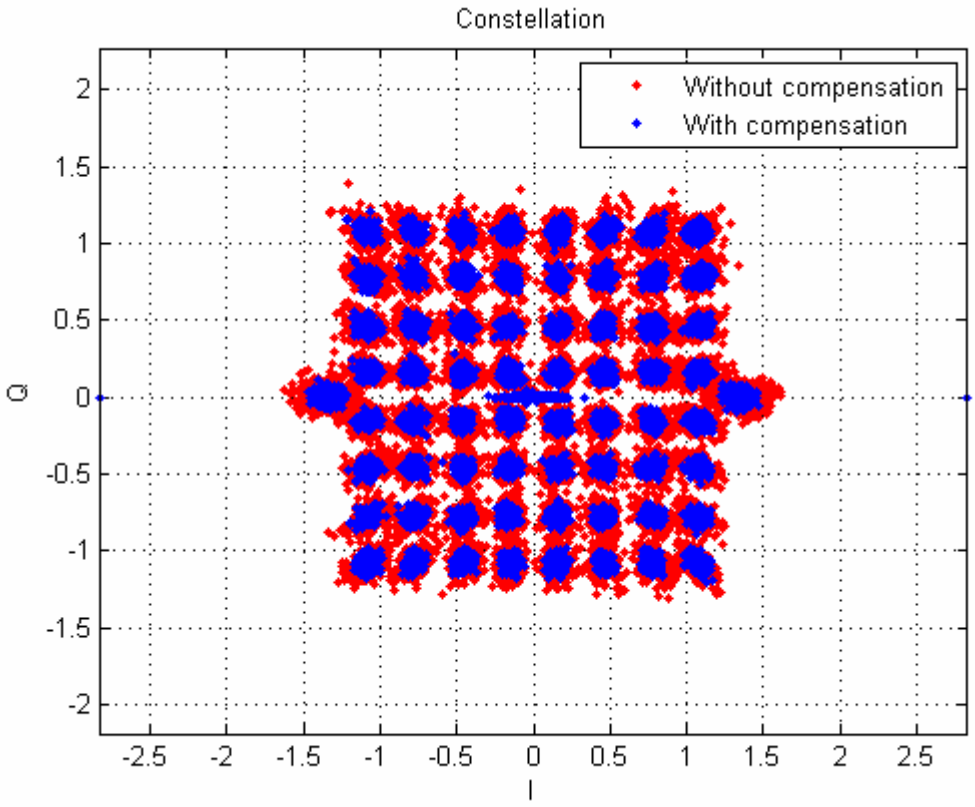

Figure 73 - Constellation without and with compensation

4-3.1.3 Summary

In this paragraph the devices and processing algorithms used in the two compensation architectures has been described.

4-3.2 Post compensation in Rx

Figure 74 diagram shows the strategy of the post compensation algorithm. The first part of preamble is used to synchronize the frames. When the frame is synchronized its preamble is also used for the channel estimation. Once the channel is estimated, the preamble or payload is used to estimate the nonlinearity. This estimation is done by projecting the known sequence on the orthonormal basis created from the memorized (reference) sequence by Gram-Schmidt orthonormalization process (5th order polynomial basis). A few points of the AM/AM and AM/PM characteristics are computed thanks to this polynomial approximation.

The compensation is carried out on signal by applying the inverse interpolation function computed from these points. This function is realized by exploiting a special property of the Lagrange polynomial interpolation. The compensation function (inverse function) is realized by swapping the absisses and ordinates of the interpolation points for the Lagrange polynomial construction. Finally the signal is compensated in the time domain before equalization.

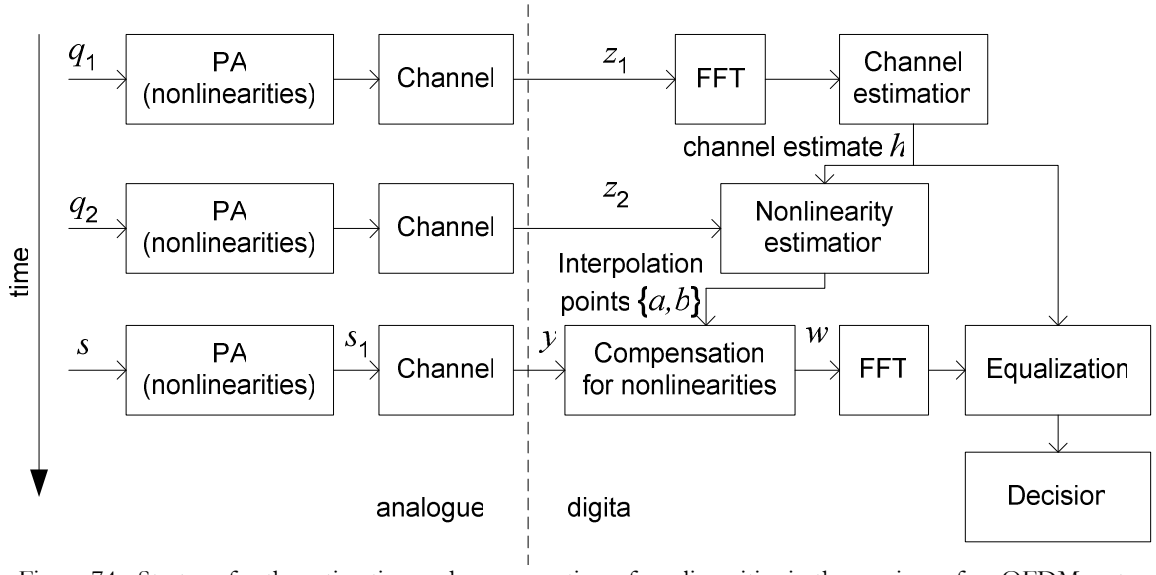

Figure 74 - Strategy for the estimation and compensation of nonlinearities in the receiver of an OFDM system

Figure 75 shows the compensation performances obtained in simulation. 3dB IBO is saved by the compensation algorithm for 64QAM modulation for 3dB SNR degradation. A test bed is presented in the next paragraph and in [66] as a proof of concept and as a performance reference for the hybrid receiver-aided compensation method.

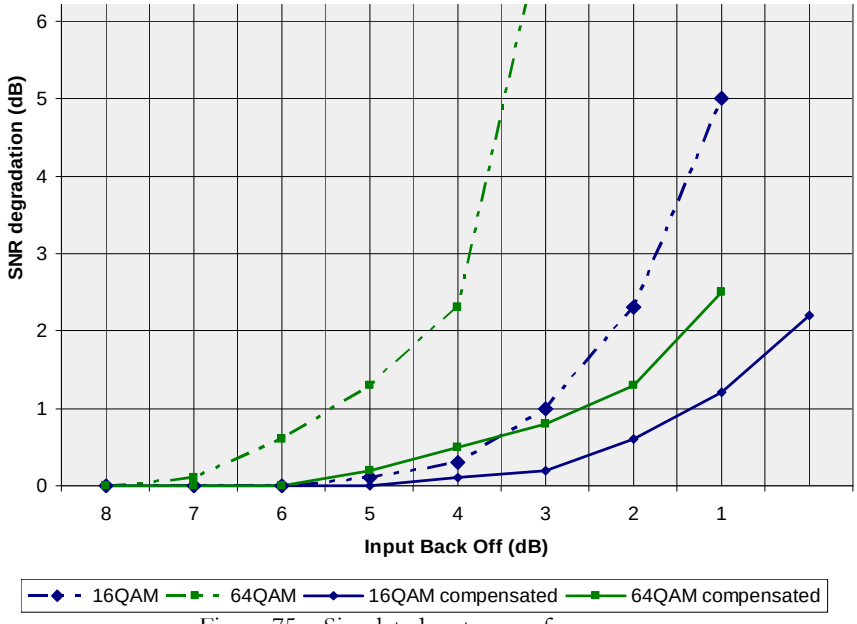

Figure 75 – Simulated system performances

4-3.3 Hybrid receiver-aided compensation method

Figure 76 shows briefly the proposed strategy for compensation of nonlinearity. The estimation of the nonlinearities is carried out in the receiver on a first frame Fr.1 with a training sequence. The reference sequence is memorized in receiver. The estimated parameters are sent back from

the receiver to the emitter thanks to software feedback. Next nonlinearities are compensated on the next frames in the emitter by a classical predistortion on the next frames.

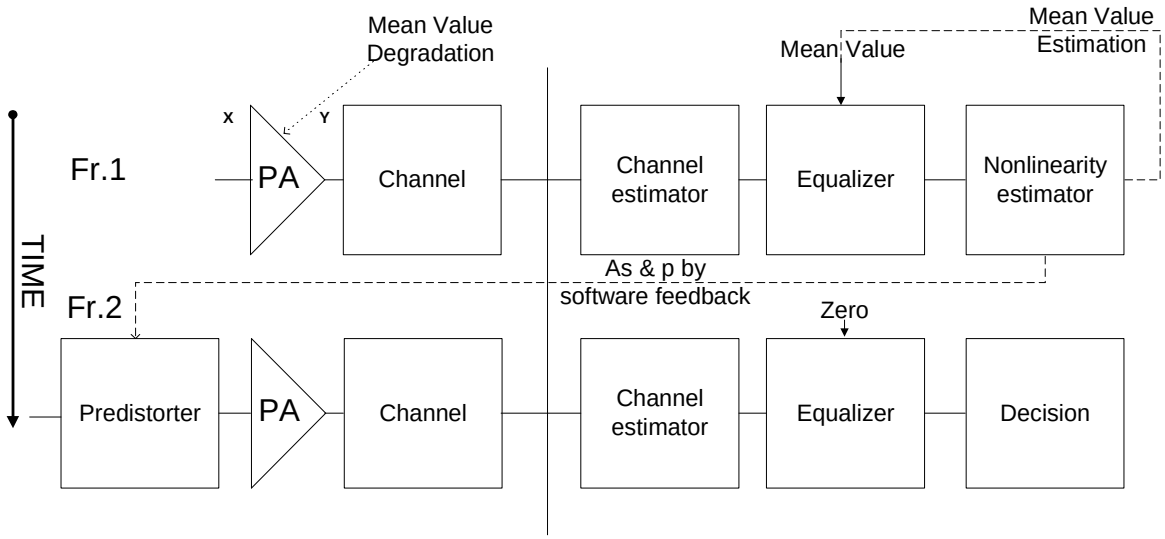

Figure 76 - Strategy for the estimation of nonlinearities in the receiver and compensation in the transmitter of an OFDM system

This architecture is fully described and tested below in the fifth chapter.

4-4 Post compensation in Rx measurements

In this section the measurement test bed is described. Then it was adapted for being used for evaluation of the algorithm in more realistic conditions by measurement in an anechoic chamber.

4-4.1 Measurement test-bed

The test bench schematic is shown in Figure 77. It consists of a vector signal generator Rohde & Schwartz SMJ100A, a power amplifier and a real-time spectral analyzer Tektronix RSA 3408. The generator is considered as a transmitter part of the link, which transmits the IEEE802.16e frames periodically. The frames are generated by Matlab in a PC with parameters in Table 10.

The baseband frames in IQ form are up-converted to 3.5GHz by a signal generator. They pass through the PA, where they are nonlinearly distorted. The signal is acquired by a real-time spectral analyzer, which plays the role of the receiver front-end in this test bed. The IQ baseband signal is recorded and post processed in a PC. The signal is demodulated in baseband. The signal is synchronized in time-frequency, [69]. Channel estimation and channel tracking are done using respectively preamble and pilots. BER is estimated without channel coding (FEC).

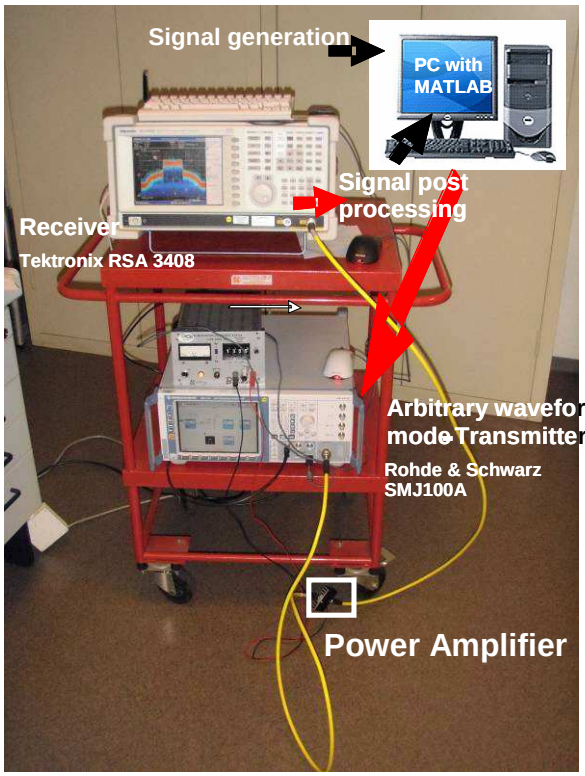

Figure 77 – Test bed

The EVM was measured without PA between 0.4% for low P_{IN} and 0.7% for high P_{IN} when the signal generator was connected directly with the real-time spectrum analyzer. This demonstrated that our test bench is valid and it might be used for further measurements. When inserting the PA in the loop, the EVM raised to 11.3% for 4.2dB backoff for non-compensated signal and 6.7% for compensated signal. Figure 78 shows EVM vs. IBO for compensated (blue) and non-compensated (green) signals. When the IBO was higher than -3.22dB the synchronization did not work, because of the PA saturation, which clipped the pilots.

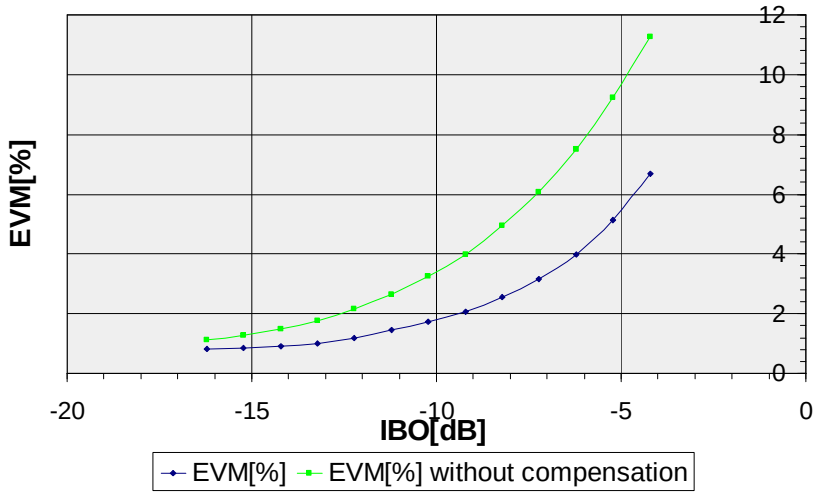

Figure 78 - EVM [%] with and without compensation vs. IBO [dB]

Table 11 shows the IBO gain for different EVM targets for 64 QAM from IEEE 802.16e-2005 standard. The IBO gain is approximately around 3dB.

EVM [%]	IBO_C [dB]	IBO_NC [dB]	IBO Gain [dB]
5,01	-5,33	-8,16	2,83
3,98	-6,22	-9,22	3
3,16	-7,24	-10,35	3,11
1,5	-11,11	-14,13	3,02

Table 11 - IBO gain for different EVM in IEEE 802.16e-2005 standard

4-4.2 Measurement in anechoic chamber

The concept was proven with coaxial cable as perfect channel. The goal of the next measurement was to evaluate the algorithm robustness in realistic channels.

4-4.2.1 Test bench description

The test bench was defined for 4 different channel configurations. At the receiver side the weak signal needs to be amplified. For that purpose the LNA Miteq AFS42-00-101000-20-10P-42 has been chosen. This LNA has a strong gain (47dB), but saturates quickly (-7dBm P_{1DB_OUT}).

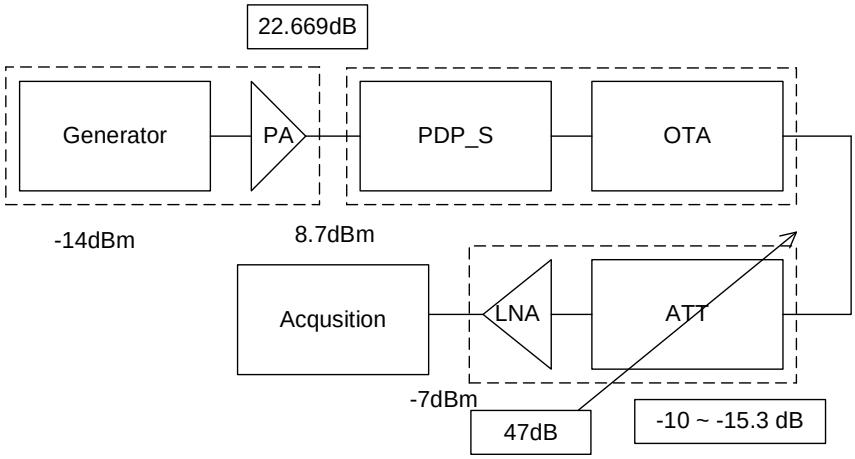

Figure 79 - Budget link

The link budget is shown in Figure 79 for the first channel (flat channel), where OTA is Over-The-Air device and PDP_S is Power Delay Profile synthesizer. The variable attenuator is necessary to control the signal dynamic at the RSA input. The noise factor was calculated in Figure 79 by Friis formula after each component. The noise figure of the attenuator is equal to its attenuation.

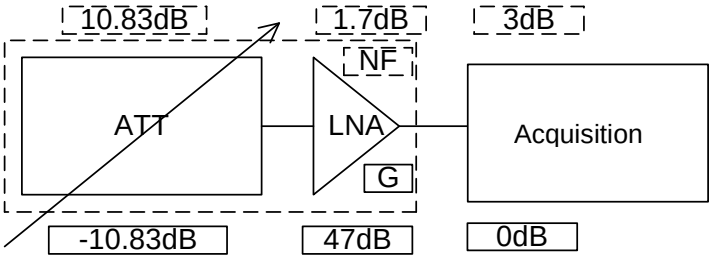

	attenuator	LNA	RSA
Nf	10,83	1,7	3
Gain	-10,83	47	0
NF_DB	10,83	13,13	13,13

	LNA	RSA
Nf	1,7	3
Gain	47	0
NF_DB	1,7	1,70

Figure 80 - Noise figure computation

As expected in Figure 80, the final noise figure with attenuator is strongly degraded compared to the noise figure of chain beginning with LNA only. Because the attenuator is necessary not to saturate the LNA input, different configurations were measured to see when the signal dynamic is degraded at the VNA input.

a) The channel only is shown in Figure 81 a) with P_{MEAN}=-18.3dBm
b) The channel with attenuator and LNA is show in Figure 81 b) with P_{MEAN}=-15.9dBm
c) The channel with attenuation by coaxial cable and LNA is shown in Figure 81 c) with P_{MEAN}=-8.1dBm
d) The channel with LNA only is shown in Figure 81 d) with P_{MEAN}=-5.6dBm

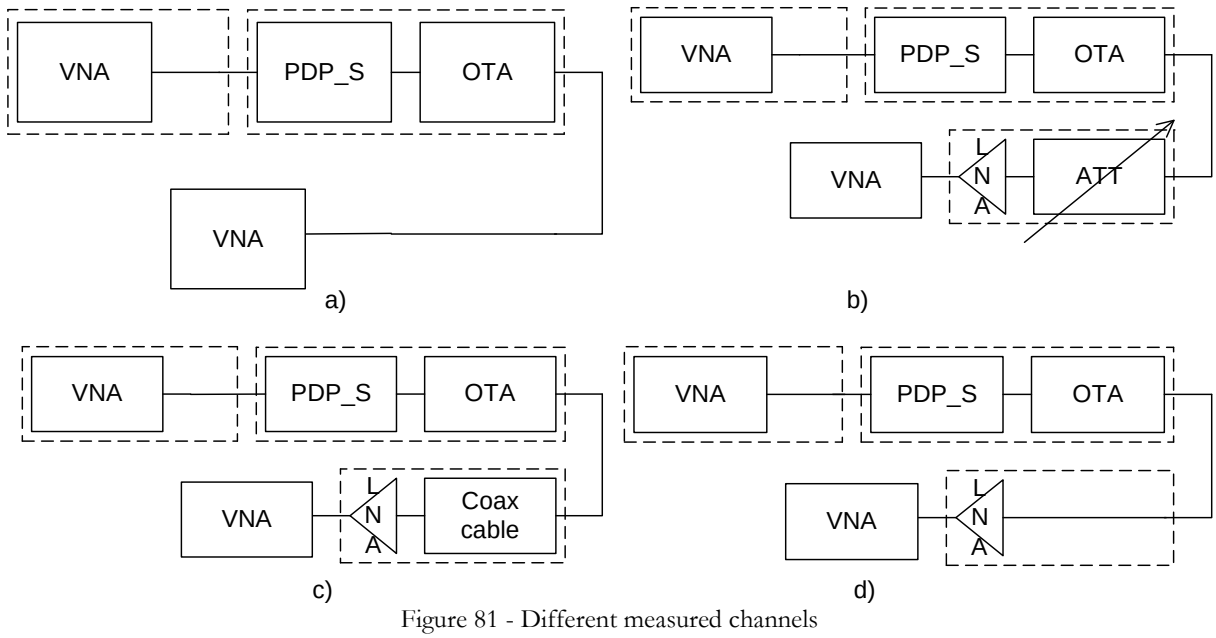

Figure 81 - Different measured channels

Figure 82 shows the measurements by the VNA. The part a) is the amplitude and b) the phase response for each configuration. The noise of the attenuator is clearly visible below -10dBm input power. When the signal is normalized we can see the different variances of the phase and amplitude shown in Figure 82 c) and d).

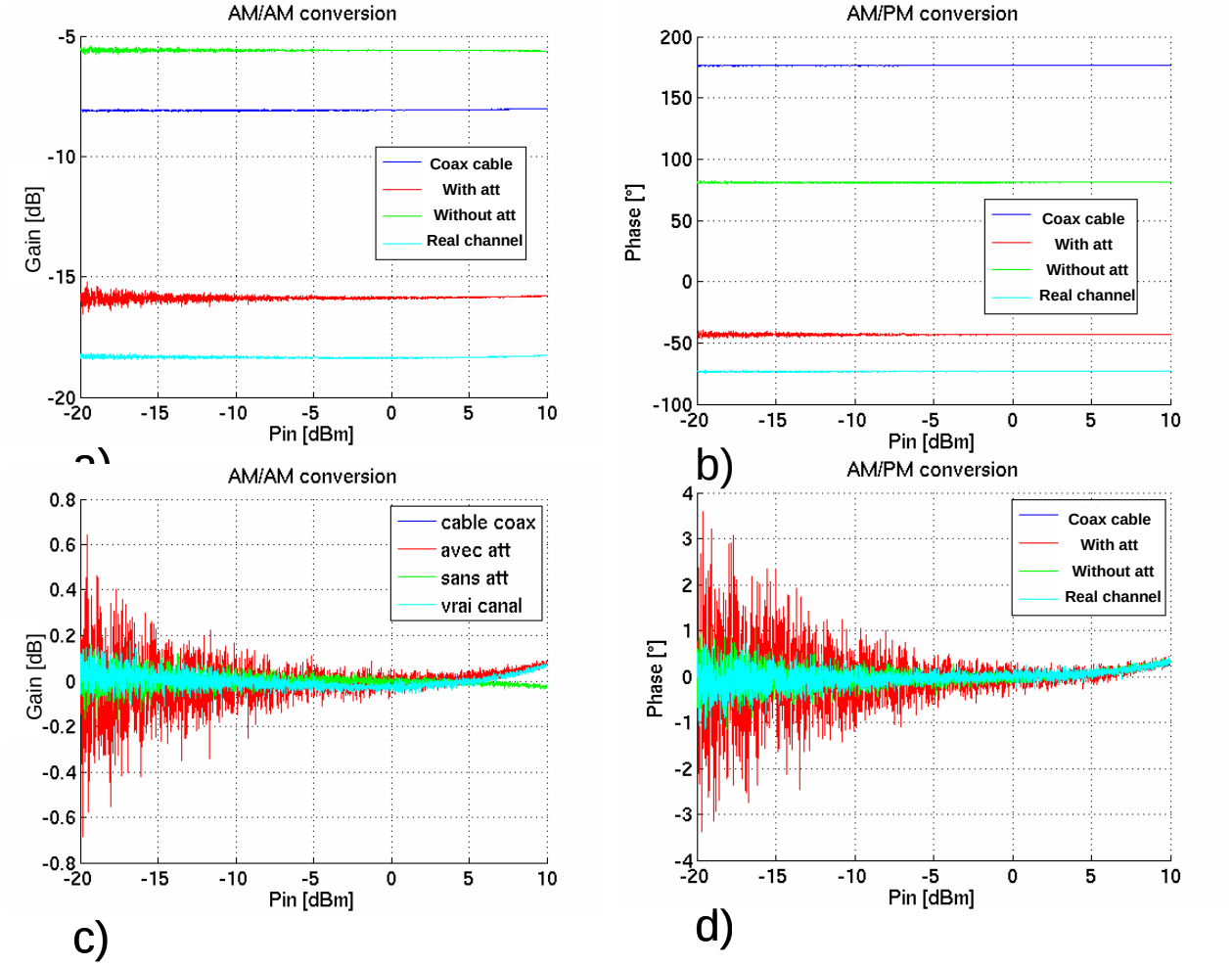

Figure 82 - Measurement a) Amplitude b) Phase c) Amplitude - mean(Amplitude) d) Phase - mean(Phase)

4-4.2.2 Conclusion

The attenuator shall be used only for the c) case (flat channel) to scale the signal to the LNA input dynamic. In case of measurements with other channels, it is better not to use attenuator.

4-4.3 EVM measurement

EVM measurement has been carried out in three synthetic channels. The goal of this measurement was to see the impact of the realistic channel on the degradation of the parameter estimation and thus the EVM after compensation.

4-4.3.1 Channel generation

Synthetic channel representative of 3.5GHz WiMax environment has been created cascading Over The Air (OTA) propagation with multiple antennas and reverberant box as described in Figure 84. The signal is amplified, sent to the emitter antenna and received by 4 directive antennas (creating multipath condition). The 4 signals are then combined and pass through a reverberant box (which spread the received signal) before being processed in PC. The angle of

the emitting antenna can be shifted to create different channel condition. Three channels are thus generated as test benches (Figure 83).

The first channel (Figure 85 a)) corresponds to Line Of Sight. According to the previous measurements, an attenuator is added so that the LNA works in its linear zone. The channel n°2 (spread channel with 0° antenna shift) and n°3 (spread channel with 45° antenna shift) correspond to multipath channels (According to the previous measurements no attenuator needed). Their impulse response appears respectively in Figure 85 b) and c). The obtained spread is quite short compared to the sampling period (78,1ns).

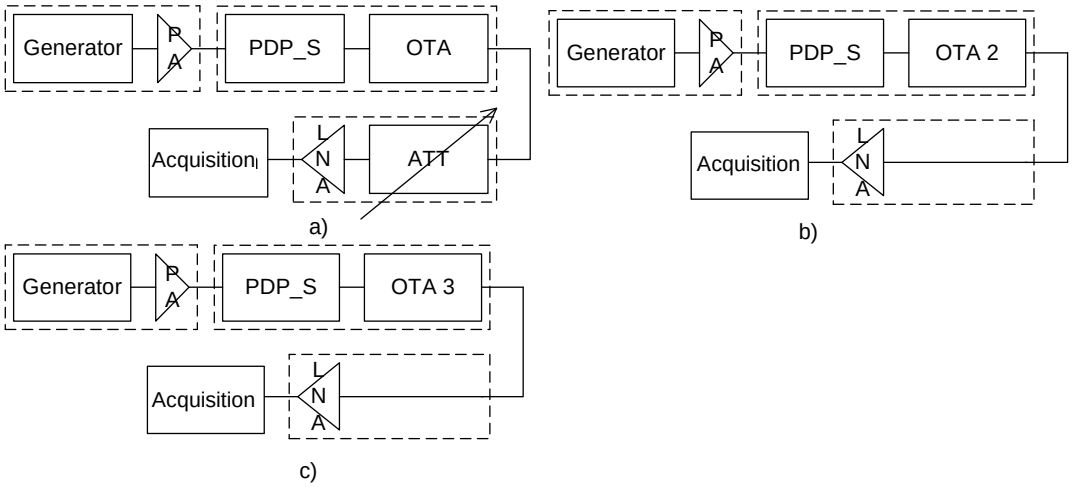

Figure 83 - Schematic of measurement for the different channels

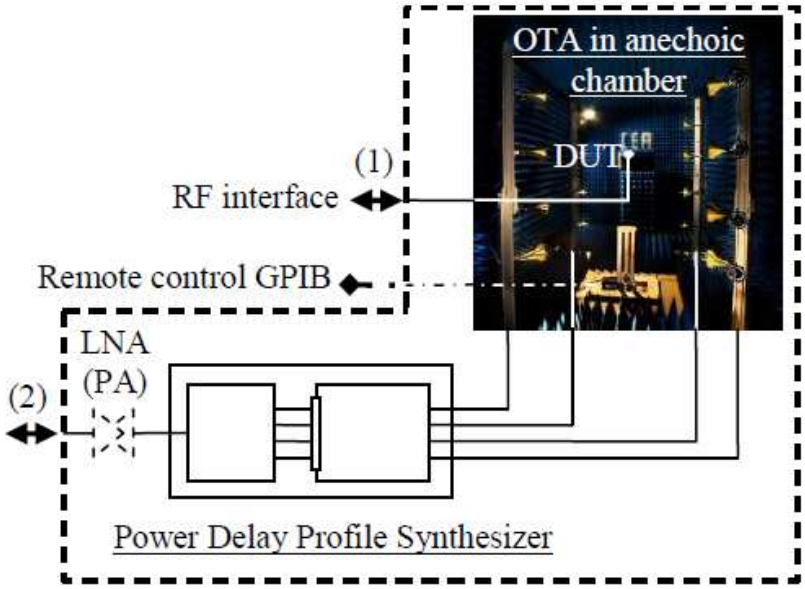

Figure 84 – OTA model [70]

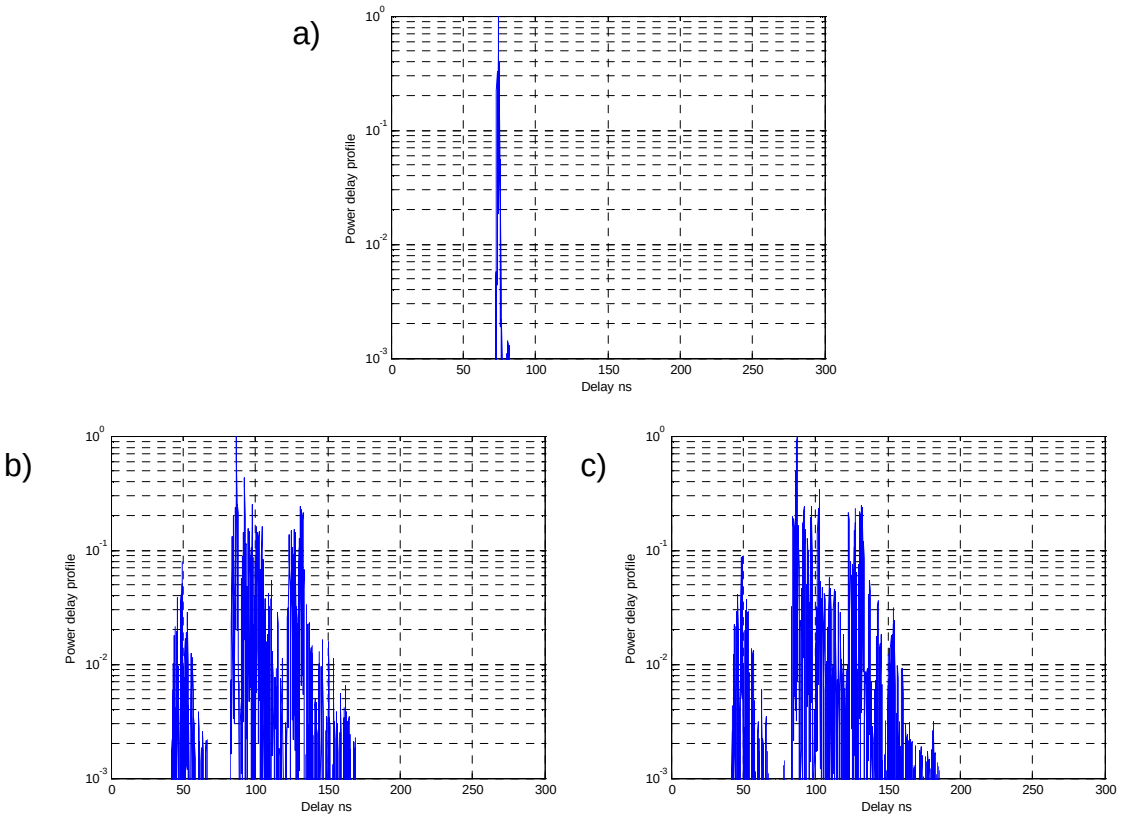

Figure 85 - Channels used for the measurement a) flat channel b) spread channel 0° c) spread channel 45°

Table 12 shows the RMS delay spread in nanoseconds. The multipath and delay spread create frequency fading as drawn in Figure 86. Over the 10MHz bandwidth around 3.5GHz, the channel response can be managed by the equalization. However the received training sequence or payload used for nonlinearity estimation can be biased by this impulse response.

	RMS delay spread [ns]
Flat	7
Spread ϕ=0°	23
Spread ϕ=45°	25

Table 12 - Channel RMS delay spread

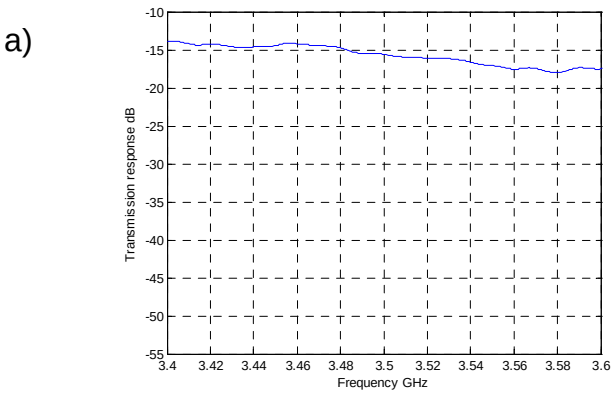

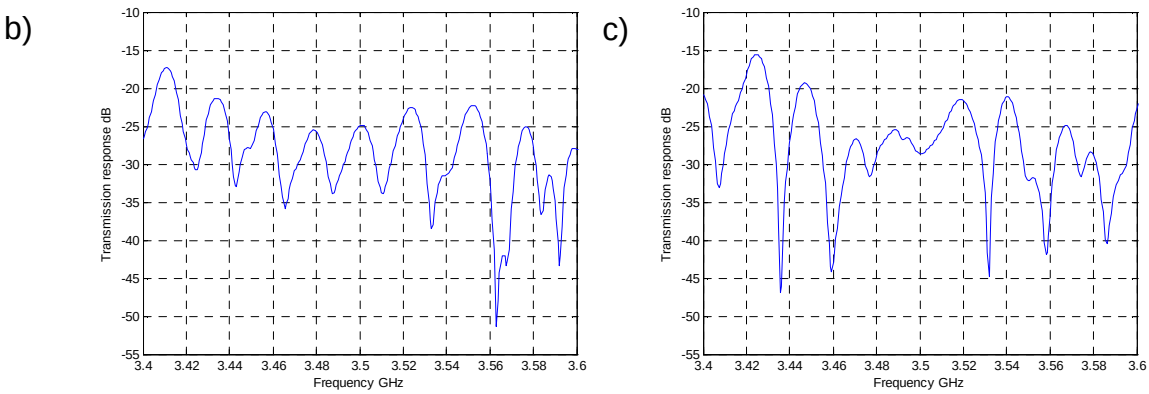

Figure 86 – Frequency transfer functions of channels used for the measurement a) flat channel b) spread channel 0° c) spread channel 45°

4-4.3.2 EVM measurement for the different channels

.Figure 87 shows the EVM for the reference (flat channel) non compensated signal (red), non-compensated signal affected by channel (blue) and post compensated signal (pink).

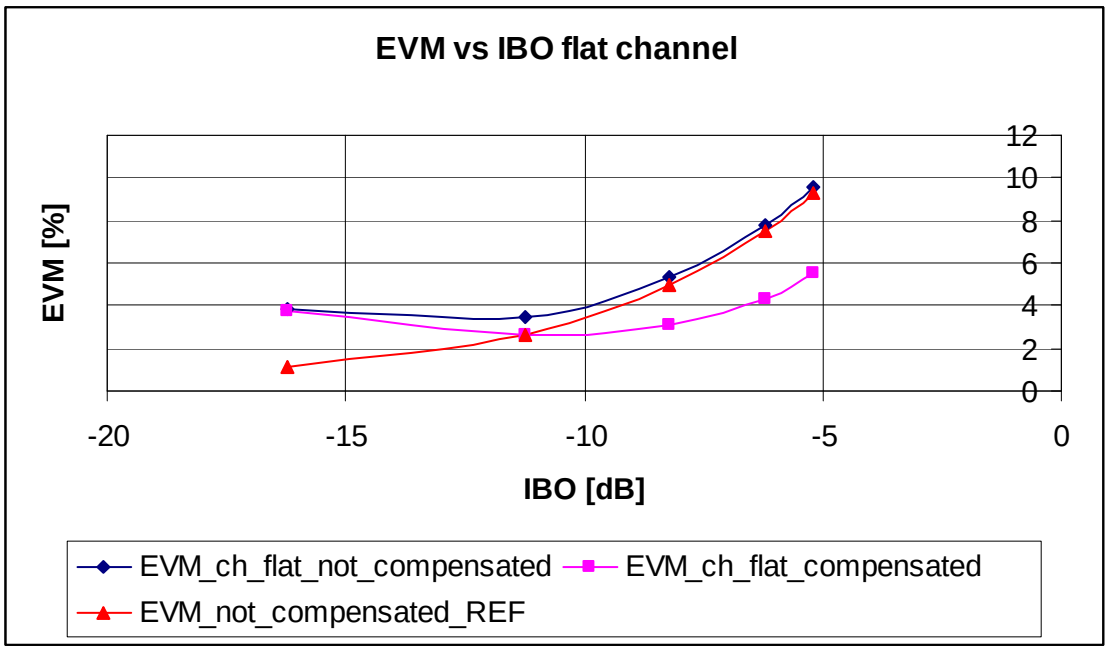

Figure 87 – EVM measured for flat channel

Table 13 shows the different values of IBO for nonlinearity compensated and non compensated signal in flat channel for different EVM requirement. IBO gain is around 2.5dB.

For low power signals (IBO around -15dB) the EVM is degraded by the noise floor (low SNR).

EVM [%]	IBO_C [dB]	IBO_NC [dB]	IBO Gain [dB]
5,01	-5,55	-8,16	2,61
3,98	-6,75	-9,22	2,47
3,16	-7,99	-10,35	2,36

Table 13 - IBO gain in channel 1 for different EVM in IEEE 802.16e-2005 standard

Figure 88 shows the compensated, non-compensated and reference EVM for spread 0° channel, with the different values of IBO in Table 14. The IBO gain is around 2.5dB also.

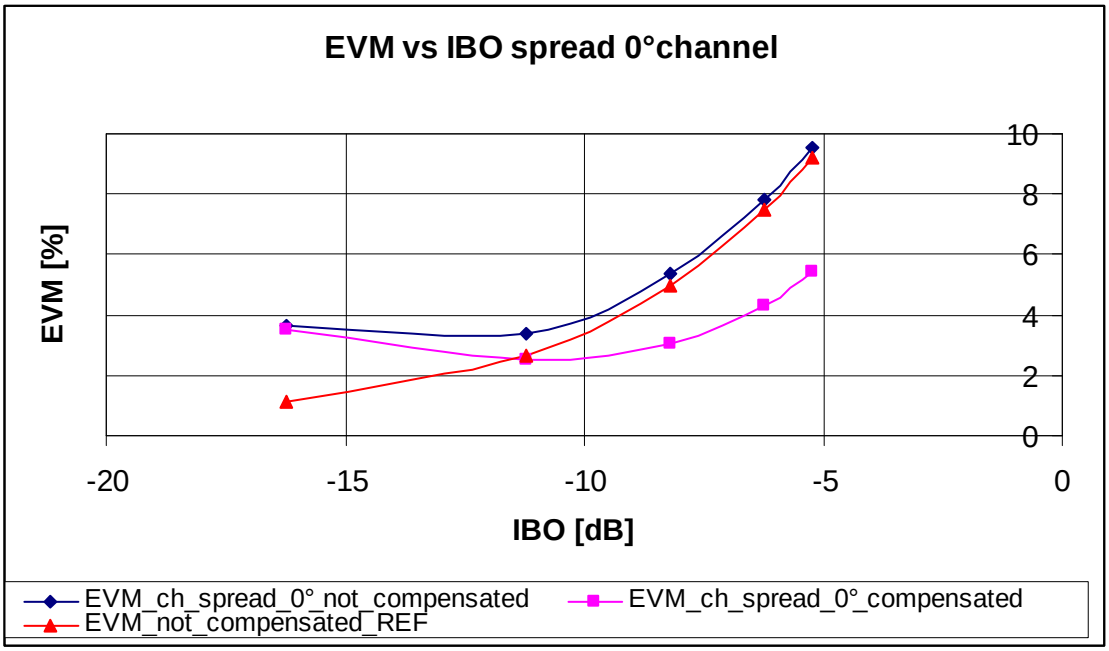

Figure 88 – EVM measured for spread channel 0°

EVM [%]	IBO_C [dB]	IBO_NC [dB]	IBO Gain [dB]
5,01	-5,5	-8,16	2,66
3,98	-6,71	-9,22	2,51
3,16	-7,94	-10,35	2,41

Table 14 - IBO gain in channel 2 for different EVM in IEEE 802.16e-2005 standard

Figure 89 shows the compensated, non-compensated and reference EVM for spread 45° channel, with the different values of IBO in Table 15. The IBO gain is around 2.5dB also.

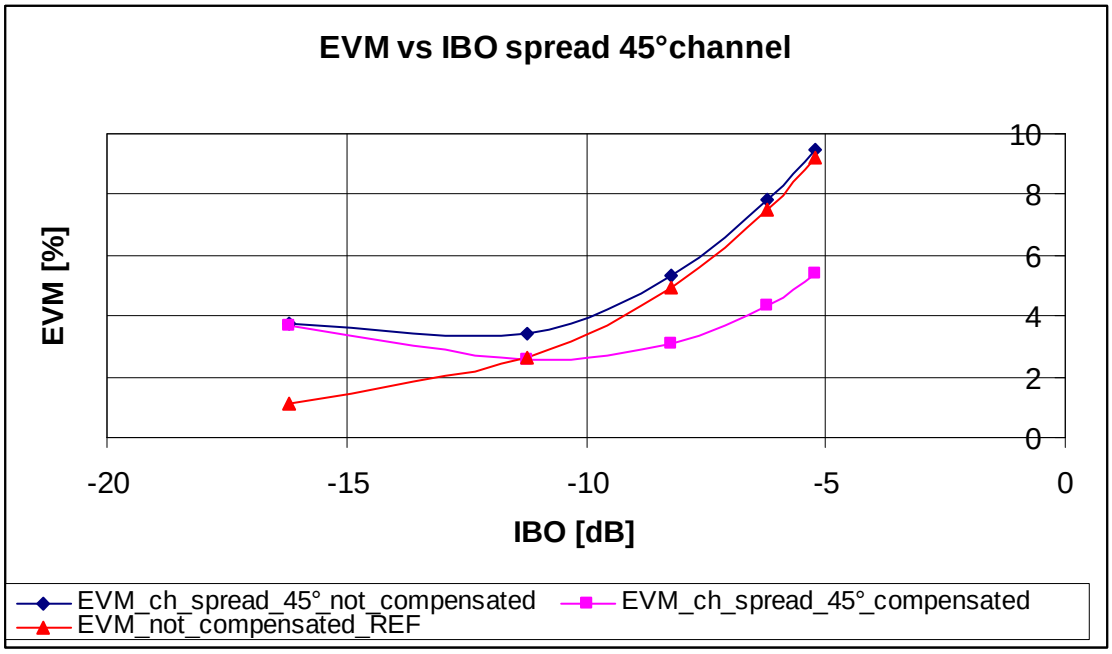

Figure 89 – EVM measured for spread channel 45°

EVM [%]	IBO_C [dB]	IBO_NC [dB]	IBO Gain [dB]
5,01	-5,5	-8,16	2,66
3,98	-6,76	-9,22	2,46
3,16	-8,01	-10,35	2,34

Table 15 - IBO gain in channel 3 for different EVM in IEEE 802.16e-2005 standard

The targeted WIMAX application requires 3% EVM. Without compensation, results highlight that more than 10dB IBO can be required to comply with the standard. These results shows that IBO can be reduce to 7,5dB with our method, whatever the propagation channel impairment.

4-4.3.3 Conclusion

The algorithm shows its robustness for the estimation and correction of the nonlinearty in the different considered channels. One can expect around 2.5dB IBO reduction for the same EVM when using the post compensation algorithm. However the IBO applied to the emitted signal shall make the emitted power spectral power density compatible with the spectrum mask of the standard.

4-5 Hybrid receiver-aided architecture

Hybrid receiver-aided architecture is investigated in this chapter. Firstly the feasibility of using a software feedback of the nonlinearity parameters is studied for WiMAX and LTE standards. The special properties of Rapp's model were used for the estimation of the nonlinearity model with fixed-point computation. Finally the simulations are proven with model approximation.

4-5.1 Software Feedback

Information about nonlinearity has to be transmitted by appropriated messages in MAC layer from the receiver to the emitter side. This exchange has not been forecasted by current standards. However we have tried to guess how it could be managed with WiMAX and LTE standard.

An example is shown on Figure 90 a) for WiMAX. The dialogue exchange consists of sending a message already included in the standard 802.16e [80] as Feedback polling information element (IE). The mobile or relay station estimates the nonlinearity and sends it back to the base station by message Feedback header using the non-used bit fields of the message. An other dialogue exchange is shown in Figure 90 b) for LTE. For the downlink and uplink a nonlinearity compensation request should be set as a mechanism similar to channel quality indication (CQI) mechanism described in [71]. It needs to append one bit into DCI which indicates the "NL_estimation" request which is transmitted in the Physical Downlink Control Channel (PDCCH). The PA model parameters are sent back in an appropriate new message. Its format is the same as the reply message which contains a part of the channel matrix CQI (20 bits available).

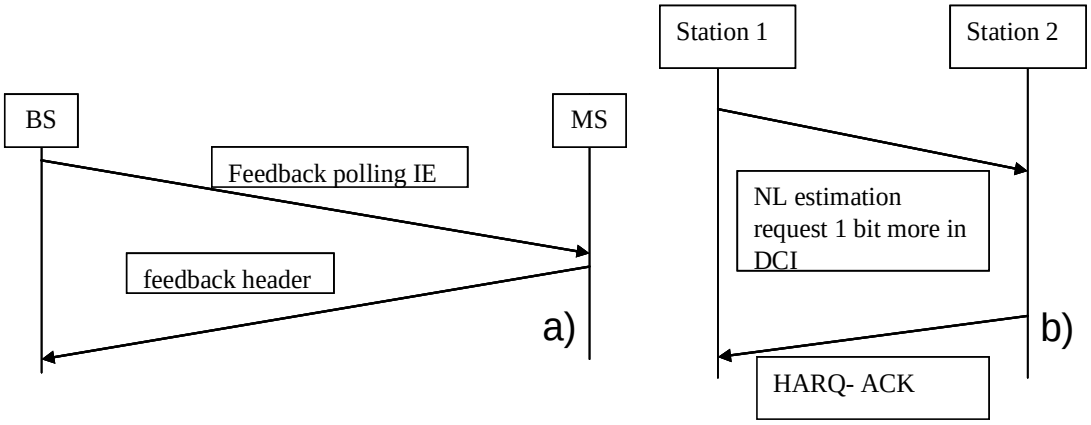

Figure 90 - MAC layer nonlinearity transfer dialogue a) 802.16e DL b) LTE

Table 16 proposes a classification of the compatibility of these mechanisms to the considered current standards. If the mechanism demands only the use of reserved bits, it corresponds to class1 (feedback feasible without modification). If a modification of existing messages is required, it falls in class 2. Otherwise if it demands the creation of a new dialogue or a new message, it corresponds to class 3. The details for other standards might be found in [72]. As a result the feedback of nonlinearity parameters is now only compatible with WiMAX for the downlink case. The future "green radio" standard should add dedicated fields in their dialogue messages for the transfer of power level, channel state information and also nonlinearity parameters to help optimizing the network's overall power consumption.

802.16e	DL	1
	UL	3
802.16j	DL/UL	3
LTE	DL	2
	UL	2

Table 16 – Compatibility of the MAC Layer Message Dialogues of Different Standards Regarding Software Feedback

4-5.2 Error function

The Rapp's model has two parameters to estimate, As and p. These parameters are dependent and related with Eq. 61, where X is the reference signal power and Y is the received signal power.

$$|As| = \frac{\sqrt{X \cdot Y}}{\sqrt[2p]{X^p - Y^p}} \qquad \text{Eq. 61}$$

The problem of nonlinearity estimation is defined as a two constant estimation from a signal having $\chi 2$ distribution which is derived as a squared sum of normal distributions. A survey on this topic can be found in [73]. Because of the ease of error calculation directly from measured and reference data, Mean Square Error (MSE) was chosen as the optimization criteria. Analytical function for perfect channel H=1 is given by Eq. 62.

$$MSE = \left(\frac{X_{power}}{\left(\left(1 - \left(\frac{X_{power}}{\hat{A}s^2} \right)^{\hat{p}} \right)^{\frac{p}{\hat{p}}} + \left(\frac{X_{power}}{As^2} \right)^p \right)^{\frac{1}{p}}} - X_{power} \right)^2 \qquad \text{Eq. 62}$$

Where Âs and $\hat{p}$ are the estimated parameters and As and p are the parameters of the model.

Finding the analytical solution of Minimum MSE leads to compute the partial derivative of the MSE function of Âs and $\hat{p}$. The obtained Jacobian matrix is badly conditioned since the parameters are correlated, which prevent its inversion. To tackle this minimization of MSE, an adaptive algorithm is proposed as an alternative.

Figure 91 shows the MSE function computed analytically. The minimum MSE appears in yellow.

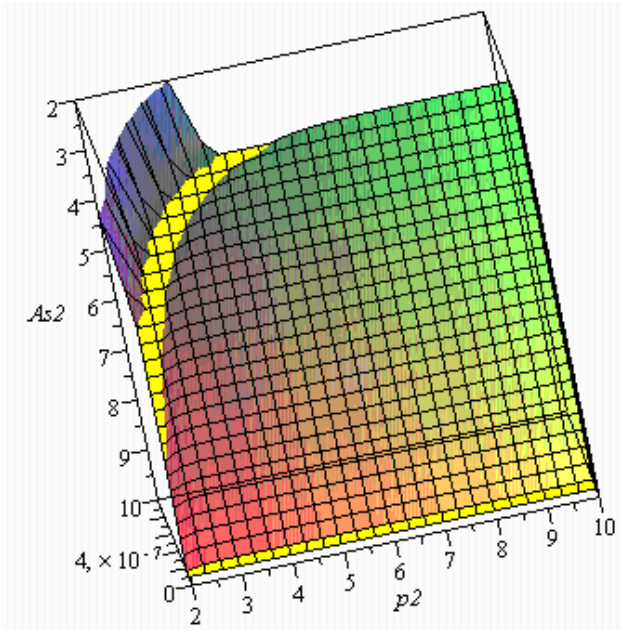

Figure 91 – MSE function

As and p have an asymmetrical impact on the MSE as it appears from Figure 91, looking on the intersection of the multicolored plane and the yellow plane. Due to As and p dependency it is difficult to estimate the minima, but if the As and p parameters are estimated only on an interval and not on all of the values from $-\infty$ to $+\infty$ the dependency became an advantage, because the model is always able to describe the power amplifier nonlinearity with low MSE. This property is important for parameter estimation algorithm robustness.

4-5.3 System Modeling

In order to carry out the estimation without bias, the gain degradation due to PA nonlinearity has to be taken into account and the modified mean value to be introduced into the nonlinearity estimation and in the OFDM equalizer, for the first frame Fr1. For the next corrected frames equalization can be carried out directly.

The bias of the gain due to the nonlinearity was analyzed in the last chapter in the section on system modeling for 802.16 signals.

The estimation algorithm is based on finding the minimum error given by Eq. 62. Finding the minimum in an analytical way was too complex; hence a numerical method is used. Also finding the minimum by 2D Lest Mean Square algorithm is complex to implement because it means handling a Jacobian matrix. Moreover, As and p have an asymmetrical impact on the MSE.

As it appears from Figure 91, looking on the intersection of the multicolored plane and the yellow plane, the minimum is larger in the As axis, hence easier to find with less iterations.

Hence an imbricated two loop dichotomy and Least Mean Square algorithm is proposed. Dichotomy is used to estimate the Âs parameter, while an adaptive LMS algorithm [74] is applied to find p, through Eq. 63. Thanks to LMS algorithm the aliased noise is reduced; hence the ADC in the receiver needs to cover only the channel bandwidth.

$$\hat{p}(n+1) = \hat{p}(n) + \mu \cdot x(n) e^{*}(n) \qquad \text{Eq. 63}$$

The residual mean square error depends on allowable algorithm complexity; as detailed in the next chapter. The algorithm stops when the residual error falls below -24,5dB. If the algorithm succeeds, the nonlinearity model fits with the nonlinear PA behavior with good precision.

Figure 92 shows the measured payload (red points) fitted with the Rapp model (blue points) using the 1D-LMS-dychotomie algorithm.

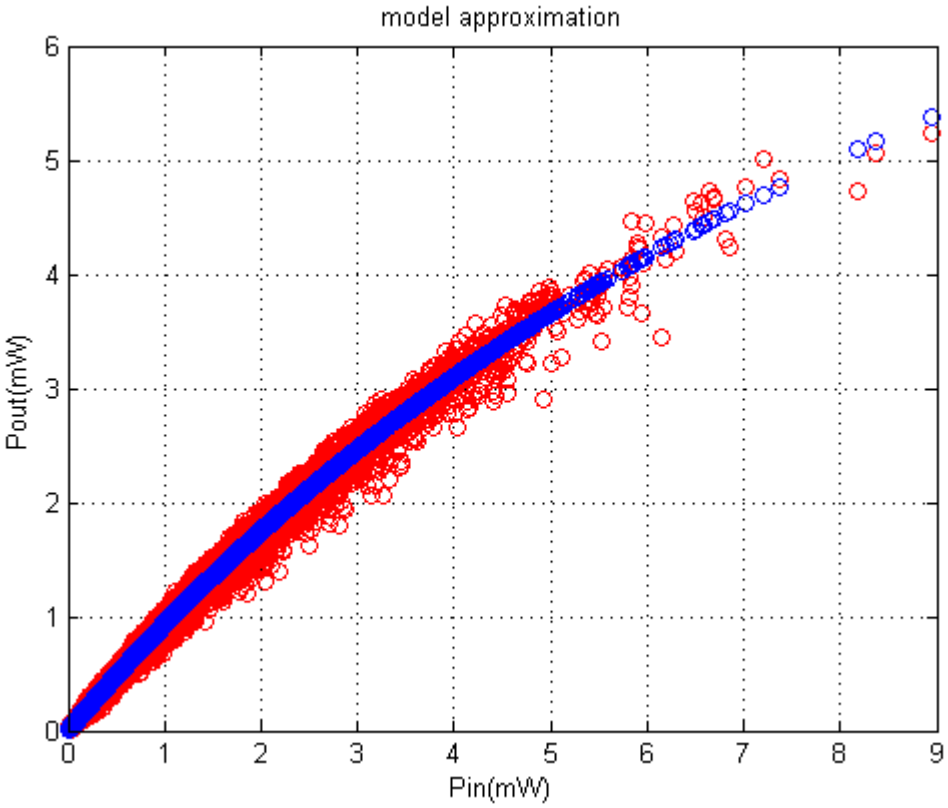

Figure 92 – Model Fitting

The algorithm was simulated for a WiMAX system in fixed point with 8 bit precision for predistorted signal and 7 bit for non-predistorted signal. The mean square error of estimation was -25.7dB. The signal EVM at receiver output was 2.3%, for 6 dB IBO.

4-6 Proof of concept of hybrid architecture

In this paragraph the concept of receiver-aided architecture is proven by measurements, firstly with coaxial cable and then in the anechoic chamber with multipath propagation. The signal is pre-processed in Matlab in fixed point arithmetics.

4-6.1 Test Bed

Hybrid architecture uses a modified existing test bed. Figure 93 shows the test bed. It is composed of an arbitrary waveform generator R&S SMJ 100A which outputs the 802.16 signals generated by Matlab on a PC quantified on 7 bits.

In the first step, the reference signal passes through a nonlinear power amplifier, where it is distorted. The distorted signal is acquired by the Tektronix RSA 3408. All data are pre and post processed in the PC with Matlab, where the parameters are extracted using the 1D-LMS-Dychotomy algorithm given by Eq. 63.

In the second step, the parameters are used to predistort the signal in Matlab. The predistorted frame is loaded into the SMJ 100A, quantified on 8 bits. The signal passes through the nonlinear PA and is again acquired by the RSA 3408. Finally the signal is processed on PC to measure the EVM.

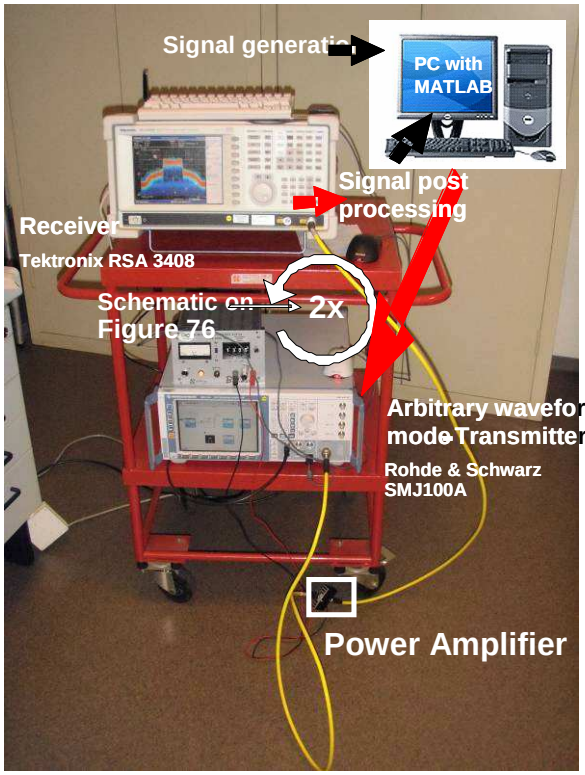

Figure 93 – Hybrid architecture test bed

4-6.2 Results

Figure 94 shows the result of the measurements, for non compensated EVM (blue) and compensated EVM (magenta), function of the power back off of the amplifier. For a target EVM of 3%, the reduction of IBO reaches 2.1dB (Table 17).

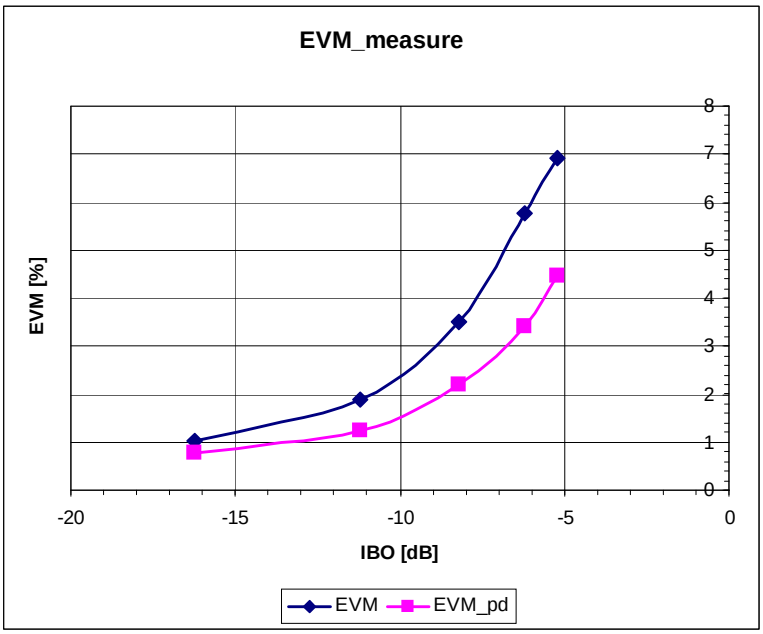

Figure 94 – Measured EVM with coax cable

EVM [%]	IBO_C [dB]	IBO_NC [dB]	IBO Gain [dB]
5,01	-4,62	-6,68	2,06
3,98	-5,65	-7,78	2,13
3,16	-6,63	-8,79	2,16

Table 17 - IBO gain in coaxial cable as channel for different EVM in IEEE 802.16e-2005 standard for receiver aided architecture

4-6.3 Over-The-Air (OTA)

After a first proof of concept on a wired link, the algorithm has been verified through a synthetic channel with a variable fading depth in 10MHz bandwidth around 3,5GHz. A principle for emulating a channel is described in [75]. In our case, the channel with fading is emulated by 2 different paths, Light of Sight (LOS) path and Non Light of Sight (NLOS) path. The total impulse response is given by the amplitude and delay of the NLOS path compared to the LOS path.

The fading deep is set by a variable attenuator and the delay is set by a lossy coaxial cable with length equal to 18.75m (Figure 95 – Schematic of OTA), creating a delay of 90ns. The specification of the OTA elements have been computed from the link power budget, as detailed in [75]. The IBO range of interest (-9,2dB; -5,2dB) is selected so that distortions and noise impact on the signal are negligible.

As a first characterization of the OTA, the nonlinearity was checked using a two tone signal. Depending on the configuration of the OTA, IIP3 at the input of test bed was measured at 23-25dBm which is equal to the IP3 of SMJ. This guarantees that the signal is not distorted by the OTA.

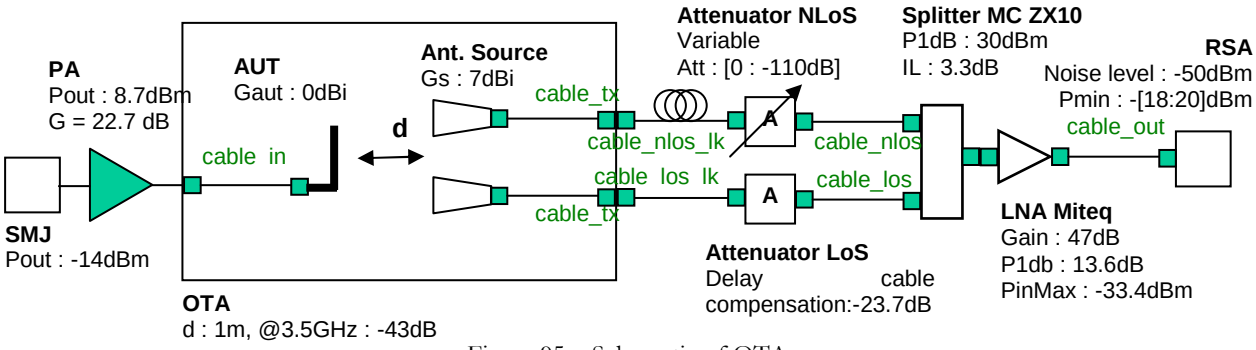

Figure 95 – Schematic of OTA

Figure 96 shows the whole test bed on red trolley. The test bed is connected with OTA components, detailed in Figure 96. The components are described in schematics in Figure 95.

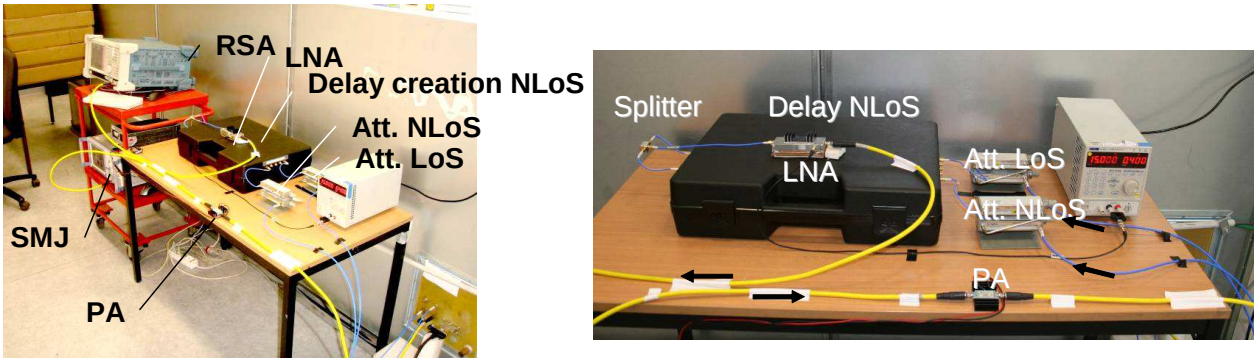

Figure 96 – Test Bed photographs

Figure 97 a) shows the schematic of testsetup inside the anechoic chamber. The photograph of two path propagation channel in anechoic chamber is in Figure 97 b).

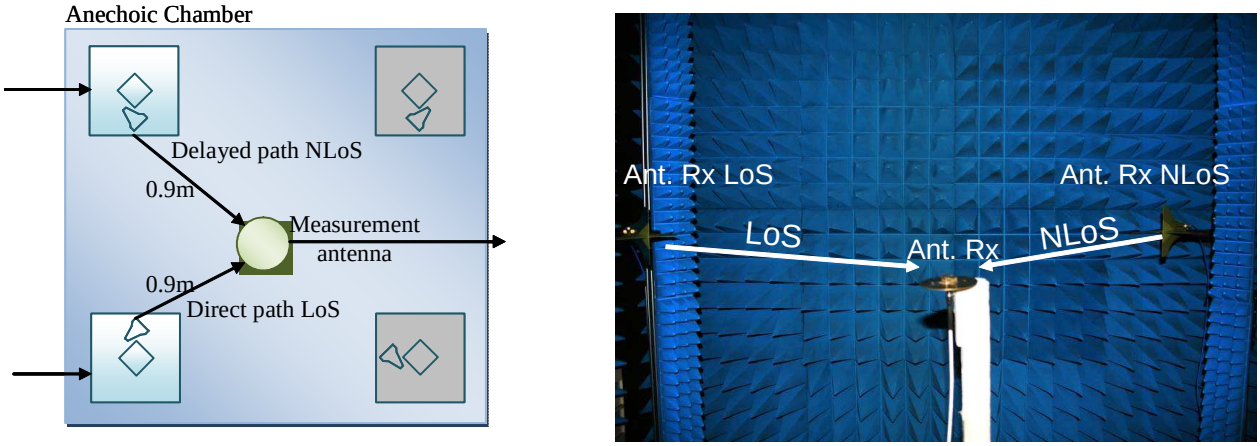

Figure 97 – a) OTA schematics b)OTA photograph

Figure 98 shows the generated channels with different fading values. Because the delay is 90 ns, the fading is created by the destructive combination of the LOS and NLOS paths in the middle of the channel bandwidth and constructive combination in the borders of the channel bandwidth.

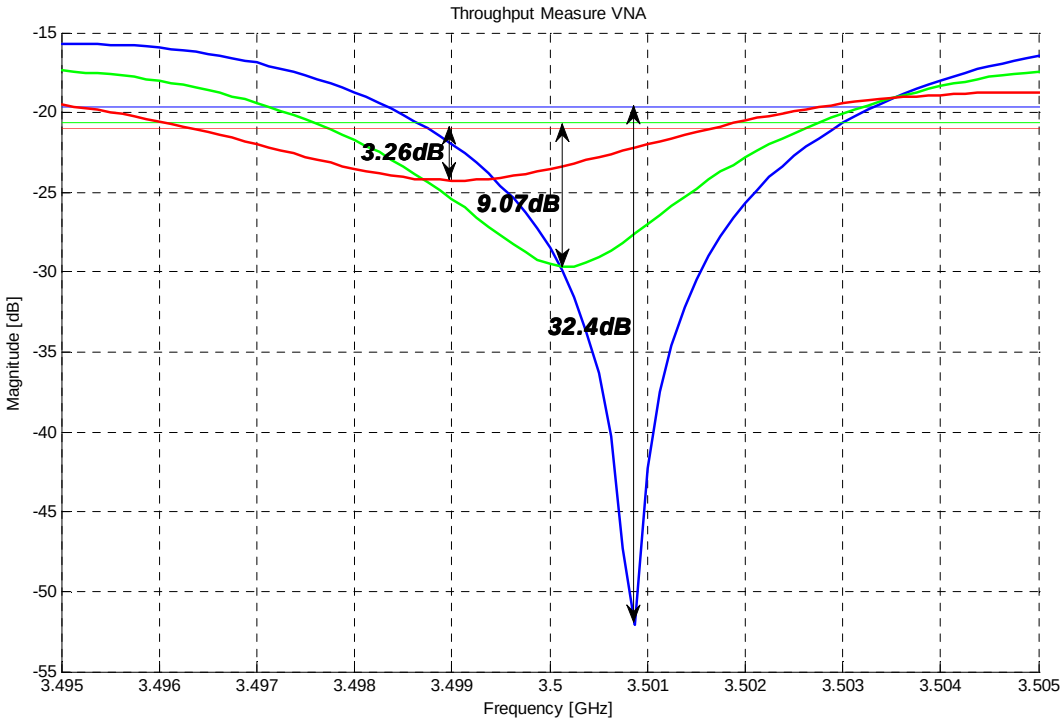

Figure 98 – Generated channels with different fading

Figure 99 shows the delay between the LOS path and NLOS path. With 12,8MHz sampling frequency, the delay of 90,2ns corresponds to about one sample. Cyclic prefix is 64 samples; hence the fading was created by phase constructive and destructive combining. Hence the flat channel has lower mean magnitude than channel with 30dB fading.

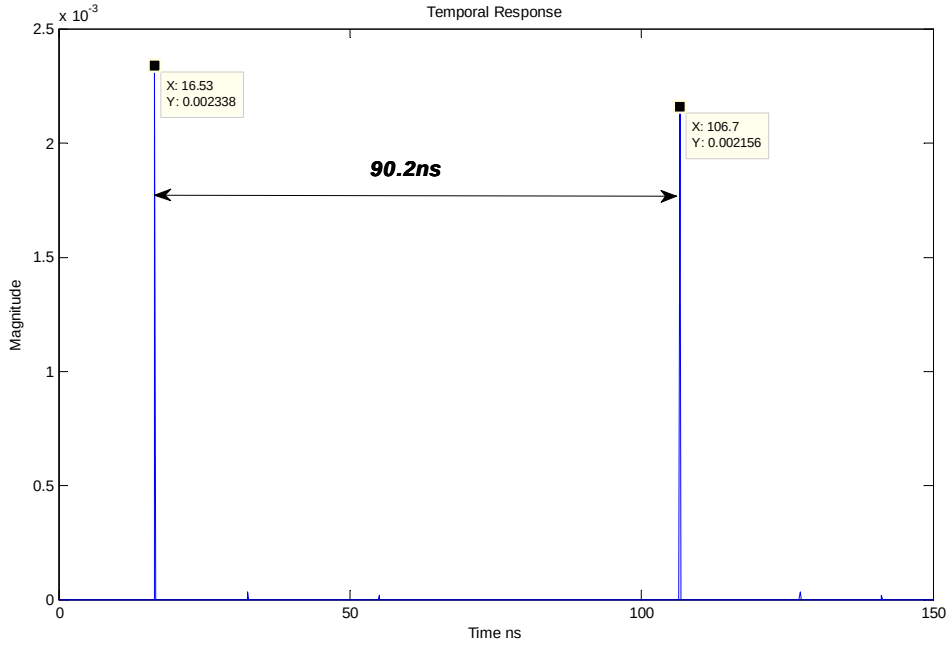

Figure 99 – Measured LOS and NLOS path delay

Figure 100 shows the printscreen from RSA before signal acquisition with the different fading values.

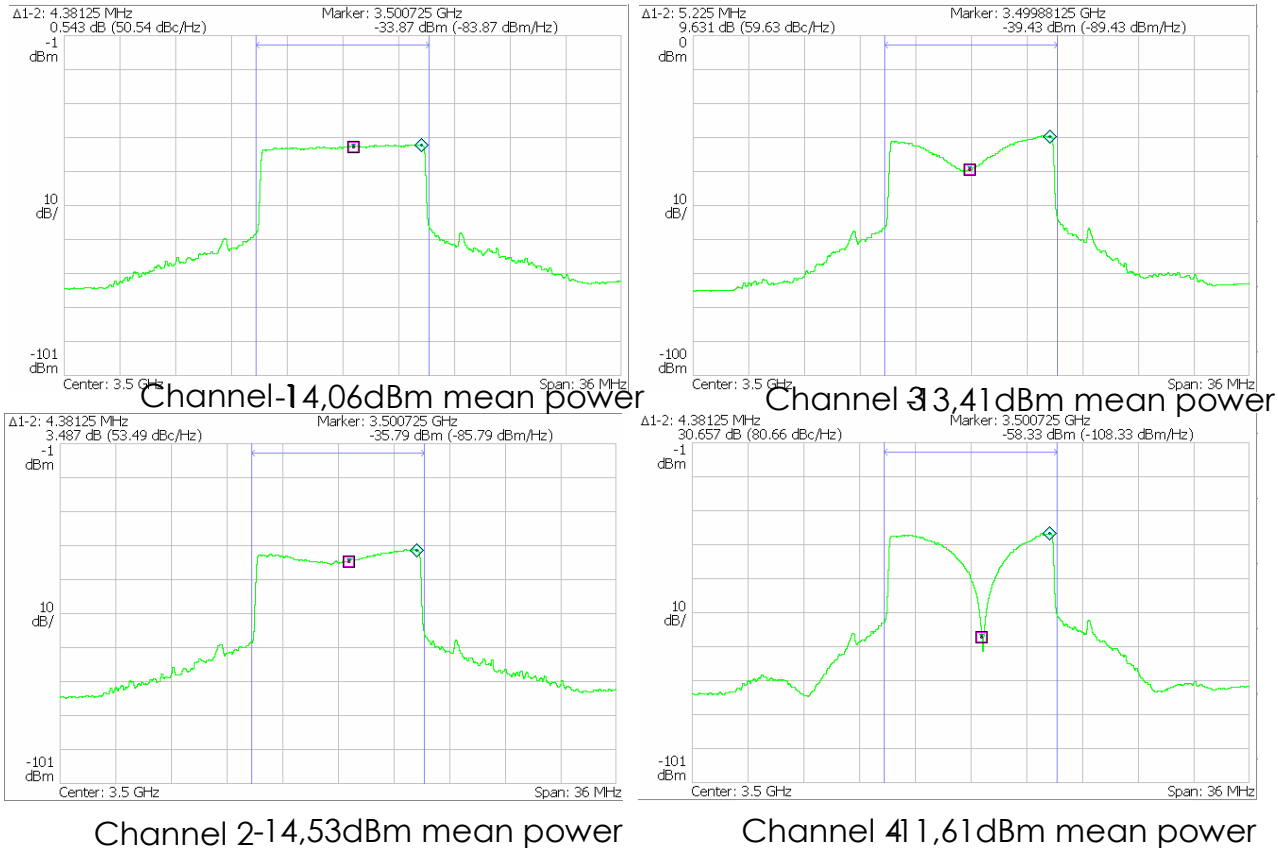

Figure 100 – Fading measured on RSA

The channels were emulated to approximate the scenarios of Figure 101 as defined in the first chapter. Strong fading corresponds to strong NLOS configuration. Fading relies on the phase of major similar power paths. Hence multipath propagation has larger probability of fading in the communication channel.

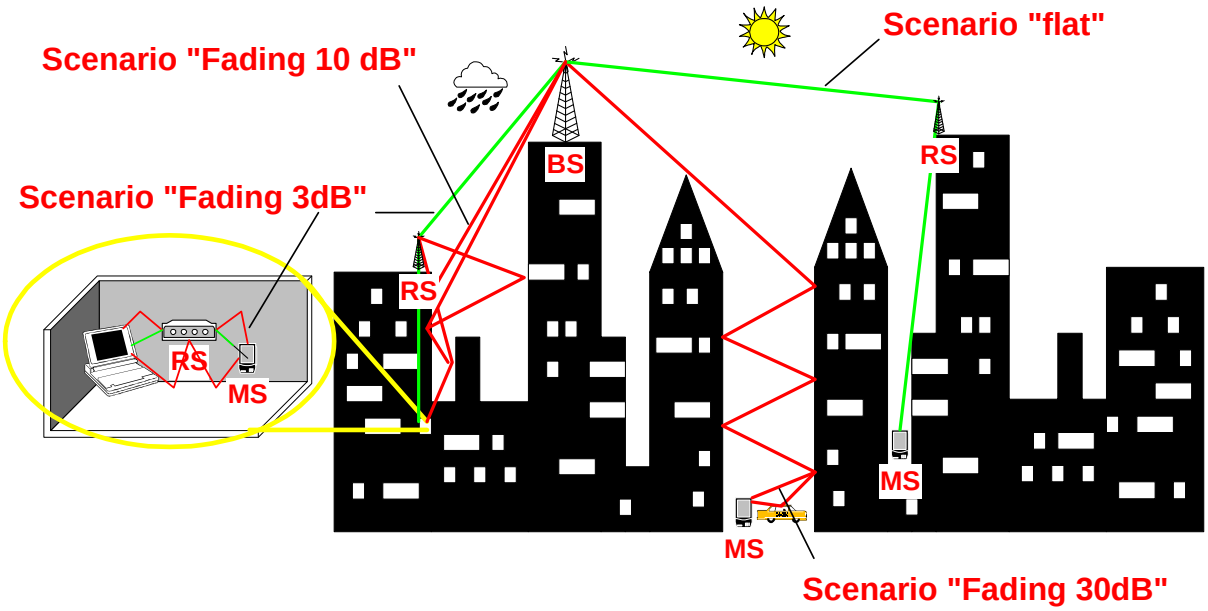

Figure 101 – Scenarios of channels with fading

Figure 102 shows the receiver-aided architecture compensation strategy with the different EVM measurement points.

- The red arrow gives the measured reference EVM. This measurement is carried out with coaxial cable as a channel. It gives us the EVM of the transmitter, which is specified by the standard.
- The blue arrow measurement point corresponds to the signal passing through a fading channel, and used for parameter estimation. The non compensated EVM is affected by the channel. As soon as the nonlinearity parameters are estimated, a predistorted signal file is created.
- In a second step on frame 2, the compensated signal EVM is measured at transmitter output (the cyan arrow).
- Finally at the green arrow, the compensated EVM is measured within the different channels. The emulated channel from frame 2 can be different from the emulated channel for frame 1, in order to account for various scenarios (for example, parameters estimated with 30dB fading channel, predistortion and transmission in flat channel).

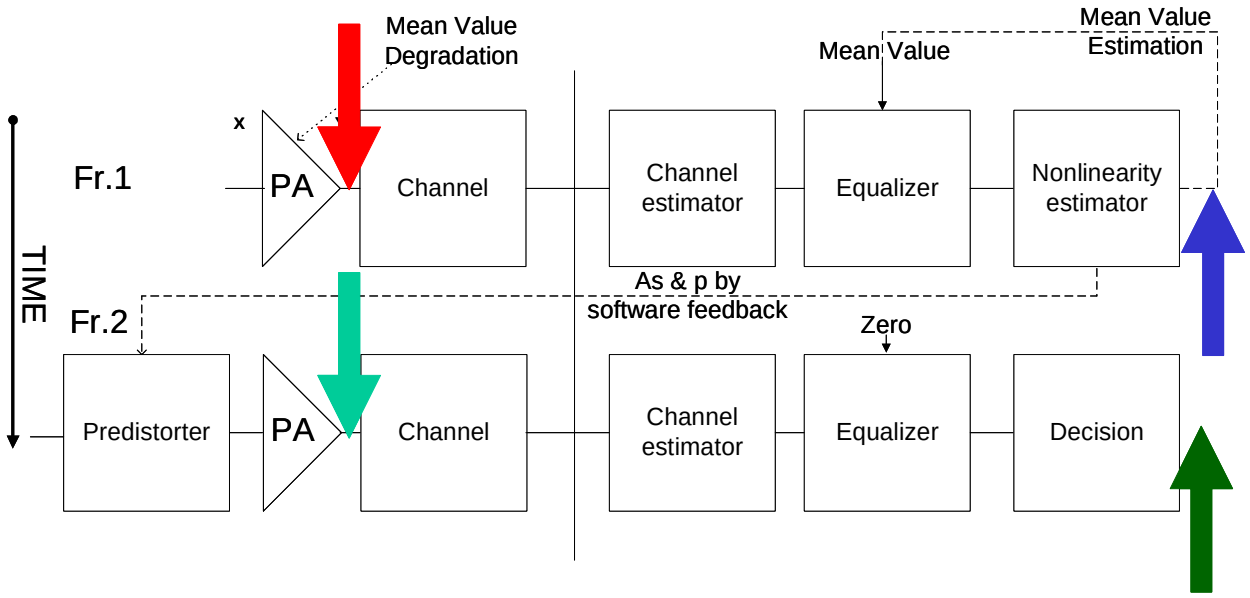

Figure 102 – Receiver aided architecture compensation strategy with measurement breakpoints

4-6.4 Back-to-back validation of the non-linearity compensation

Figure 103 shows the EVM measured back to back with parameters estimated through different channels. As shown in Figure 103 the algorithm seems very robust to channel degradation.

The power amplifier back off might be lowered up to 3dB @ EVM = 3% while still meeting the linearity conditions. Then the power consumption improvement computed as in [76] could reach 50%.

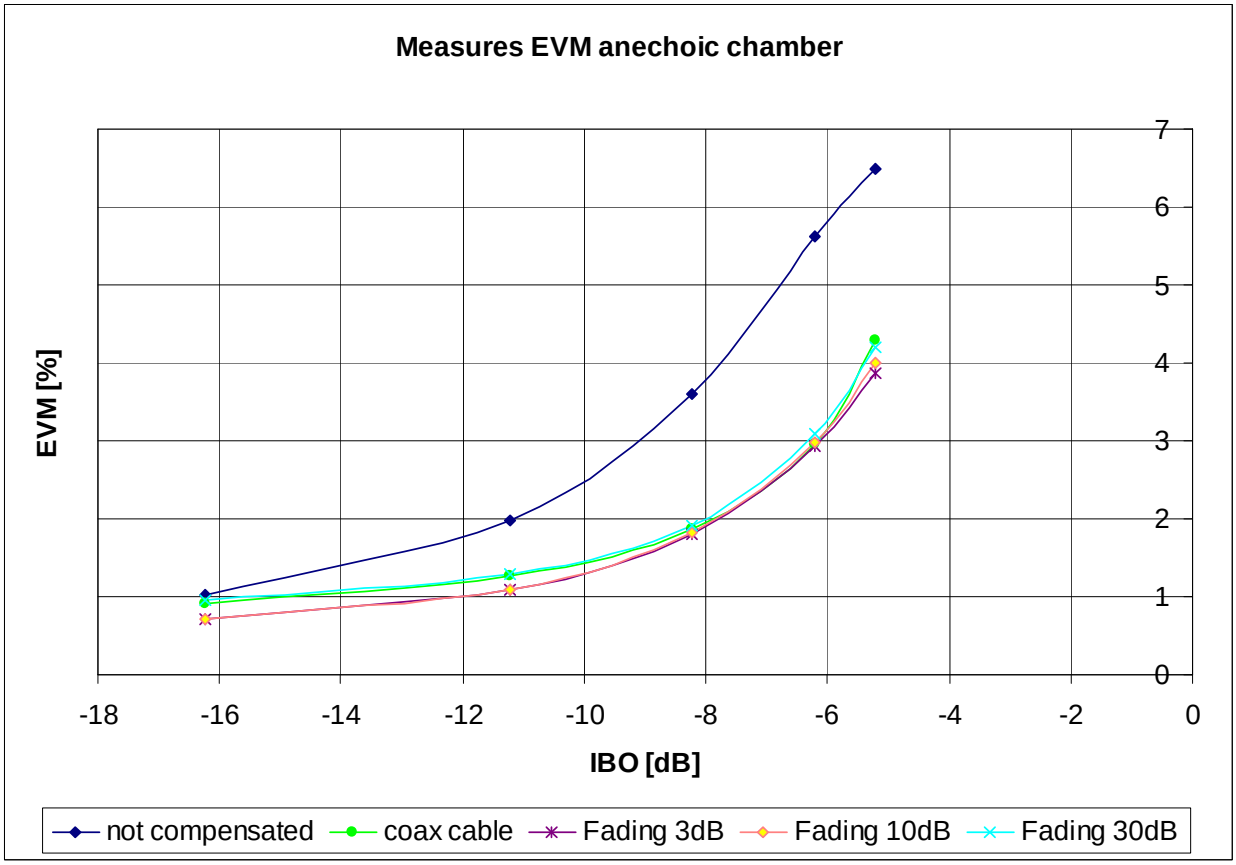

Figure 103 – Back to back validation of concept with over the air parameter estimation

4-6.5 Multi-user scenario

Figure 101 illustrates a multi-user scenarios. Usually relay stations and base stations are in direct visibility; channels with low fading appear usually between relay and base stations. The channels with significant fading are usually between mobile station and base station without direct visibility. With these assumptions, it seems interesting to estimate the nonlinearity parameters on a base station with a relay station, before making the communication between base station and mobile station.

The goal of the multi-user scenarios is to evaluate the interactions between the channel, the nonlinear power amplifier, and the processing algorithms.

Figure 104 shows the impact of the channel on the predistorted signal with parameters estimated in a"flat channel" and applied in other channels. Channel with fading 30dB degrades significantly the EVM. The other channels show degradation due to noise for IBO below -10dB.

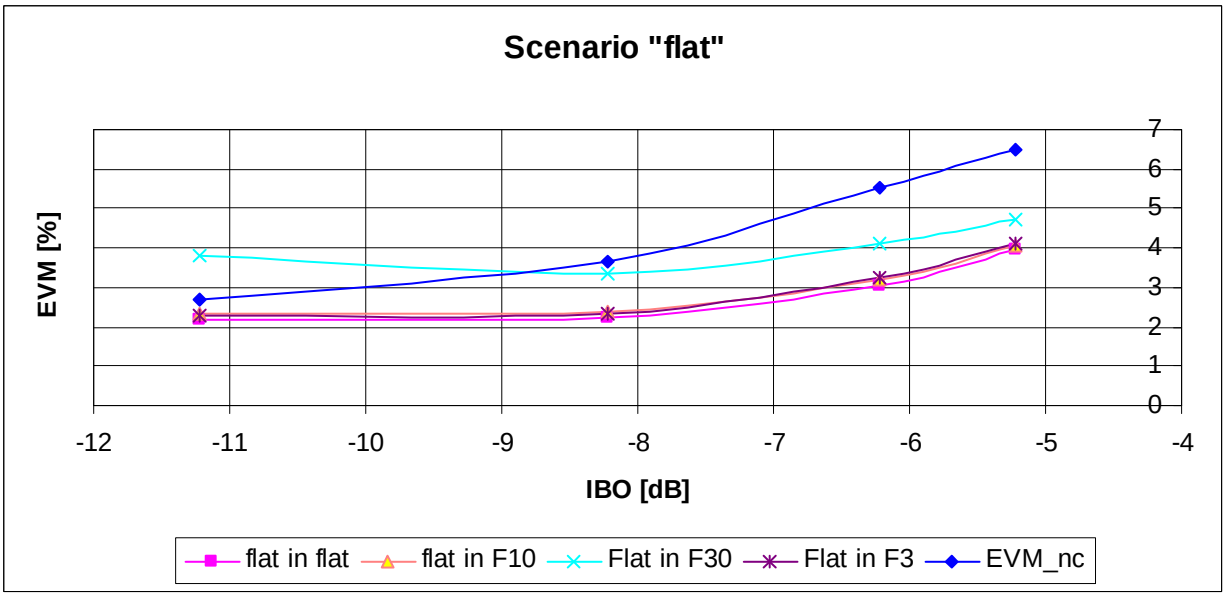

Figure 104 - EVM vs. IBO for parameters estimated in "flat channel" applied in each channels

Figure 105 shows the EVM results for parameters estimated in channel with 3dB fading. As the nonlinearity estimation is not affected by such a channel, EVM results are the same as previously.

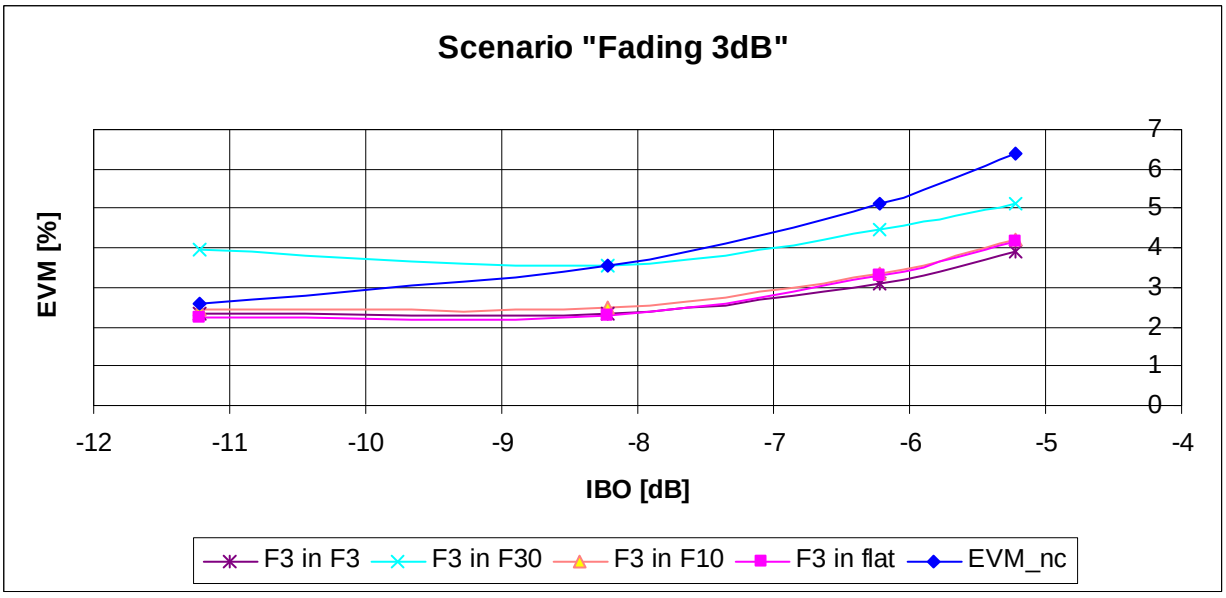

Figure 105 - EVM vs. IBO for parameters estimated in "channel with 3dB fading" applied in each channels

Figure 106 shows EVM results for parameters estimated in channel with 10dB fading. As the nonlinearity estimation is not affected by such a channel, EVM results are the same as previously.

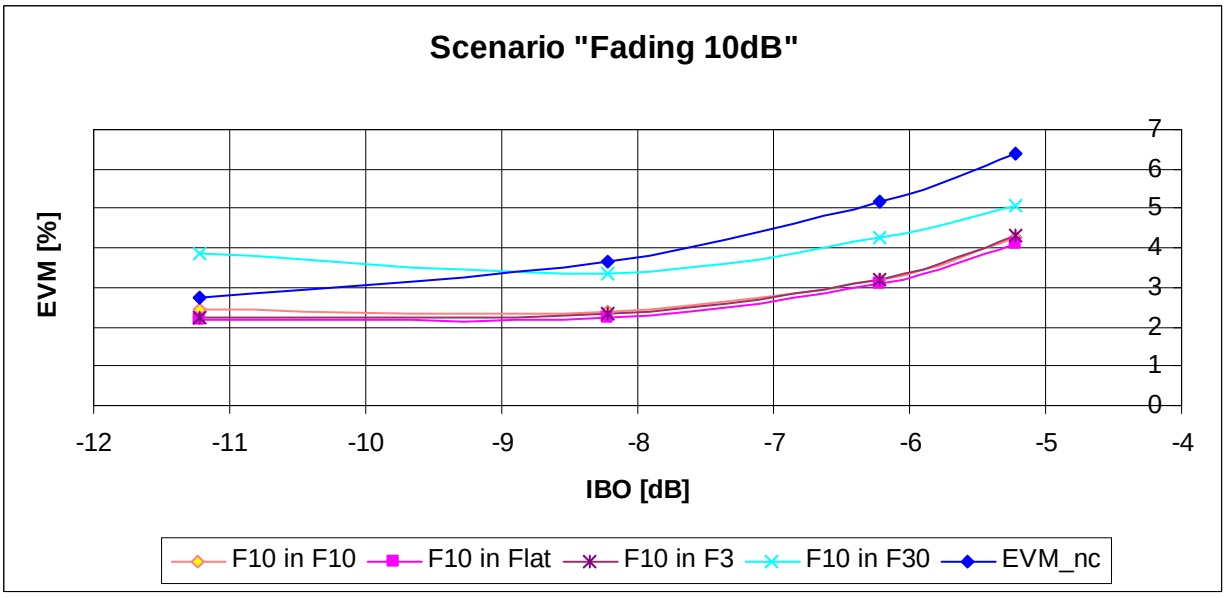

Figure 106 - EVM vs. IBO for parameters estimated in "channel with 10dB fading" applied in each channels

Figure 107 shows EVM results for parameters estimated in channel with 30dB fading. The result exhibits a low sensitivity of the nonlinearity estimation algorithm to the channel. The channel impact might be clearly seen in deep fading channels. The signal does not meet EVM requirements only because of channel degradation.

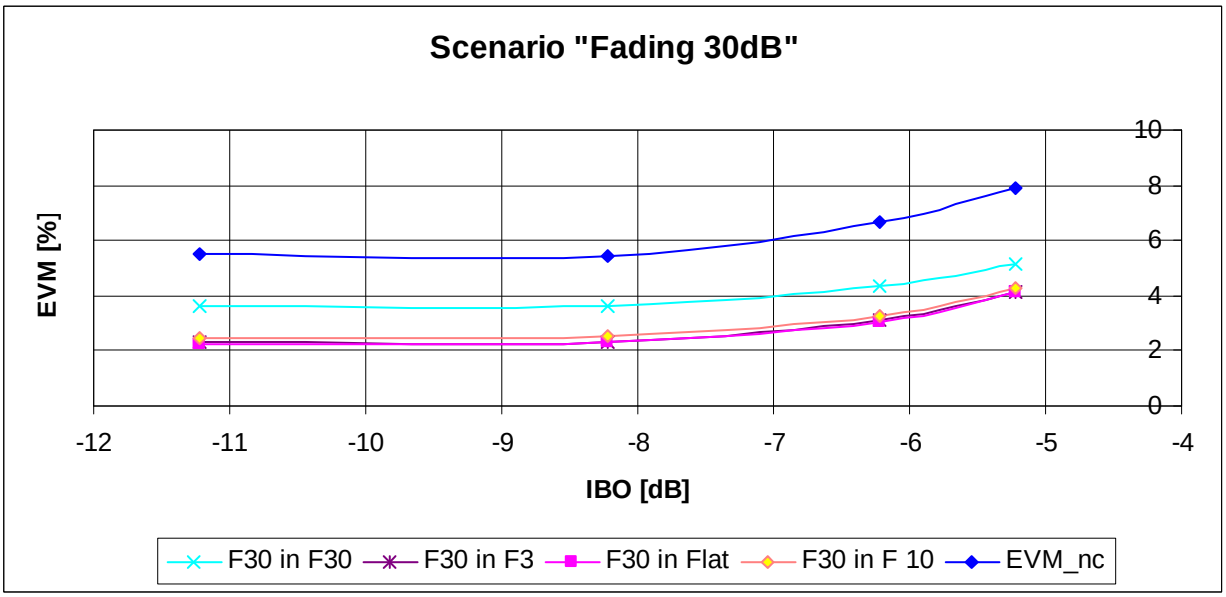

Figure 107 - EVM vs. IBO for parameters estimated in "channel with 30dB fading" applied in each channels

4-6.6 Conclusion and perspectives

More realistic channel scenarios for joint PA/antenna characterization have been described in this chapter. The measurements highlight that estimation of nonlinearity at the receiver is robust

to channel fading. The IBO is lowered by up to 3dB for different channels @ EVM = 3%. The power consumption can then be reduced by up to 50%.

A novel approach of using the OTA has been shown. The OTA is favored for possibility of emulating reproducible channels simply from two path propagation and scattering box.

4-7 Summary

The classical adaptive predistortion architecture needs extra consuming ADCs and components to realize its feedback path. As an alternative, architectures using post compensation in Rx and architecture with hybrid receiver-aided compensation are described and tested.

The different approaches of nonlinearity compensation have been studied. The first one with projection of a received training sequence onto orthogonal basis and direct compensation has the main drawback that the power amplifier by itself has to be linear enough to satisfy the standard's spectral mask and emitter EVM requirements.

The second approach uses the LMS algorithm to estimate a Rapp's model which is inversed analytically to predistort the emitted signal. Hence there is no added complexity for embedded computation. In this case the PA nonlinearity is compensated before the signal emission. The drawback of this architecture is that it may require some changes in telecommunication standards such as creation new MAC layer messages. Table 18 summarizes pros and cons of those architectures.

Architecture	*NL compensation before emission*	*HW complexity*	*SW complexity*	*Standard modification*
Predistortion	Yes	high	zero	Not needed
Postcompensation	No	zero	low	Not needed
Hybrid	Yes	zero	high	May be needed

Table 18 - Architectures summary

The impact of SW complexity on effective power consumption is evaluated it the next chapter.

Chapter 5 : Evaluation of Power Consumption & Complexity

5-1 Introduction

This chapter investigates algorithm complexity and digital consumption of the nonlinearity compensation algorithms. The first part deals with power consumption modeling. The Class A and Class B PA efficiencies are modeled allowing IBO gain to be linked to power consumption gain. Baseband unit consumption depends on algorithm complexity and hardware implementation. Different combinations are studied in a second part. In the last part the effective power consumption gain is evaluated. Studies are carried out to help finding an optimal tradeoff between extra base band unit consumption and memory size taking into account algorithm precision, robustness and refreshment rate.

5-2 Power Consumption

The evaluation of power consumption gain is based on the projection of IBO improvement values taken from EVM measurements.

5-2.1 Consumption savings

Figure 108 shows theoretical efficiency vs. IBO for class A (blue) and class B (green) power amplifiers. Class AB amplifiers are situated between those two curves, function of their conducting angle. Curves are obtained from maximal theoretical drain efficiency $\eta=P_{OUT}/P_{DC}$ multiplied by input backoff in linear domain, where P_{OUT} and P_{DC} are obtained from the equations in [77].

In [77] the maximal power efficiency is formulated as Eq. 64, where V_{DC} is the supply voltage, V_{OUT} is the output voltage, I_{DC} is given by Eq. 65 and I_1 is given by Eq. 66. α is the conduction angle, which determines the PA class. Class A PAs have a maximum efficiency equal to 50% and class B PA's maximum efficiency is given by $\pi/4 = 78.5\%$.

$$\eta = \frac{P_{OUT}}{P_{DC}} = \frac{\frac{V_{OUT}}{\sqrt{2}} \cdot \frac{I_1}{\sqrt{2}}}{V_{DC} \cdot I_{DC}} \quad \text{Eq. 64}$$

$$I_{DC} = \frac{I_{MAX}}{2\pi} \frac{2\sin(\alpha/2) - \alpha\cos(\alpha/2)}{1-\cos(\alpha/2)} \quad \text{Eq. 65}$$

$$I_1 = \frac{I_{MAX}}{2\pi} \frac{\alpha - \sin(\alpha)}{1-\cos(\alpha/2)} \quad \text{Eq. 66}$$

For class A PAs, when back off is applied, the efficiency is given by Eq. 67, where IBO is the input back off defined as P_{1dB}-P_{IN} in dB. Because of the conduction angle, which is equal to 2π, the PA is active all the time so $I_{MAX}=V_{DC}/R$; hence the dependency of efficiency to IBO is linear.

$$\eta(IBO) = IBO_{LIN} \cdot \eta_A \qquad \text{Eq. 67}$$

For class B PA, when back off is applied the efficiency is given by Eq. 68. Because the supply current is dependent on the conduction angle $\alpha=\pi$, the supply current is 0 half the time $I_{MAX}=V_{OUT}/R$; hence the dependency of efficiency to IBO is of square root form.

$$\eta(IBO) = \sqrt{IBO_{LIN}} \cdot \eta_B \qquad \text{Eq. 68}$$

Equations Eq. 67 (blue) and Eq. 68 (green) are shown in Figure 108. The curves of class AB amplifiers are between the blue and green one depending on the conduction angle.

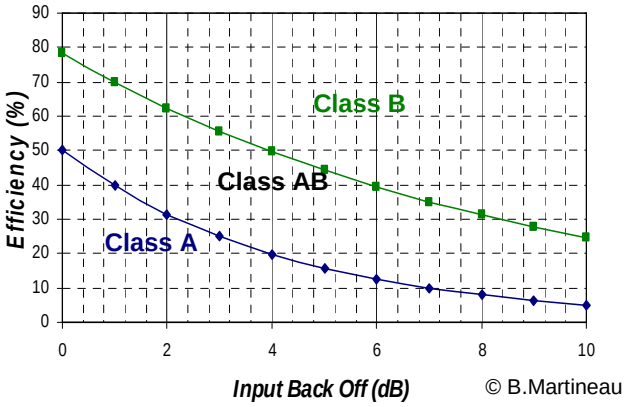

Figure 108 – Efficiency vs. IBO

These relations are fundamental for determining power consumption gain for power amplifiers of class A, AB and B.

5-2.2 Projection into consumption domain

Figure 109 left recalls the measured EVM versus input back off. The green curve corresponds to EVM without compensation. The blue curve is the measured EVM of compensated signal. Figure 109 shows the projection of the signal compensation performance into power supply savings. For a defined EVM of 3%, the IBO difference from Eq. 67 gives us the efficiency for non compensated system with class A power amplifier η_1=16.84%, and η_2=10.45% for compensated system with the same PA. This can be translated into 38% efficiency improvement.

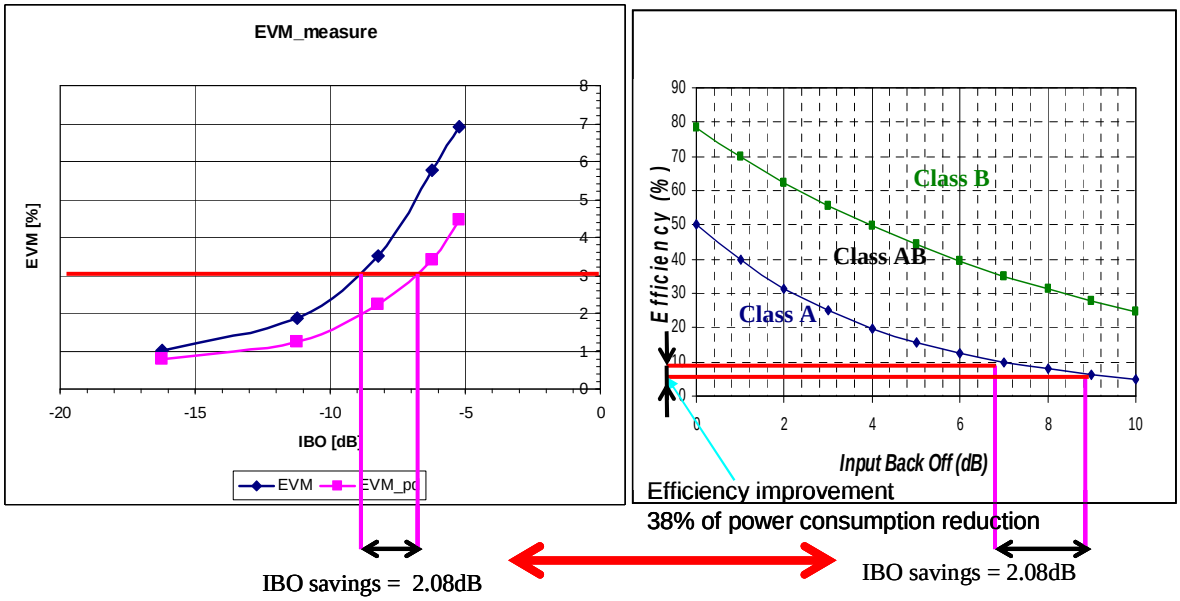

Figure 109 – Illustration of the method evaluation of power amplifier consumption savings from EVM measurements

Table 19 and Table 20 show the theoretical efficiency ratio for class A and class B, which might be projected as a theoretical gain in power consumption.

Class A / EVM [%]	Efficiency_C [%]	Efficiency_NC [%]	Efficiency ratio	Consumption gain [%]
5,01	17,26	10,74	1,61	37,77
3,98	13,61	8,34	1,28	38,72
3,16	10,37	6,61	1,57	36,26

Table 19 - Class A efficiency savings

Class B / EVM [%]	Efficiency_C [%]	Efficiency_NC [%]	Efficiency ratio	Consumption gain [%]
5,01	46,12	36,38	1,27	21,12
3,98	40,96	32,05	1,28	21,75
3,16	35,76	28,53	1,25	20,22

Table 20 - Class B efficiency savings

5-2.3 Conclusion

The class A-AB power amplifier consumption might be reduced by 38% by hybrid predistortion. At this time, the main improvement is achieved by amplitude compensation. The AM/PM distortion and memory effect impact were neglected comparing to the compensated AM/AM distortion, because of the low gross power consumption gain. The net power consumption gain is determined by gross power consumption gain minus power consumption

needed to estimate the parameters. To have a positive consumption gain, the complexity of algorithms and hardware solution are essential.

5-3 Complexity and power consumption of the signal processing

This section gives an evaluation of the digital baseband unit extra consumption for both the emitter and the receiver. The estimation of the nonlinearity algorithm has to be carried out periodically (function of PA biasing, ageing, temperature) while predistortion should run permanently at the emitter.

The hardware complexity is measured in MMACs (Mega Mutliply-ACcumulate). The predistortion unit complexity depends on the hardware implementation of the exponential function used in Eq. 69, or its equivalent. The Matlab code complexity is reformulated by [78] to compute hardware complexity in MACs.

$$X_{POWER} = \frac{Y_{power}}{\left(1-\left(\frac{Y_{power}}{As^2}\right)^p\right)^{\frac{1}{p}}} \qquad \text{Eq. 69}$$

This hardware complexity determines the architecture and consumption of base band unit needed for power amplifier predistortion.

5-3.1 Fixed point computation

Figure 110 shows the signal to clipping and quantization noise ratio for OFDM systems with signal parameters from Table 10 - Signal parameters, where μ is clipping factor. The methodology found in [79] was applied to set the fixed point optimal quantization. Due to minimum SNR needed to demodulation and the other noises the optimal quantization is 7 bits in our case for real part I and imaginary part Q of the transmitted signal.

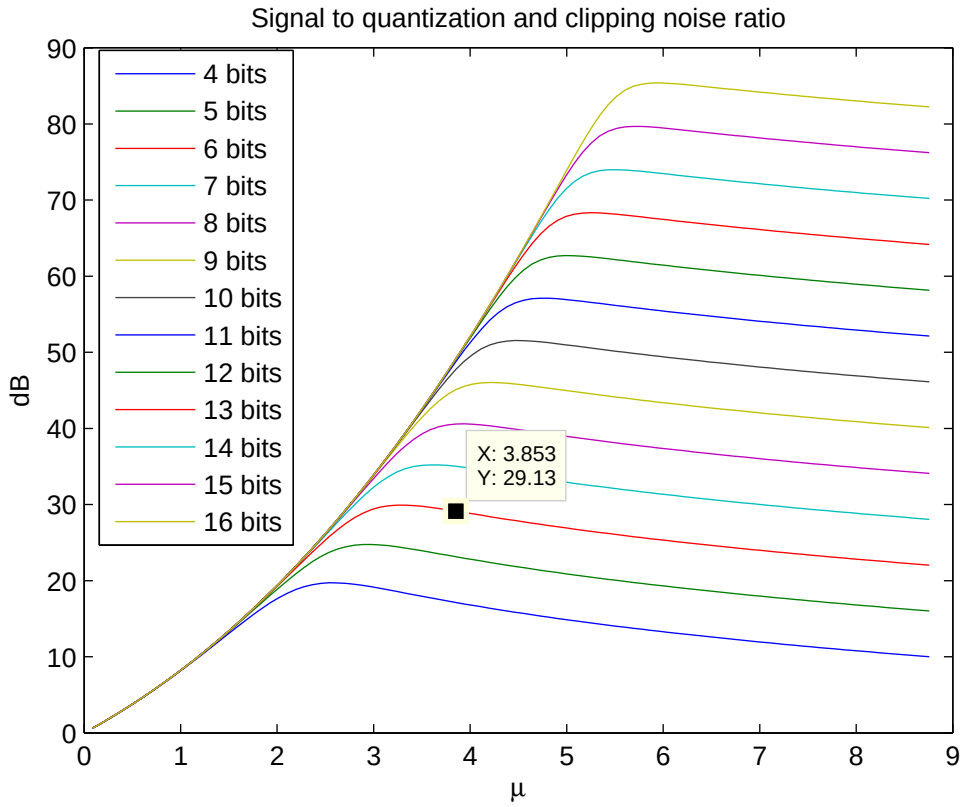

Figure 110 – Optimal signal to clipping and quantization ratio

The predistortion function increases signal dynamic before the power amplifier. To keep the same quantization noise, one bit more is allocated to the new signal dynamics. The predistorted signal is then quantized on 8 bits for I and 8 bits for Q.

The main loop of the estimation algorithm modifies the As parameter to minimize the MSE. The minimum error value is first found for every As in a 9 points interval. Then the new computation interval is reduced to the 5 points (As_vect_division) around the minimal error value. At the next iterative step, MSE is computed again on 9 points covering this new interval. The dichotomy stops when the desired MSE precision of 0,01 is reached. At this step As is coded with 9 bits.

Figure 111 shows the algorithm progress on finding the lowest MSE. The red curve is the first iteration, the green curve is second iteration and the blue curve is third iteration.

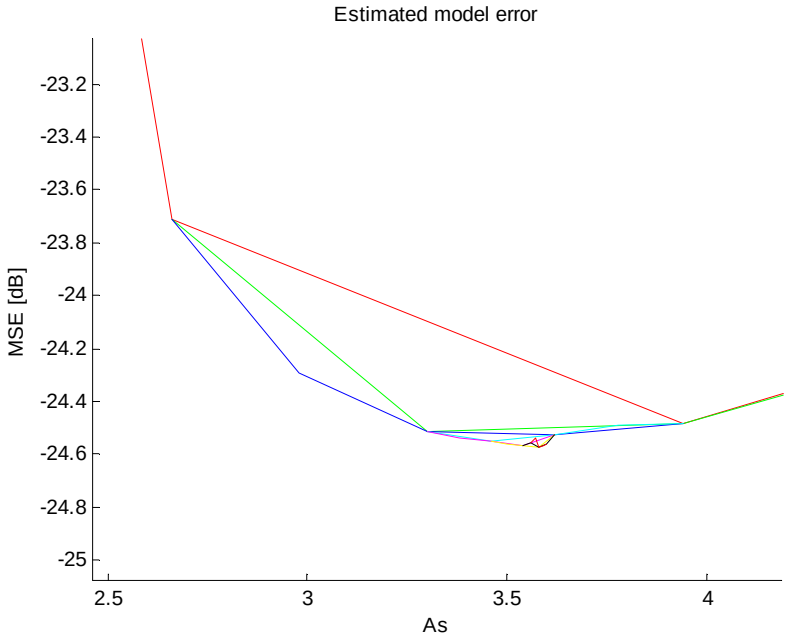

Figure 111 – Zoomed MSE [dB] vs. As parameter of Rapp model

The p parameter is estimated by LMS algorithm inside the dichotomy loop. Figure 112 shows iterative convergence curves. From the extreme value (interval border) the p value converges to the right value with minimal mean error in combination with As parameter. This makes algorithm very robust. Due to parameters dependency given by equations in the previous chapter, even with non optimal As the p converges to a value giving low MSE error. Hence the p parameter which is coded on 7 bits needs in the worst case 2^7 iterations to reach the right value.

The coding of As and p is optimized for PA nonlinear functions. Minimal and maximal values are determined for As on 9 bits (min=1,38; max= 6,5) and p on 7 bits (min=0,8; max=2,08).

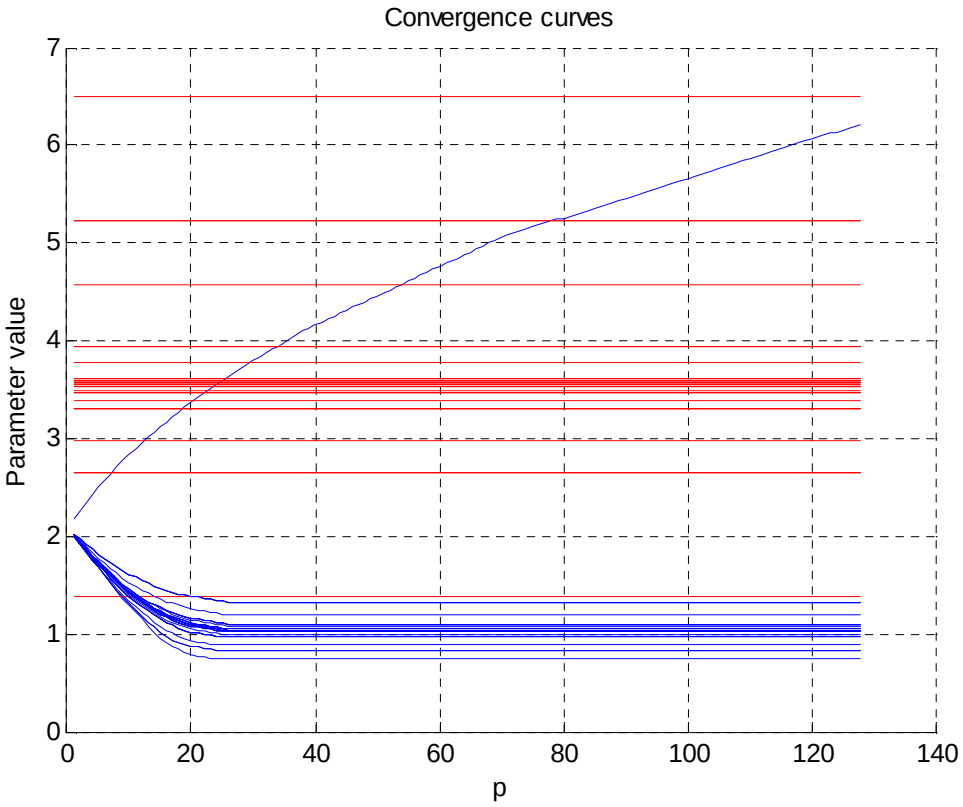

Figure 112 – Convergence curves of LMS sub algorithm

To estimate the parameters with a good accuracy, only 64 samples is needed.

With these assumptions, the predistortion unit complexity is evaluated to 2025MACs/sample while the nonlinearity estimation complexity is evaluated to 8.15MMACs per estimation for the parameters of Table 21. With computation of the exponential function, the implementation of the predistortion is clearly unmanageable. As a result, a Look Up Table is proposed to carry out the predistortion at the emitter.

As_vect division	5	iterations
Dichotomy loops	9	loops
Bits number	16	Bits
Samples number	64	Samples
p max iterations	2^7	iterations

Table 21 -Algorithm parameters

The algorithm summarizing graph is given in Figure 113. The couple of As and p parameters which approximates the nonlinearity with lowest MSE are given as results.

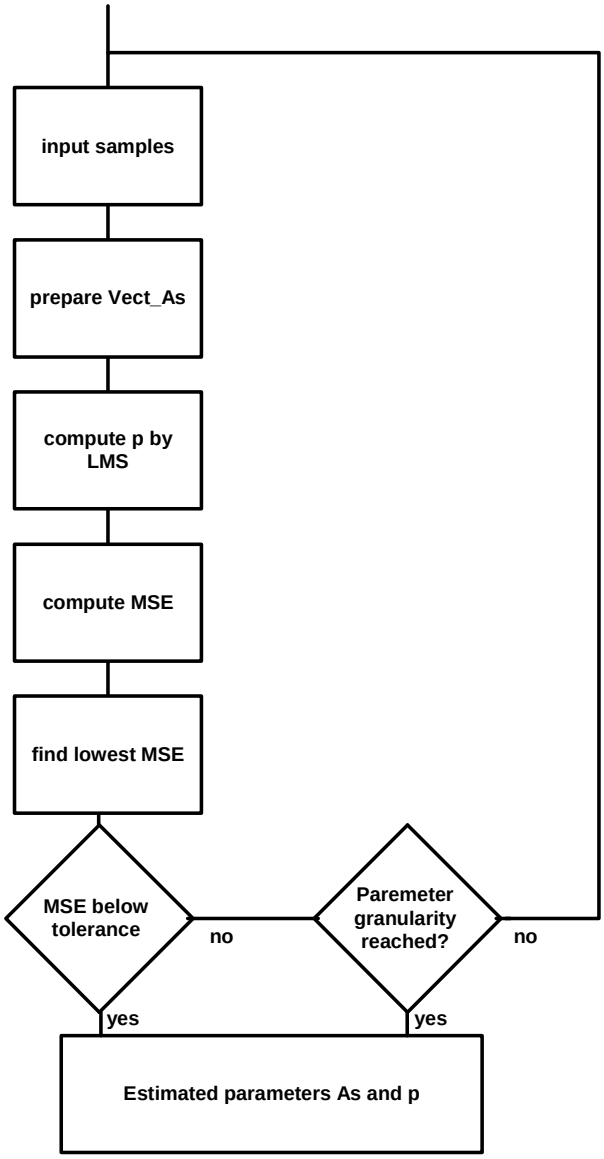

Figure 113 – Algorithm diagram

Figure 114 shows the residual MSE error after parameter estimation for different channels and IBO.

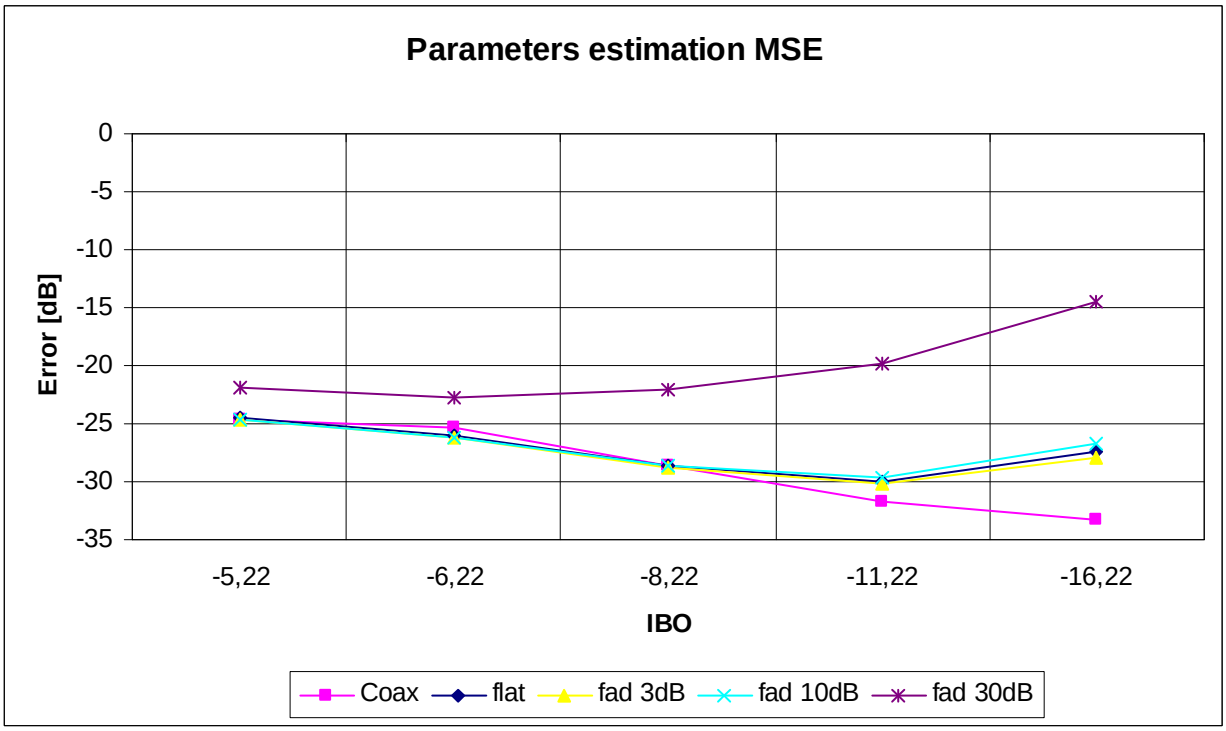

Figure 114 – Estimated MSE vs. IBO for different channels

5-3.2 Hardware implementation

In this chapter suggestions of hardware realization are proposed. The first part describes an implementation of the algorithms as hardware computation. The complexity study has been carried out for a DSP. As an alternative, the second part describes a realization based on Look Up Table to avoid computation complexity. The third part shows a combination of the two approaches as a trade-off for optimizing the power consumption.

5-3.2.1 Hardware computation

The algorithm can be divided into 2 different parts. The first part, which is needed to predistort one sample, requires 2025 MACs. This part is active all the time when the predistortion is applied. The second part of algorithm is parameter estimation. This algorithm complexity has been estimated to 8,15MMACs per estimation. Hence is needed only for occasional refreshment. As an example, a DSP (ADAU 1702) with 25 Mega Instructions per Second (MIPS) consumes 0,16W. When all algorithms are executed on the DSP, the consumption and execution time are summarized in Table 22. Inversion of model requires no complexity because it has been done analytically.

DSP 0,16W	Needed energy	Needed time
Estimation – occasionally on	53,8[mJ/Estimation]	0,33[s/Estimation]
Predistortion – always on	13.4 [µJ/SAMPLE]	81 [µs/SAMPLE]

Table 22 - Energetic budget of algorithms computed by DSP

If the refreshment parameter rate is not important (lower than 1s) the power consumption becomes weak. The con of this solution is that for predistortion the emitter power consumption stays at 0,16W.

5-3.2.2 LUT solution

Look Up Tables are proposed as an alternative in Figure 115 to algorithm computation at emitter and receiver side. The LUT is used at emitter for predistortion, with table entries corresponding to the nonlinearity coefficients transmitted by software feedback.

The Tx LUT is composed of elementary 65536 LUTs (for each As and p couple, as detailed below) with 2^6 I and Q input entries and 1576 I and Q output amplitude levels. For each LUT entry are memorized I and Q predistorted signal corresponding to {As,p} and input power. The predistorted signal is quantified on 8 bits. As the predistortion operates on input power (positive values) the number of power levels can be reduced to 7 bits for I and Q paths, and the sign is added to signals afterwards. The required elementary LUT size is then 1576*2*7=22064 bits. The global Tx LUT memory size is then 65536*22064=1.4Gbits or 0.18Gbytes.

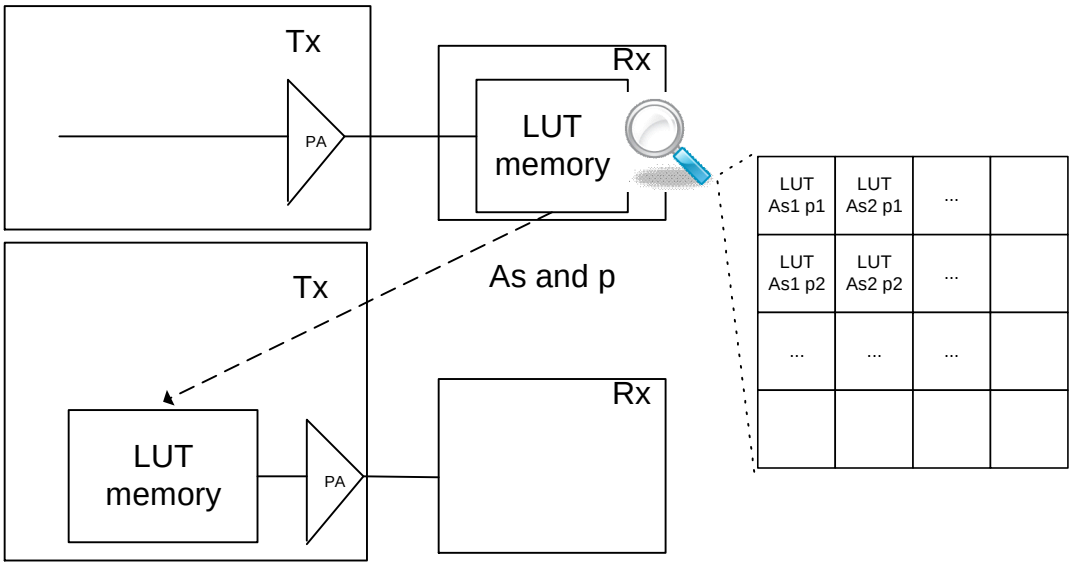

Figure 115 – LUT only solution

The required number of {As,p} couple entries in LUT are determined by the range and precision of the As and p parameters. For As on 9 bits (min=1,38; max= 6,5, step 0.01) and p on 7 bits (min=0,8; max=2,08, step 0.01), 65536 elementary LUTs are needed.

The model is base only on AM/AM distortion and the first bit of the signal is used for the sign. So the number of bits which determine the LUT levels decreases from 7 to 6 for non-predistorted signal and from 8 to 7 for predistorted signal. Hence in the elementary LUT for one combination of nonlinearity parameters As and p, the input is determined by 2 six-bit inputs and 2 seven-bit outputs. Two six-bit inputs create 4096 combinations. However when considering the square value of imaginary part Q and real part I as I^2+Q^2 and using the I and Q symmetry (Figure 116), the LUT might be compressed from 4096 to 1576 levels only.

	1	2	3	4	5	6	7	8	9	10	11
1	1	2	3	4	5	6	7	8	9	10	11
2	2	4	6	8	10	12	14	16	18	20	22
3	3	6	9	12	15	18	21	24	27	30	33
4	4	8	12	16	20	24	28	32	36	40	44
5	5	10	15	20	25	30	35	40	45	50	55
6	6	12	18	24	30	36	42	48	54	60	66
7	7	14	21	28	35	42	49	56	63	70	77
8	8	16	24	32	40	48	56	64	72	80	88
9	9	18	27	36	45	54	63	72	81	90	99
10	10	20	30	40	50	60	70	80	90	100	110
11	11	22	33	44	55	66	77	88	99	110	121

Figure 116 – Demonstration of number symmetry

The global LUT size reaches 0,18GB. This is not possible to implement such a huge LUT without power hungry memories.

5-3.2.3 Adaptive LUT solution

Figure 117 shows the proposed adaptive LUT solution. This solution combines the advantages of hardware computation with the pretty small size of an elementary LUT. The idea is to estimate the nonlinearity parameters {As,p} by hardware computation, transmit them from receiver to transmitter by software feedback and compute in the transmitter the elementary LUT only for the {As,p} couple. In that case, only 25kbit of memory is needed for LUT.

As memory consumption is evaluated between 10 and 100 times lower than equivalent hardware consumption, the power saving becomes important.

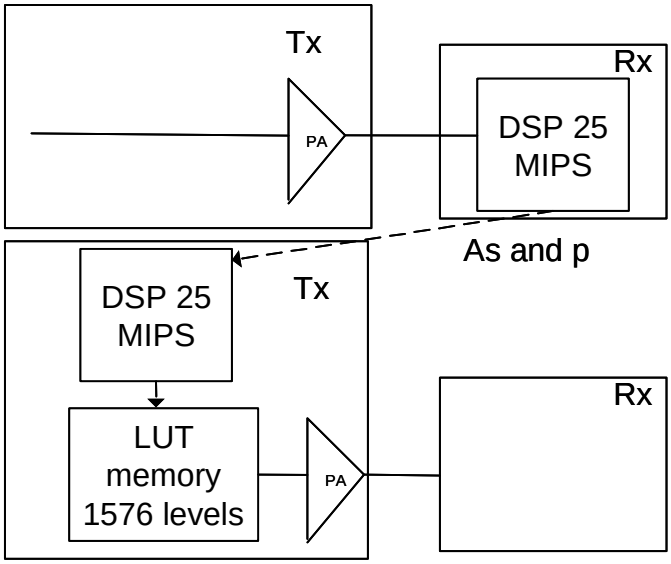

Figure 117 – Adaptive LUT solution

5-3.3 Conclusion

In this paragraph the algorithm is described in details with all the aspects of the hardware implementation. The hardware implementation finally converges to adaptive LUT solution

because of pretty small size of elementary LUT and its consumption for predistortion. In the next chapter, DSP is used as a reference for power consumption of the hardware computation.

5-4 LUT impact on final consumption

In this paragraph the baseband unit consumption is evaluated, as a comparison to power savings on the power amplifier. The algorithm complexity is translated into an estimated energy budget, taking into account the refreshment rate of the nonlinearity estimation. This refreshment rate is obviously related to channel and components stationarity.

5-4.1 Refreshment rate

In the receiver-aided hybrid architecture, the estimation of the overall network power consumption depends on the refreshment rate of the estimation of the nonlinearity parameters. The energy needed for parameter estimation in the receiver and LUT adaptation in transmitter is divided by refreshment rate to evaluate the algorithm's power consumption.

Assuming a DSP (ADAU 1702) consuming 160mW, the average power consumption of the hardware computation is evaluated at 68.7mW, 1,2mW, 19µW, 0.8µW, respectively for 1s, 1min, 1hour, 1day refreshment period, (Figure 118).

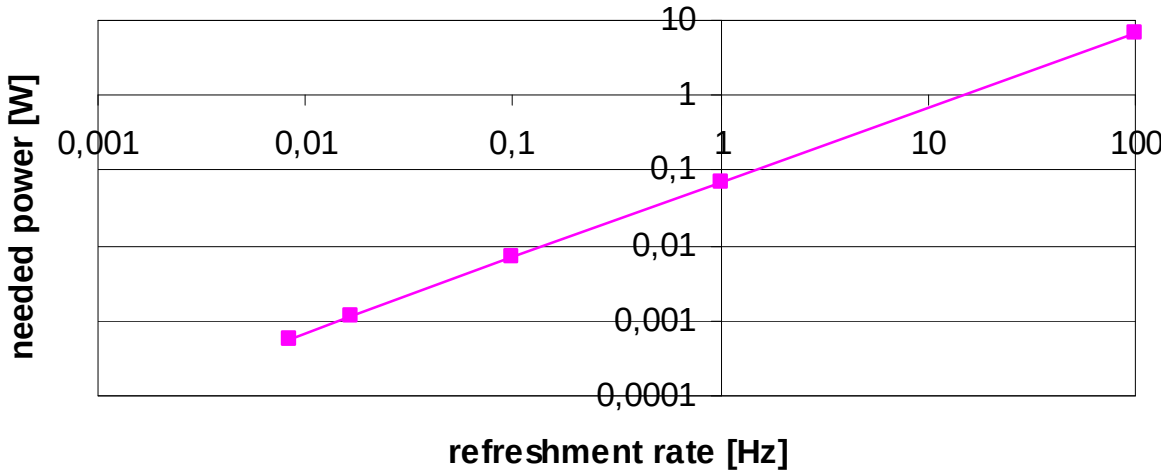

Figure 118 – DSP power consumption vs. refreshment rate

5-4.2 Power consumption of base band unit

From Figure 109 the efficiency of compensated and non compensated systems are estimated for class A power amplifier to η_2=16.84%, and η_1=10.45%. The efficiencies are translated into power consumption savings domain by Eq. 70. For instance for a 20dBm conducted power amplifier the power saving is 360mW.

$$P_{SAVED} = P_{OUT\_LIN}\left(\frac{1}{\eta_2} - \frac{1}{\eta_1}\right) \quad \text{Eq. 70}$$

However on the other hand, the compensation architecture needs extra base band consumption at emitter and receiver side. The effective power savings is given by Eq. 71.

$$P_{SAVED\_EFF} = P_{SAVED} - P_{BASEBAND} \quad \text{Eq. 71}$$

For instance if the LUT is implemented with two 16kbit memories (Microchip 93AA86A/B/C), having consumption of 3.6mW with refreshment rate equals to 1min, the LUT consumes 1.2mW and the overall baseband consumes 4.8mW. Hence the global power budget for a 20dBm PA output power falls to P_{SAVED_EFF} = 355.2mW. Function of the refreshment rate, the saved power decreased. For high refreshment rate, the power balance can become negative. Table 23 shows the emitted power for which the balance becomes negative between the saved and the consumed power at the given refreshment period. For instance with 1s refreshment rate, the hybrid receiver-aided architecture would save power if the emitted power is higher than 12.8dBm. From this chart it becomes easy to determine if the compensation of the nonlinearity by this architecture is relevant for fixed or mobile applications.

Refreshment period	0,01 s	1 s	10 s	1 min	1 h	1 day
P_PA[dBm]	37,8	12,8	2,8	-5	<-20	<-20

Table 23 – Minimum emitted power function of refreshment period

Figure 119 shows an estimation of the saved power function of the PA output power for different refreshment periods. In the figure are marked the maximal output power levels allowed by the standards, from Table 24. For the considered standard, the receiver-aided architecture would allow to save power both in downlink at base station and in uplink at mobile station, assuming a refreshment rate of 1s or higher.

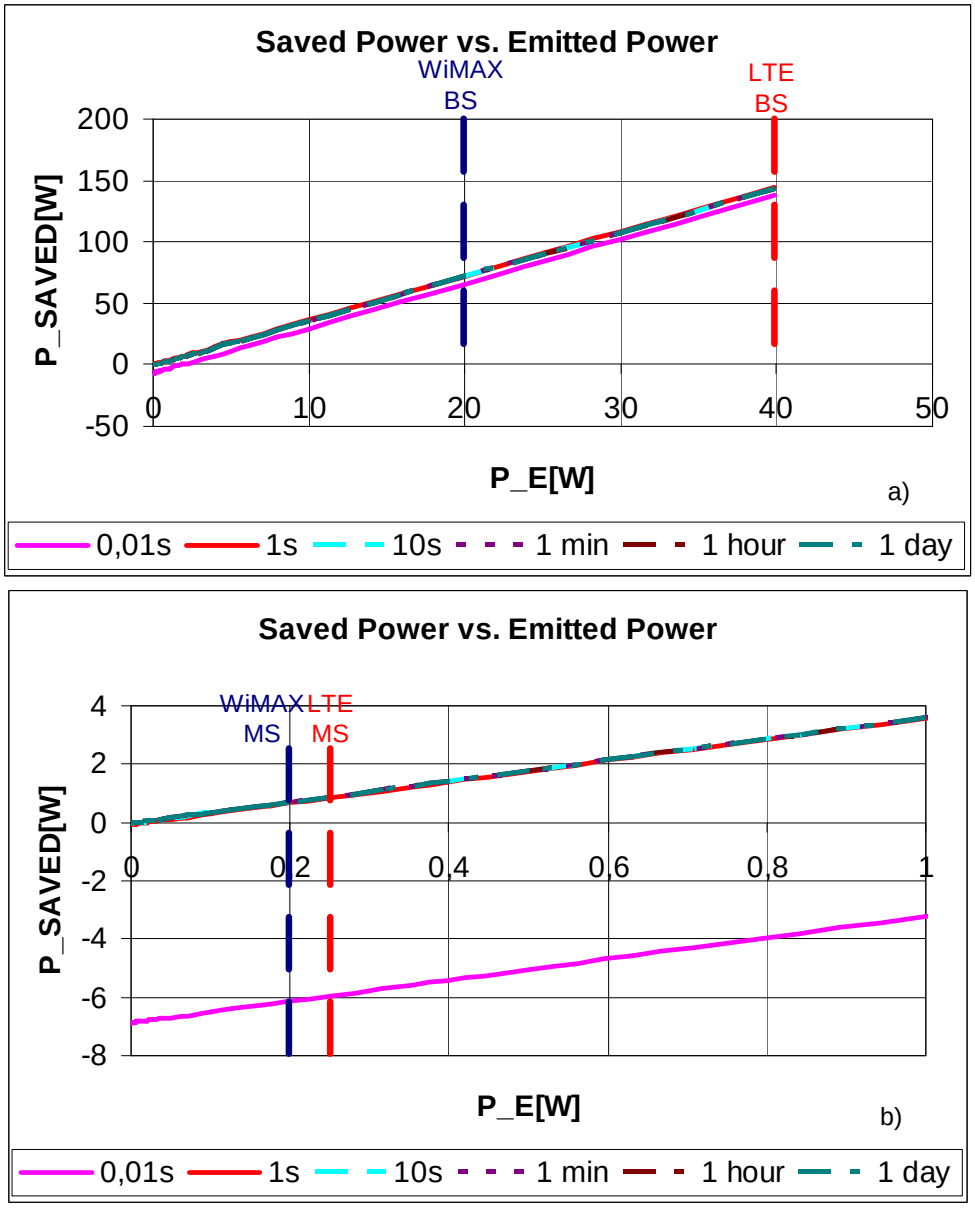

Figure 119 – Saved power vs. PA output power a) entire zone (LTE & WiMAX BS output power) b) zoom on region close to zero (LTE & WiMAX MS)

Standard / Device PA's output power	BTS	MS
WiMAX	43 dBm	23 dBm
LTE	46 dBm	24 dBm

Table 24 - Power amplifier's output powers for different standards

5-4.3 Conclusion

As a conclusion, Figure 120 shows the overall power consumption ratio between compensated PA and non-compensated PA. The red line shows us the level where the consumption of a non compensated system is equal to a compensated system. This graph highlights that the receiver aided architecture could not only be suitable for base stations, but is also interesting for compensation of mobile station power amplifiers.

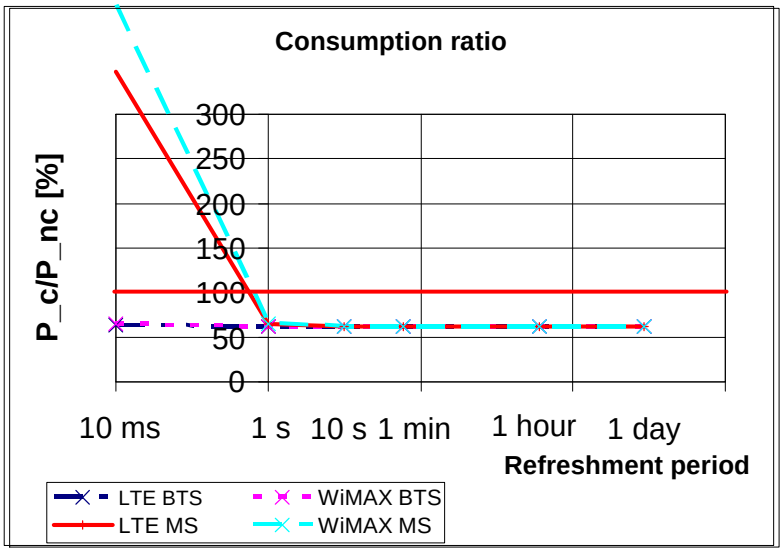

Figure 120 – Consumption ratio vs. refreshment period

5-5 Consumption & complexity summary

This chapter focuses on the optimization of baseband unit signal processing. Firstly the power consumption gain achieved by the predistortion is determined. The associated complexity of baseband unit processing related to the nonlinearity estimation algorithm application is evaluated. A predistortion scheme is combined from memory approach and calculation unit approach to avoid their drawbacks. The results exhibit that the energy can be saved in the base station case and also in the mobile station case with frequent refreshment rate.

Chapter 6 : General Summary

6-1 Relevance for Green Radio

In the first chapter is stated that power amplifier consumes 12.5% of overall cellular network power supply. This figure increases more when considering PA heat dissipation and the need for cooling fans.

In order to reduce this consumption, a new receiver-aided compensation architecture has been proposed to enhance power amplifier efficiency thanks to low complexity algorithms. This solution should be applicable in base stations, relay stations and even in mobile stations. From our evaluation, up to 40% of the power amplifier consumption could be saved using this new kind of predistortion. The consumption of the cooling fans could also be reduced significantly.

Because of its simplicity of implementation, it could be widely spread in rural environment, allowing .the replacement of diesel generators by solar panels or windmills. Then the base station deployment could avoid to be linked to the power grid.

More generally, the percentage of fossil fuel in overall cellular network consumption might be decreased in favor of renewable energy sources, because the base station power demand is decreased

6-2 Practical implementation

A novel receiver aided hybrid architecture has been proposed to increase power amplifier efficiency. This architecture combines the advantages of the digital architectures of the state-of-the-art, i.e. predistortion and post compensation. The compatibility of the software feedback loop needed for this architecture with WiMAX and LTE standard has been checked. This software feedback allows transmitting a limited quantity of data. Hence a low complexity and few parameters model has been chosen for the estimation of the nonlinearity at the receiver. The estimation of this model is carried out by an algorithm based on minimization of mean square error on a training sequence with a mixed dichotomy/LMS adaptive algorithm. Linked issues have been investigated such as gain control or equalizer impact on nonlinearity estimation.

An important part of the document deals with the evaluation the hardware consumption of the implemented algorithm. An approach combining the advantages of low-consumption Look Up Tables for predistortion algorithm and hardware computation for estimation of the nonlinear model has been proposed. Finally, the concept has been tested and validated by measurement in a synthetic NLOS channel environment.

The estimation algorithm has proved to be very robust to channel degradation of the received training sequence. This would allow using the algorithm in a cooperative network where estimation of the nonlinearity parameters is done by cooperative users before communicating with other ones. Thus a base station in a LTE cell with 300 users might only send a request to one user device in the cell. After adaptation, the predistortion should be valid for the communication with all the 300 user devices.

6-3 Perspectives

A perspective of this work would be to develop a compact portable demonstrator which is able to evaluate the performances of the receiver-aided predistortion in real channel or with real BS, RS and MS stations. In this scope it would be needed to develop an ASIC whose specifications are brought by this thesis. Then the consumption saving could be validated by measurement.

Thanks to low power consumption the algorithm could be used in cooperative network or ad-hoc network when the predistortion is adapted mutually between the neighbors. Hence the algorithm is suitable for reduction of power consumption in ad-hoc networks.

In the case of cellular networks such as LTE advanced with OFDMA modulation, one device per cell could calculate the predistortion of the base station power amplifier whenever the emitted power and channel information per block time/frequency are changed (already envisaged in LTE advanced standard). With the maximal number of 300 mobile devices per cell and thanks to estimation algorithm's channel robustness the refreshment rate per device does not need to be increased. Hence the algorithm is suitable for power optimization of the cell in a cellular network.

Bibliography

[1] Richter F. et al: "*Energy Efficiency Aspects of Base Station Deployment Strategies for Cellular Networks*" IEEE VTC2009-fall

[2] Liu Silu "*The green CDMA base station*" Huawei Communicate, Dec 2008, Issue 45

[3] Louhi J.T.: "*Energy Efficiency of Modern Cellular Base Stations*" Telecommunications Energy Conference, 2007. INTELEC 2007

[4] "*Eco-sustainable wireless service*" Strategic white paper Alcatel-Lucent

[5] "*Energy-savings solutions helping mobile operators meet commercial and sustainity goals worldwide*" Ericsson press information, June 2008

[6] P. Grant et al.: "Green Radio – Towards Sustainable Wireless Networks" Research brief on IET April 2009

[7] Frank Meywerk.:"*The Mobile Broadband Vision – How to make LTE a success*" LTE world summit, November 2008, London

[8] H. Karl: *"An overview of energy-efficient techniques for mobile communication systems*" Telecommunication Networks Group, Technical University Berlin, September 2003

[9] 802.16e-2009 IEEE standard

[10] IST-2001-34561/LETI/WP3/R/PU/002 : *"Predistortion Techniques"*, Project MUMOR, CEA-LETI, 2001

[11] J.G. Andrews et al.: "*Fundamentals of WiMAX: understanding broadband wireless networking*" ISBN 0-13-222552-2 Prentice Hall 2007

[12] Proakis J.G., Manolakis D.G.: "Digital Signal Processing – Principles, Algorithms & Applications", ISBN 0-13-373762-4 Prentice Hall, 1996

[13] Kenington P.B.: "*High-Linearity RF Amplifier Design*", ISBN-10: 1-58053-793-6 Artech House, 2000

[14] Cripps S.C.: "*RF Power Amplifiers for Wireless Communications*" ISBN 0-89006-989-1 Artech House Publishers

[15] Kenington P.B.: "*High-Linearity RF Amplifier Design*", ISBN 1-58053-143-1, Artech House Publishers, 2000

[16] Flament A.: "*Conversion N/A Radiofrequence 1 bit multivoies a filtrage programmable integre en technologies CMOS 65nm en IPD*" Ph.D. thesis USTL 2008

[17] Stauth J.T. et al.: "*Pulse-Density Modulation for RF Applications: The Radio-Frequency Power Amplifier (RF PA as a Power Converter*" Power Electronics Specialists Conference 2008

[18] Grebennikov A. et al.: " *Switchmode RF Power Amplifiers*", ISBN 978-0-7506-7962-6, Newnes 2007

[19] P. Nagle et.al.: "*A Wideband Linear Amplitude Modulator for Polar Transmitters Based on the Concept of Interleaving Delta Modulation*" ISCCC 2002

[20] Jeckeln E. et. al.: "US20020191710_A1"US patent 2002

[21] Bummam Kim et. al.: "*Performance Enhancement of Linear Power Amplifier Employing Digital Technique*" ISCAS 2008

[22] Pipilos S. et al.: "*A transmitter IC for TETRA Systems Based on a Cartesian Feedback Loop Linearization Technique*" IEEE Journal of Solid-State Circuits, vol 40, n°3, March 2005

[23]Cho H. et al.: "*A High-power Cartesian Feedback Transmitter Including a Compact Doherty Amplifier*", Microwave and Optical Technology Letters, vol. 50, n° 4, April 2008

[24]Sowlati T et al.: "*Quad-Band GSM/GPRS/EDGE Polar Loop Transmitter*", IEEE journal of solid-state circuits, vol. 39, n° 12, December 2004

[25]Norris G. et al: "*Optimized Closed Loop Polar GSM/GPRS/EDGE Transmitter*" 2006 IEEE

[26]Ito M. et al.:"*Variable Gain Amplifier in Polar Loop Modulation Transmitter for Edge*", Processing of ESSCIRC, Grenoble, France, 2005

[27]Akamine Y. et al.: "*A Polar Loop Transmitter with Digital Interference including a Loop-Bandwidth Calibration System*" , IEEE International Solid-State Circuits Conference, 2007

[28]Cox D.C.: "*Linear Amplification with Nonlinear Components*", IEEE Transactions on Communications, December 1974

[29]Helaoui M. et al.: "*A New Mode-Multiplexing LINC Architecture to Boost the Efficiency of WiMAX Up-Link Transmitters*", IEEE Transactions on Microwave theory and Techniques; vol. 55, n° 2, February 2007

[30]Panseri L et al.: "*Low-Power Signal Component Separator for a 64-QAM 802.11 LINC Transmitter*", IEEE Journal of Solid-State Circuits, vol. 43, n° 5,May 2008

[31]Birafane A. et al.: "*Phase-Only Predistortion for LINC Amplifiers With Chireix-Outphasing Combiners*", IEEE Transactions on microwave theory and techniques, vol 53, n°6, June 2005

[32]Poitau G. et al.: "*Experimental Characterization of LINC Outphasing Combiners, Efficiency and Linearity*", RAWCON,2004

[33]Abd Elaal M. et al.: "*Modified LINC Amplification System for Wireless Transceivers*", VTC-2006 Fall

[34]Yun Woo Y., Yi J., Yang Y., Kim B.:"*SDR Transmitter Based on LINC Amplifier with Bias Control*", Microwave Symposium Digest, 2003 IEEE MTT-S International, Vol.:

[35]Gerhard W. et al.: "*WCDMA outphasing power amplifier with a software defined transmitter/receiver architecture for determination of the predistortion function* " Advances in Radio Science, Copernicus GmbH 2006

[36]Wurm P. et al.: "*Radio Transmitter Architecture with All-Digital Modulator for Opportunistic Radio and Modern Wireless Terminals*" Cognitive Radio and Advanced Spectrum Management, 2008.

[37]Staszewski R.B.et al: "*All-Digital PLL and Transmitter for Mobile Phones*", IEEE Journal of Solid-State Circuits, vol. 40, n° 12, December 2005

[38]Seah K.-H. et al.: "*Digital polar transmitter for ultra wideband system using OFDM modulation*", Electronic letters, 12th April 2007, vol.43, n° 8

[39]Li C.J. et al: "*High Average-Efficiency Multimode RF Transmitter Using a Hybrid Quadrature Polar Modulator*", IEEE Transactions on Circuits and Systems –II: Express Briefs, vol.55, n° 3, March 2008

[40]Kenington P.B.: "*A Wideband Lineariser for Single and Multi-Carrier 3G CDMA*", VTC 1999 - Fall

[41]Kenington P.B. et al.: "*Power Amplification Techniques for Linear TDMA Base Stations*" GLOBECOM 1992

[42]Ding L. et al.: "*Memory polynomial Predistorter based on the indirect learning architecture*", GLOBECOM 2002

[43]Mueller J.-E., Ceylan M.: "*Transmission device with adaptive digital predistortion, transceiver with transmission device, and method for operating a transmission device*", US patent n° US 7,372,918 B2, 13. May 2008

[44]Ding L. et al: "*A memory polynomial predistorter implemented using TMS320C67XX*", School of Electrical and Computer Engineering, Georgia Institute of Technology, Atlanta

[45]Marsalek R: "*Contributions to the power ampli¯er linearization using digital baseband adaptive predistortion*" PhD thesis Universite Marne la Valee2003

[46]Baudoin G. et al.: "*Adaptive Polynomial Pre-Distortion for Linearization of Power Amplifiers in Wireless Communications and WLAN*" EUROCON 2001

[47]Liu T.et al.: "*Augmented Hammerstein Predistorter for Linearization of Broad-Band Wireless Transmitters*" Transactions on Microwave Theory and Techniques, IEEE 2006

[48]Kusonoki S. et al.: "*Power-Amplifier Module With Digital Adaptive Predistortion for Cellular Phones*", Transactions on Microwave Theory and Techniques IEEE 2002

[49]Safari N. et al.: "*A Block-Based Predistortion for High Power-Amplifier Linearization*", Transactions on Microwave Theory and Techniques IEEE 2006

[50]Dehos C. et al.: "*Digital Compensation of Amplifier Nonlinearities in the Receiver of a Wireless System*" SCVT 2007

[51]Boumaiza S. et al: "*Systematic and Adaptive Characterization Approach for Behavior Modeling and Correction of Dynamic Nonlinear Transmitters*", IEEE Transactions on Instrumentation and Measurement, VOL. 56, NO. 6, DECEMBER 2007

[52]Schenk T.C.W. et al: "*Receiver-based compensation of transmitter-incurred nonlinear distortion in multiple-antenna OFDM systems*" VTC 2007 fall

[53]Hagh-S H. et al.: "*CMOS wireless phase-shifted transmitter*", IEEE Journal of Solid State Circuits Vol. 39 (8) , pp. 1241-1252School: Edward S. Rogers Sr. Dept. Elec. E. University of Toronto, Toronto, Ont. M5S 3G4, Canada

[54]Vuolevi J.: "*Analysis, measurement and cancellation of the bandwidth and amplitude dependence of intermodulation distortion in RF power amplifiers*" ISBN 951-42-6514-9 Oulu University press 2001

[55]Dominique Schreurs et.al.: "*RF Power Amplifier Behavioral Modeling*", Cambridge University Press 2009 ISBN-13 978-0-511-43721-2

[56]Kibangou A.Y.: "*Modeles de Volterra a complexite reduite: estimation parametrique et applications a l'egalisation des canaux de communication*", Ph.D. thesis Nice-Sophia Antipolis, 2005

[57]Ahmed A. et al. "*Efficient PA Modeling Using Neural Network and Measurement Setup for Memory Effect Characterization in the Power Device*" Microwave Symposium Digest, IEEE 2005

[58]Draxler P. et. al.: "*Time domain characterization of power amplifiers with memory effects*", 2003 IEEE MTT S International Microwave Symposium Digest CatFf

[59]Myslinski et al.: "*Large-Signal Behavioral Model of a Packaged RF Amplifier Based on QPSK-like Multisine Measurements*" 13th GAAS Symposium – Paris 2005

[60]Clark C.J. et al.: "*Time-Domain Envelope Measurement Technique with Application to Wideband Power Amplifier Modeling*" IEEE Transactions on Microwave Theory and Techniques, VOL. 46, NO. 12, DECEMBER 1998

[61]Ahmed A. et al. "*Measurement of Envelope Frequency Dependent Nonlinearity in GaN HEMT Power Device*" International Workshop on Integrated Nonlinear Microwave and Millimeter-Wave Circuits, IEEE 2006

[62]Saleh, A.A.M., "*Frequency-independent and frequency-dependent nonlinear models of TWT amplifiers*," IEEE Trans. Communications, vol. COM-29, pp.1715-1720, November 1981.

[63]Rapp, C., "*Effects of HPA-Nonlinearity on a 4-DPSK/OFDM-Signal for a Digital Sound Broadcasting System,*" in Proceedings of the Second European Conference on Satellite Communications, Liege, Belgium, Oct. 22-24, 1991, pp. 179-184.

[64]Brette R. et al..:"*Piecewise-polynomial interpolation*", Lesson ENS, 2008 {http://www.di.ens.fr/~brette/calculscientifique/lecture3.pdf}

[65]Zeleny J. et al.: "*A Digital Cartesian Feedback Path Design for 2.4GHz ISM Band Standards*" ICECS 2009

[66]Zeleny J. et al.: "*Digital Compensation of the Power Amplifier Nonlinearities at Relay Station Receivers in 802.16j very high data rate systems*" RWW 2010

[67]Pedro J.C. et al.: "*Intermodulation Distortions in Microwave and Wireless Circuits*" ISBN 1-58053-356-6 Archtech House 2003.

[68]Bhatt, Tejas et al., "*Initial Synchronization for 802.16e Downlink*", Asilomar Conference on Signals, Systems and Computers, 30 Oct - 2 Nov 2006, Asilomar, CA, USA, p.6pp, (2006)

[69]ICT-ROCKET "*6D2 package*" 2010

[70]L. Rudant et al.: "*Wideband Over-The-Ait Test-Bed Reproducing Channel Delay Dispersion Characteristics*" Antennas and Propagation (EuCAP), 2010 Proceedings of the Fourth European Conference on, vol., no., pp.1-5, 12-16 April 2010

[71]TS 36.212 LTE standard norm, 3GPP.

[72]Panayiotopoulos I. et al.: *"Method for predistortion in a communication system* ", PCT patent application n° 2010/060851

[73]Hrdina Z.: "*Statisticka radioelektronika*" CTU 1996

[74]Shetty, Kiran Kumar: "*A Novel Algorithm for Uplink Interference Suppression using Smart Antennas in Mobile Communications*" PhD thesis Florida state university 2004

[75]Robin M.: "*Emulation du canal de propagation en chambre anéchoïde*", 29 march 2011 INPG

[76]Zeleny J. et al: "*Receiver-Aided Predistortion of Power Amplifier Nonlinearities in Cellular Networks*" submitted to IET 2011

[77]Cripps S.C.: "*RF Power Amplifiers for Wireless Communications*" ISBN 0-89006-989-1 Artech House Publishers

[78]Goyot A., "Introduction aux Opérateurs Arithmétiques", University course TIMA CNRS

[79]Dardari D.:" *Joint Clip and Quantization Effects Characterization in OFDM Receivers*" IEEE Transactins on Circuits ans Systems I, Regular Papers, vol. 53, n°. 8, August 2006

[80]IEEE Std 802.16™-2009

[81]Tim C.W. Schenk, "*RF Imperfections in High-rate Wireless Systems: Impact and Digital Compensation*", Springer Publisher, ISBN 978-1402069024, Feb. 2008.

ANNEXE A SUPPLEMENTARY WORK

The work in the period of March 2008 – middle of June 2009 was to develop a Cartesian feedback path of digital transmitter architecture in the context of opportunistic radio. Figure i shows the feedback path schematics. The signal is taken by a splitter to the base-band unit by Cartesian feedback path where is digitized by an ADC. The ADC clock frequency creates an intrinsic tunable filter, which is essential for being able to be adapted to the different standard's bandwidth for the opportunistic radio context.

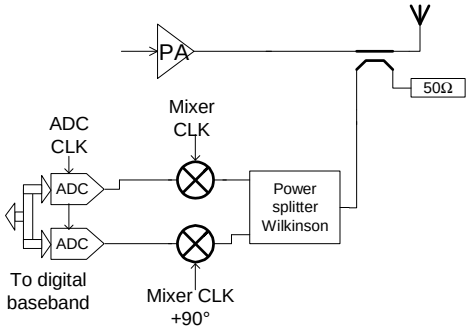

Figure i– Feedback Path with charge sampling

A publication was written in this period: "A Digital Cartesian Feedback Path Design for 2.4GHz ISM Band Standards" ICECS 2009

Figure ii shows the developed demonstrator (only on paper). From this work no publication was done, because the work stopped suddenly and the project was totally changed.

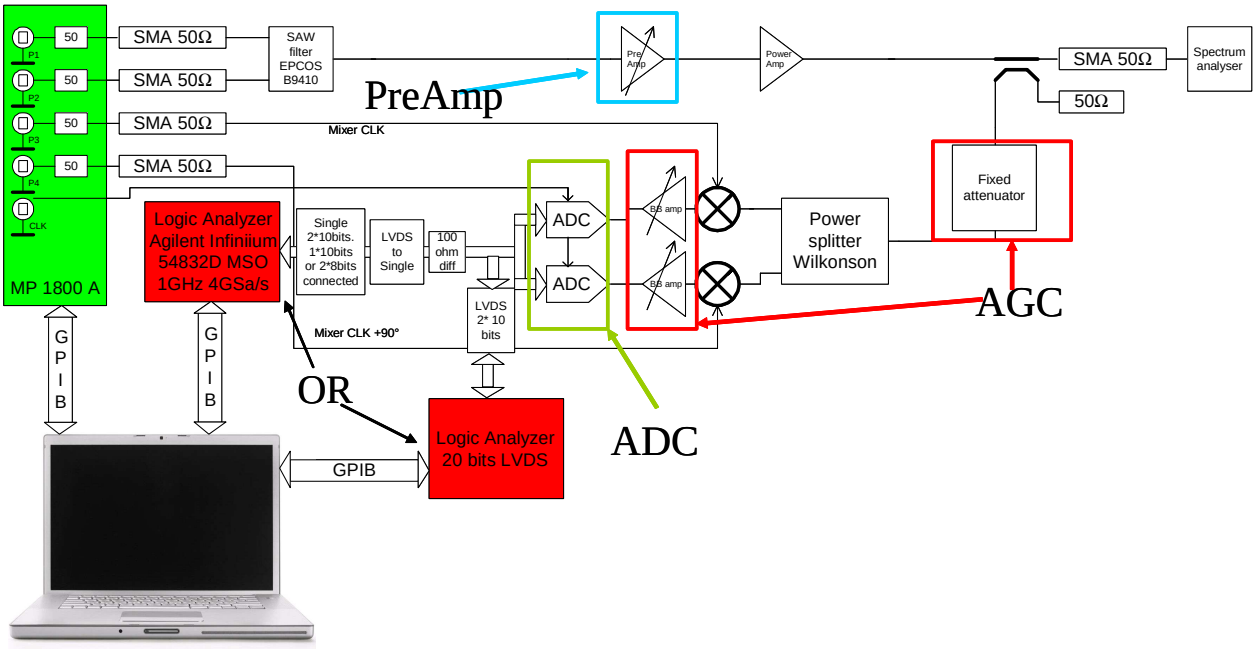

Figure ii – Card schematics

ANNEXE B GLOSSARY

1D-LMS	One Dimensional Least Mean Square
3GPP	3rd Generation Partnership Project
ACPR	Adjacent Channel Power Ratio
ADC	Analog to Digital Converter
AGC	Automatic Gain Control
AWGN	Additive White Gaussian Noise
BER	Bit Error Ratio
BS	Base Station
BTS	Base Transceiver Station
CDMA	Code Division Multiple Access
DSP	Digital Signal Processor
EDGE	Enhanced Data rates for GSM Evolution
EE&R	Envelope Elimination and Restoration
EVM	Error Vector Magnitude
FEC	Forward Error Correction
FPGA	Field Programmable Gate Array
GSM	Global System for Mobile Communications
GPRS	General Packet Radio Service
IBO	Input Back-Off
IIP3	Input Third Intercept Point
IIR	Infinite Impulse Response
LINC	Linear Amplification with Nonlinear Components
LMS	Least Mean Square
LNA	Low Noise Amplifier
LOS	Light of Sight
LTE	Long Term Evolution
LUT	Look Up Table
MAC	Medium Access Control
MS	Mobile Station
MSE	Mean Square Error
NARMA	Nonlinear Autoregressive Moving-Average
NLOS	Non Light of Sight
OFDM	Orthogonal Frequency Division Multiplex
OFDMA	Orthogonal Frequency Division Multiple Access
OTA	Over The Air
PA	Power Amplifier
PAPR	Peak to Average Power Ratio
PDP_S	Power Delay Profile Synthesizer
PSD	Power Spectral Density
QAM	Quadrature Amplitude Modulation
QPSK	Quadrature Phase Shift Keying

RF	Radio Frequency
RSA	Real time Spectral Analyzer
SNR	Signal to Noise Ratio
TWT	Traveling Wave Tube
VNA	Vector Network Analyzer
VSWR	Voltage Standing Wave Ratio
WiMAX	Worldwide Interoperability for Microwave Access